

# **The role of metabolite receptors in tumor progression**

Dissertation  
zur Erlangung des Doktorgrades  
der Naturwissenschaften

vorgelegt beim Fachbereich Biochemie, Chemie und Pharmazie  
der Johann Wolfgang Goethe-Universität  
Frankfurt am Main

von  
Isabell Brandenburger  
aus Bad Belzig

Frankfurt am Main, (2020)  
(D30)

vom Fachbereich Biochemie, Chemie und Pharmazie der

Johann Wolfgang Goethe-Universität als Dissertation angenommen.

Dekan: Prof. Dr. Clemens Glaubitz

Gutachter: Prof. Dr. Dieter Steinhilber  
Prof. Dr. Stefan Offermanns

Datum der Disputation:

---

## CONTENTS

<b>1</b>	<b>ABBREVIATIONS.....</b>	<b>6</b>
<b>2</b>	<b>INTRODUCTION.....</b>	<b>8</b>
2.1	Tumor metabolism .....	8
2.2	Regulation of tumor growth via metabolites .....	10
2.2.1	Lactate.....	12
2.2.2	Free fatty acids .....	14
2.3	Tumor models.....	15
2.3.1	Syngeneic tumor model .....	16
2.3.2	AOM-DSS colorectal cancer model .....	17
2.3.3	MMTV-PyMT breast cancer model .....	18
<b>3</b>	<b>AIM OF THIS STUDY.....</b>	<b>20</b>
<b>4</b>	<b>MATERIALS .....</b>	<b>21</b>
4.1	Chemicals/reagents/plates.....	21
4.2	Buffers .....	21
4.3	Enzymes.....	23
4.4	Primers .....	24
4.5	Plasmids .....	25
4.6	Antibodies.....	25
4.7	Cell lines .....	25
4.8	Bacterial strains .....	26
4.9	Medium.....	26
4.10	Kits .....	29
4.11	Genetic mouse models .....	29

<b>5</b>	<b>METHODS</b> .....	<b>31</b>
5.1	CRISPR/Cas.....	31
5.2	Cell culture.....	36
5.3	Expression analysis .....	36
5.4	Adipocyte isolation.....	37
5.5	BrdU and H&E staining.....	37
5.6	X-Gal staining.....	39
5.7	Immunofluorescence .....	40
5.8	Syngeneic tumor model .....	40
5.9	Colorectal cancer model .....	41
5.10	Breast cancer model.....	41
5.11	Statistical analysis .....	41
<b>6</b>	<b>RESULTS</b> .....	<b>42</b>
6.1	Metabolite receptor expression in human solid tumors .....	42
6.1.1	HCA1 is expressed in breast tumor samples .....	42
6.1.2	FFA4 is expressed in colon tumor samples.....	44
6.2	Metabolite receptor expression in tumor cell lines.....	47
6.3	Generation of <i>Ffar4<sup>fllox</sup></i> mice.....	48
6.4	Syngeneic LLC1 tumor model.....	52
6.4.1	HCA2, FFA2 and FFA4 are expressed in tumor stroma of LLC1 tumors.....	52
6.4.2	Knockout of HCA2, FFA2 or FFA4 does not cause change of volume and weight of LLC1 tumors.....	55
6.4.3	Knockout of HCA2, FFA2 or FFA4 does not change metastasis in the LLC1 syngeneic tumor model.....	56
6.5	AOM-DSS colorectal cancer model .....	57
6.5.1	HCA2, FFA2 and FFA4 are expressed in tumor stroma of colorectal tumors .....	57
6.5.2	Knockout of HCA2 or FFA4 does not change tumor growth of colorectal tumors .....	61
6.5.3	Knockout of FFA2 increases tumor number but not area in the AOM-DSS model.....	62

6.6	MMTV-PyMT breast cancer model .....	64
6.6.1	HCA1, HCA2 and FFA2 are expressed in the stroma of MMTV-PyMT tumors.....	64
6.6.2	Knockout of HCA1 or HCA2 does not influence onset and growth of MMTV-PyMT tumors significantly .....	67
6.6.3	Knockout of FFA2 leads to earlier onset of MMTV-PyMT tumors.....	69
6.6.4	Knockout of HCA1, HCA2 or FFA2 does not change metastasis in MMTV-PyMT breast cancer model .....	71
<b>7</b>	<b>DISCUSSION.....</b>	<b>73</b>
7.1	The role of HCA1 in breast cancer .....	73
7.2	Expression of HCA2 in tumor-associated macrophages and its role in tumor development.....	75
7.3	FFA4 effects in tumor growth remain unclear.....	77
7.4	The tumor-protective effect of FFA2.....	77
7.5	Studying metastases formation in the LLC1 syngeneic tumor model and the MMTV-PyMT breast cancer model .....	80
<b>8</b>	<b>REFERENCES.....</b>	<b>82</b>
	<b>SUMMARY.....</b>	<b>96</b>
	<b>ZUSAMMENFASSUNG .....</b>	<b>97</b>
	<b>ACKNOWLEDGEMENTS .....</b>	<b>103</b>
	<b>CURRICULUM VITAE.....</b>	<b>104</b>
	<b>LEBENS LAUF .....</b>	<b>105</b>
	<b>SCHRIFTLICHE ERKLÄRUNG .....</b>	<b>106</b>

## 1 ABBREVIATIONS

ALA	$\alpha$ -Linolenic acid
AOM	Azoxymethane
ATP	Adenosine triphosphate
BrdU	5-Bromo-2'-deoxyuridine
CAF	Cancer associated fibroblast
cDNA	Complementary deoxyribonucleic acid
CREB	cAMP response element binding protein
DAG	Diacylglycerol
DSS	Dextran sulfate
EGF	Epidermal growth factor
EMT	Epithelial to mesenchymal transition
ES cell	Embryonal stem cell
GAPDH	Glycerinaldehyd-3-phosphat-dehydrogenase
gDNA	Genomic deoxyribonucleic acid
GPCR	G-protein coupled receptor
FA	Fatty acid
FADH <sub>2</sub>	Flavin adenine dinucleotide
FFA	Free fatty acid
FFAR	FFA receptor
GLUT	Glucose transporter
3-HB	3-Hydroxy butyrate
HCA	Hydroxy carboxylic acid
HCAR	HCA receptor
HDAC	Histone deacetylase
HER2	Human epidermal growth factor receptor 2
HIF-1	Hypoxia-inducible factor -1
IHC	Immunohistochemistry
IF	Immunofluorescence
IFN	Interferon
IL	Interleukin
IP3	Inositol-1,4,5-trisphosphate
KRAS	Kirsten rat sarcoma
lacZ	Gene coding for $\beta$ -galactosidase enzyme

LCFA	Long-chain fatty acid
LLC1	Lewis lung carcinoma cell line 1
loxP	Locus of X-over P1
LPA	Lysophosphatidic acid
MCT	Monocarboxylate transporter
MMTV-PyMT	Mouse mammary tumor virus Polyoma Virus middle T antigen
mRFP	Murine red fluorescent protein
mRNA	Messenger ribonucleic acid
mTOR	Mammalian target of rapamycin
NADH	Nicotinamide adenine dinucleotide
NADPH	Nicotinamide adenine dinucleotide phosphate
PAM	Protospacer adjacent motif
PD-L1	Programmed cell death protein 1 ligand
PGE <sub>2</sub>	Prostaglandin E <sub>2</sub>
PIA	(R)-N <sup>6</sup> -(2-Phenylisopropyl) adenosine
PI3K	Phosphatidylinositol 3-kinase
ROS	Reactive oxygen species
SCD1	Stearoyl-CoA desaturase
SCFA	Short-chain fatty acid
S1P	Spingosine-1-phosphate
SREBP	Sterol regulatory element-binding protein
ssODN	Single-stranded donor oligonucleotide
TAB1	TGF- $\beta$ -activated kinase 1 binding protein
TAK1	TGF- $\beta$ -activated kinase 1
TAM	Tumor associated macrophage
TGF	Transforming growth factor
TCA	Tricarboxylic acid
TNF	Tumor necrosis factor
T-reg cells	Regulatory T-cells
VEGF	Vascular endothelial growth factor

## 2 INTRODUCTION

### 2.1 Tumor metabolism

Cancer is a disease characterized by abnormal cells dividing without control. Globally it is the second leading cause of death with estimated 9.5 million cases in 2018 (1). The treatment of cancer faces multiple challenges founded in the properties of cancerous diseases. In 2000 these properties were consolidated as the hallmarks of cancer comprising self-sufficiency in growth signals, insensitivity to antigrowth signals, evasion of apoptosis, limitless replicative potential, sustained angiogenesis as well as tissue invasion and metastasis (2). A decade later two emerging hallmarks of cancer were added: evasion of immune destruction and reprogramming of energy metabolism (3). The latter describes a change of metabolic activities in cancer cells compared to benign cells in order to obtain or maintain a malignant character (4).

The reprogramming of energy metabolism comprises several independent and coherent characteristics such as altered bioenergetics, enhanced biosynthesis and an intact redox balance (5). In order to accomplish these characteristics a particular set of pathways is frequently deregulated. The tumor suppressive protein p53 is known to support DNA repair, cell cycle arrest, senescence of cells and apoptosis. However, recent studies indicate its involvement in the regulation of tumor metabolism. A loss of p53 enhances the glycolytic flux and promotes proliferation and redox balance (6). A gain of function of the transcription factor *c-myc* stimulates the expression of genes supporting anabolic growth by promoting the generation of transporters and enzymes involved in glycolysis, fatty acid synthesis and glutaminolysis (7). Furthermore, the phosphatidylinositol 3-kinase (PI3K)-AKT pathway is known as a master regulator of glucose uptake (8). In normal cells this pathway is activated by stimulation with growth factors whereby in the following hypoxia-inducible factor -1 (HIF-1) and sterol regulatory element-binding protein (SREBP) induce glycolysis and fatty acid (FA) synthesis (9). In cancer cells, mutations in the PI3K-AKT pathway frequently lead to independence from external stimuli such as growth factors (10, 11). In the course of the PI3K-AKT signaling, mRNA for the glucose transporter 1 (GLUT1) is expressed and GLUT1 is translocated to the cell surface resulting in substantial glucose uptake (12). Tumors have an increased demand of glucose and glutamine. In their catabolism carbon intermediates, which can serve as building blocks for macromolecules, are generated. The increased uptake of glucose into tumor cells has been discovered nearly a century ago by Otto Warburg (13, 14). Likewise, the increased uptake of glutamine is a well-known process in tumor metabolism since the 1950s (15). In quiescent cells, the glycolysis is used to generate acetyl-CoA that is oxidized in the tricarboxylic acid (TCA) cycle in order to generate electrons to fuel the



production of ATP. Proliferating cells regularly experience a change in these processes (16). Today it is known that the pyruvate, which accumulates as a product of aerobic glycolysis, is not supplied to the TCA cycle for adenosine triphosphate (ATP) production but transformed to lactate. Thus, glycolysis is not primarily used to fuel ATP production but to provide building blocks and reducing equivalents for the synthesis of biomolecules.

The alterations in bioenergetics are founded in the metabolic flexibility of tumor cells which allows them to endure a constantly changing availability of nutrients (17). Although mechanisms to ensure glucose and glutamine supply come into effect, tumors are often faced with nutrient depletion because of insufficient vascularization and rapid growth of the tumor itself (18). In this state of emergency, mutations of Kirsten rat sarcoma (KRAS) or inhibition of the mammalian target of rapamycin (mTOR) pathway can enable the tumor cells to take up extracellular proteins and living or apoptotic cells (19-21). The engulfment of proteins or cells by the cell membrane, the following transport of the vesicles to lysosomes and the proteolytic degradation to free amino acids is known as macropinocytosis (22) respectively entosis (20, 21). Another consequence of insufficient tumor vascularization is the occurrence of hypoxic areas. Therefore, biosynthetic reactions involving molecular oxygen as an electron acceptor can be abolished (4). For instance, the introduction of double bonds into newly synthesized FAs is catalyzed by stearoyl-CoA desaturase 1 (SCD1). A lack of unsaturated FAs can trigger the tumor cell to secure the supply through the uptake from the surrounding of the cell (23).

For replicative cell division and tumor growth a constant biosynthesis of macromolecules is required. Basic nutrients are taken up from the extracellular space followed by the conversion into intermediates by core metabolic pathways such as glycolysis, nonessential amino acid synthesis and the TCA cycle. These intermediates from TCA cycle and glycolysis are stored in pools to be available for the synthesis of biomolecules such as FAs, cholesterol, glycerol or nonessential amino acids. For these processes reducing power in form of Nicotinamide adenine dinucleotide phosphate (NADPH) is required which originates from the controlled oxidation of carbon substrates derived from TCA cycle or glycolysis (4).

In order to preserve the redox balance the reducing equivalent NADPH is a key factor in the maintenance of antioxidant defense systems. Tumors harbor increased levels of reactive oxygen species (ROS) such as hydrogen peroxide, because of hypoxia, the activation of oncogenes and the induction of PI3K signaling (24). Low levels of ROS can activate signaling pathways and transcription factors to stimulate tumor growth whereas ROS levels exceeding a certain threshold cause cellular damage. Therefore, NADPH is required to maintain a redox homeostasis. It is

assumed that upon tumor initiation an increased metabolic activity leads to an increase of ROS resulting in the activation of signaling pathways that promote cell proliferation and survival (25). Then, the antioxidant capacity of tumor cells increases to prevent toxic ROS levels and thus, facilitate tumor progression (26).

## 2.2 Regulation of tumor growth via metabolites

Metabolites are of central importance in the bioenergetics and biosynthetic processes of tumor cells. To obtain and maintain a malignant character aberrant cell proliferation is required. The alterations in tumor cell metabolism frequently result in increased levels of metabolites such as glucose, lactate, glutamine, acetate and many others. Several mechanisms how metabolites contribute to tumor proliferation are known. For example, the transcription factor *c-myc* is a key regulator of glutamine uptake and utilization in proliferating cells (27). It induces the transcription of glutamine transporters ASCT2 and SN2 and stimulates the production of enzymes that convert glutamine to glutamate that cannot leave the cells by the use of glutamine transporters (28). In addition, *c-myc* regulates the synthesis of enzymes that are substantial for purine and pyrimidine biosynthesis (29, 30). For the generation of nucleotides one to three molecules of glutamine are necessary and the attachment of the purine and pyrimidine rings requires glutamine derived intermediates from the TCA cycle. Hence, glutamine is an indispensable building block for nucleotide biosynthesis and its uptake is crucial for the proliferation of tumor cells. Both, glucose and glutamine do not only act as donors for carbon intermediates but oxidation of the intermediates in the TCA cycle provides the cell with the electron donors  $\text{FADH}_2$  and  $\text{NADH}$  that are required for ATP generation (31). Furthermore, glutamine can provide nitrogen for the generation of pyrimidine and purine nucleotides and nonessential amino acids.

Another domain of metabolite-dependent tumor promotion is the execution of epigenetic alterations. Changing disposability of glucose and oncogenic signaling promoted by KRAS mutation or AKT are likely to increase the total histone acetylation which in the following is inducing an increased gene expression in favor of tumor progression (32). The constant metabolism of glucose leads to a buildup of acetyl-CoA which acts as a substrate for the histone acetylation, i.e. the deposition of acetyl marks on histones. Moreover, the deposition of crotonyl marks on histones is reported to induce gene expression to an even higher degree than acetyl marks (33). The therefore obligatory Crotonyl-CoA is a catabolism product of different amino acids such as lysine and tryptophan and of the short chain fatty acid (SCFA) butyrate. Generally, these posttranslational modifications cohere with an improved accessibility of the genomic DNA (gDNA) for the assemblage of transcription factors and thus an enhanced gene expression.

Metabolites in tumor and tumor stroma cells can act via different targets including G-protein coupled receptors (GPCRs) that are a receptor class existent in nearly all living organisms. Their ubiquity determines them as a prominent therapeutic target in pharmacology. A GPCR is commonly activated by a ligand resulting in G-protein activation, change of receptor conformation and following signal transduction in the cell. Besides exogenous ligands, an organism can also use, store, generate or metabolize endogenous ligand molecules. GPCRs are present in numerous physiological and pathophysiological activities. This work focusses on two groups of GPCRs that possess a pivotal role in metabolism because they are activated by abundant metabolites: Hydroxy carboxylic acid receptors (HCARs) and free fatty acid receptors (FFARs) (Figure 1). Henceforth they will be named metabolite receptors. In the group of HCARs HCA1 is activated by lactate whereas HCA2 is activated by ketone bodies such as 3-hydroxy butyrate (3-HB) (34-36). Among the FFARs FFA2 is activated by SCFAs including acetate, butyrate and propionate while FFA4 is activated by long-chain fatty acids (LCFAs) (36-40). The metabolites activating these GPCRs do not just occur in regular metabolism, they also appear in the stroma of solid tumors as products of tumor cell metabolism. Solid tumors do not only consist of tumor cells but they can harbor a variety of different cell types such as leukocytes, fibroblasts, pericytes, endothelial cells, epithelial cells and adipocytes. While it has to be investigated which of the receptors can be expressed on tumor cells themselves, present data is showing the expression of metabolite receptors in stromal cell. HCA1, a  $G_i$ -coupled receptor, formerly known as GPR81, is mainly expressed on adipocytes (34, 41, 42). HCA2, formerly known as GPR109a, is also  $G_i$ -coupled and is expressed on monocytes, macrophages and adipocytes (35, 43-46). The SCFA receptor FFA2, formerly known as GPR43, can either be  $G_i$ - or  $G_q/11$ -coupled. Adipocytes and different leukocytes express FFA2 (47-49). FFA4, formerly known as GPR120, is a receptor with  $G_q/11$  coupling and its expression can be found on macrophages and to a minor degree on adipocytes (38, 50, 51).

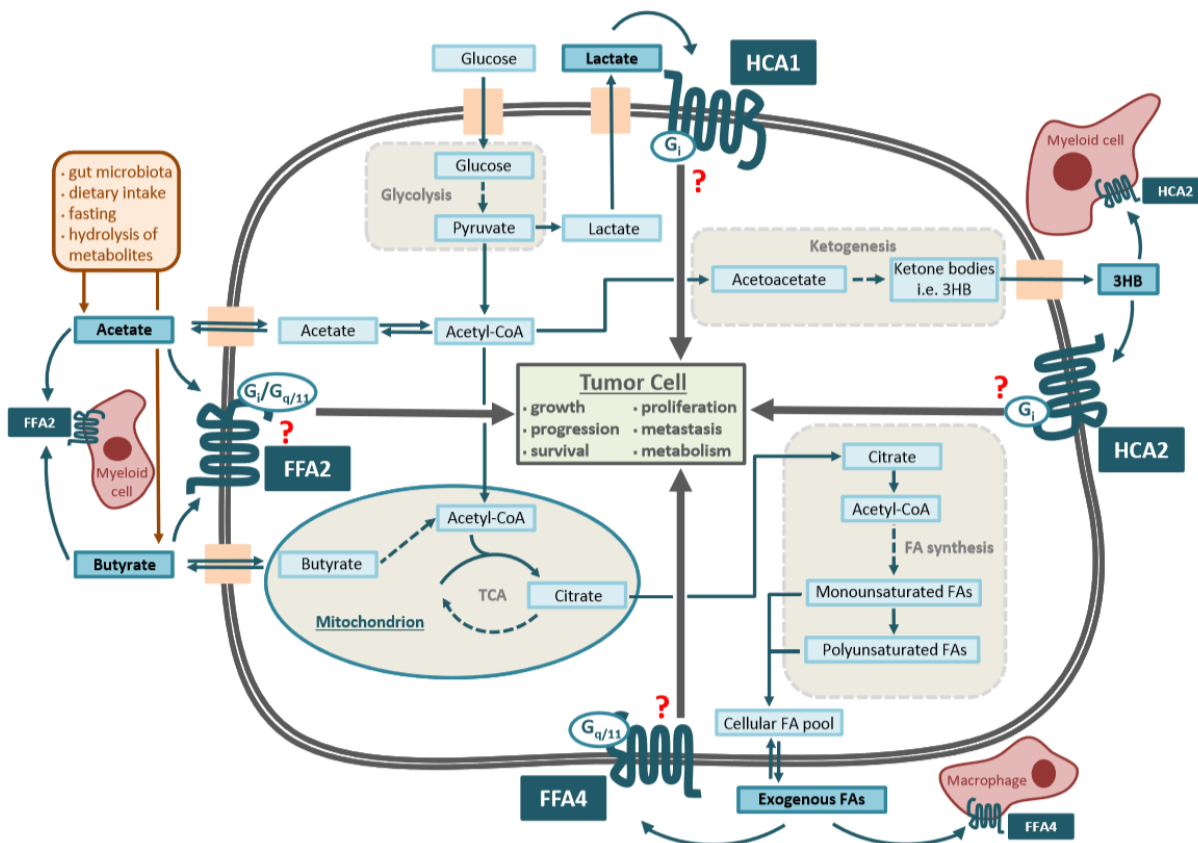


**Figure 1: The role of metabolite receptors in tumor growth and progression.** Overview of metabolite receptor expression and coupling. Shown are simplified metabolic processes to depict ligand origin and binding. The effect of receptor activation on tumor cell growth, progression, proliferation, survival, metabolism and metastasis is the subject of this work.

### 2.2.1 Lactate

The role of lactate in tumor metabolism first came into focus when Otto Warburg discovered its high occurrence in tumor cells (13). Aerobic glycolysis in tumors was named after him and is now known as the Warburg effect. This phenomenon was also confirmed for a variety of tumor cell lines and solid tumors (52, 53). Warburg's initial hypothesis described the aerobic glycolysis as a mechanism to generate ATP in order to compensate impaired mitochondria function (54, 55). However, further research in the area revealed not only mitochondria in tumor cells being fully functional (56-58), but also proved that aerobic glycolysis is present in benign proliferating cells as well (59). Thus, lactate resulting from aerobic glycolysis presumably has other functions to promote tumor cell growth and progression as its necessity for those processes is meanwhile well acknowledged (60-62). Furthermore, a high lactate concentration in solid tumors is inversely correlated with patient survival (63-65). Tumors can benefit from aerobic glycolysis and the resulting lactate in several ways.

Tumor growth requires the immune system to fail in eliminating abnormal cells. Therefore, tumors have different mechanisms to avoid destruction of their cells. They can increase the release of inhibitory molecules, they can release immunosuppressive cytokines and they are also able to downregulate the secretion of immune cell stimulating molecules (66). Moreover, it was shown that extracellular lactate inhibits the differentiation of monocytes and dendritic cells and impedes dendritic cells and cytotoxic T-cells from secreting cytokines (67, 68). Hence, extracellular lactate is able to incapacitate the main actors of the immune system's antitumoral response. The underlying mechanism is the fact that cytotoxic T-cells use glycolysis as their primary source of energy and thus seek to release the nascent lactate into the extracellular matrix. For the transport of lactate via monocarboxylate transporters (MCTs), the additional secretion of H<sup>+</sup> is required. Both, a low pH and the extracellular lactate impair the transport by abrogating the pH and lactate gradients. As a result, T-cells cannot clear themselves of lactate and glycolysis slows down (68-70). Meanwhile, regulatory T-cells (T-reg cells) using FA oxidation as their main energy source are not affected by high extracellular lactate concentrations (71).

Lactate is also capable of promoting tumor metastasis by inducing cell migration and vessel formation. Experiments in a Boyden chamber showed that lactate levels as they are obtained in solid tumors *in vivo* are sufficient to initiate migration of single tumor cells as well as of associations of tumor cells (72). The transforming growth factor (TGF)  $\beta$ 2 pathway was identified as a possible mediator of lactate induced migration effects (73). In contrast an increased lactate concentration can hinder the migration of monocytes and abolish their secretions of cytokines such as tumor necrosis factor  $\alpha$  (TNF- $\alpha$ ) and interleukin 6 (IL-6) (72). Additionally, lactate can stimulate endothelial cells to produce vascular endothelial growth factor (VEGF) and thus promote angiogenesis (74). Besides the effect on tumor cells, immune cells and endothelial cells, lactate can also act on cancer associated fibroblasts (CAFs). An enhanced production of hyaluronan through the CAFs generates an environment that favors motility and growth of tumor cells (63, 75).

Lactate is the main ligand of HCA1. The receptor is weakly expressed in brain, skeletal muscle, gastric ghrelin cells, liver and kidney (34, 76-79), whereas its expression in white and brown adipose tissue is remarkable (34, 41, 42). To date, there is no convincing data showing HCA1 expression in immune cells what leaves a direct action between ligand and receptor on tumor associated immune cells unlikely. On the contrary, adipocytes interfusing the tumor stroma could be activated by extracellular lactate. Whether HCA1 expression can be found on tumor cells and

which impact such an expression possibly has on tumor growth and progression is one of the endeavors of this work (Figure 1).

### 2.2.2 Free fatty acids

In former times the assumption was that tumors generate lipids by the conversion of glucose and acetate (80). Soon it came clear that this process cannot fulfill proliferating cells' need for lipids. Now it is widely acknowledged that cellular FAs are produced by *de novo* FA synthesis with fatty acid synthase (FASN) playing a major role (81). Therefore, FA synthesis and FASN form attractive targets in cancer therapy (82). In a healthy body condition, FA synthesis is mainly limited to adipose tissue, liver and lactating mammary tissue (83). However, cancer cells might experience genetic alterations promoting FA synthesis (84). Enzymes involved in FA biosynthesis as well as NADPH production, which is crucial for the synthesis, are for instance controlled by SREBPs (85-87). The theory is that cell growth stimulates the activity of the mTOR complex followed by the activation of AKT which can induce the build-up of cellular SREBPs (88). Other transcription factors regulated by nutrient availability such as MondoA are known regulators of FA biosynthesis. MondoA can be induced by *c-myc* and then promotes lysis of glutamine and formation of lipids (89). Additionally, cancer cells have the ability to cover their demand in lipids by the uptake of extracellular FAs (90). The uptake of exogenous FAs presents one mechanism of tumors to deal with often-faced hypoxic conditions (23). Under normoxic conditions, not only the blood but also stromal adipose tissue can serve as a source of exogenous lipids (91).

The functions of lipids in tumors are multifaceted and not only compromise their role as intermediates for membrane formation and ATP synthesis. Lipids often act as signaling molecules. Lysophosphatidic acid (LPA) and sphingosine-1-phosphate (S1P) are able to orchestrate cell migration, inflammation and survival in cancer cells (92, 93). The LPA receptor on tumor, immune and endothelial cells promotes migration, proliferation, inflammation and angiogenesis when stimulated with its ligand LPA in an auto- or paracrine manner (93). Second messengers such as diacylglycerol (DAG) and inositol-1,4,5-trisphosphate (IP3) are other examples for lipids as key players in cell signaling (94, 95). Furthermore, lipids have essential functions in tumor progression. Epithelial to mesenchymal transition (EMT) creates an environment favoring cell mobility and migration and is promoted by TGF- $\beta$  induced release of Prostaglandin E<sub>2</sub> (PGE<sub>2</sub>) (96, 97). Another crucial factor of tumor metastasis is angiogenesis (98). PGE<sub>2</sub>, LPA and S1P stimulate vessel formation and the recruitment of macrophages that are required to prime the metastatic niche of future metastasis locations (99, 100). In addition, antitumoral M1 type macrophages can be polarized into protumoral M2 type macrophages by PGE<sub>2</sub> (101). Another example of

immunoediting is the PGE<sub>2</sub> mediated release of the cytokine IL-10, which causes immunosuppression (102). Last, a metabolic competition might occur when regulatory and memory T-cells as well as cancer cells are dependent on the uptake of extracellular FAs in order to perform lipid oxidation to serve their energy need (103).

The FAs activating metabolite receptors are primarily acetate, butyrate and propionate as representatives of SCFAs and  $\alpha$ -linolenic acid (ALA) and linoleic acid as representatives of the LCFAs. Acetate has a variety of sources. It can enter the body through dietary intake or it can be generated through deacetylation of metabolites (104). However, the majority of acetate is produced by gut microbiota breaking down dietary fibers (105). Acetate and other SCFAs are able to pass the intestinal wall and after they pass through the liver, they enter in the circulation and may be employed by tumor cells (106-108). The synthesis of FAs in tumor cells starts with the ligation of acetate to CoA followed by the carboxylation of the resulting acetyl-CoA. Then, FASN condensates one molecule of acetyl-CoA either to another one or to one molecule of malonyl-CoA. In that way acetate can ensure tumor growth by serving as a FA biosynthesis substrate in metabolic stress conditions characterized by low glucose and oxygen conditions (109-111). In the TCA cycle, the oxidation of acetate provides reducing equivalents required for energy production by oxidative phosphorylation (109). The role of acetate as a signaling molecule activating FFA2 in cancer cells is discussed controversially. One study suggests that the FFA2 had an oncogenic effect because its overexpression in NIH 3T3 fibroblasts enhanced tumor growth in immunocompromised mice (112). Another study postulates a tumor-suppressive effect of FFA2. The inhibition of FFA2 signaling in murine colorectal cancer impaired cancer cell proliferation and promoted cancer cell death (113). Recent research confirms the tumor-protective properties of FFA2. A loss of FFA2 in colon cancer led to epigenetic dysregulation of inflammation suppressors (114). Likewise, little is known about the role of FFA4 and its ligand ALA in tumor cells. Existing studies suggest a beneficial effect of the incorporation of ALA by cancer cell lines and tumor bearing mice (115, 116). The mechanism behind remains to be clarified although data offers the mediation of mitochondrial apoptosis and the inhibition of FA biosynthesis as possible ALA functions (117). The expression and functions of fatty acid receptors on tumor and stromal cells will be investigated in this work.

### 2.3 Tumor models

In order to study cancer the use of *in vitro* models is often insufficient to reflect the complexity of physiologic and pathophysiologic processes. Therefore, a variety of *in vivo* tumor models particularly in mice has been developed. Commonly used are xenograft, syngeneic, carcinogen-



inducible and genetically engineered tumor models. In a xenograft model human cancer cells, such as A549 adenocarcinoma cells or NCI-H226 squamous carcinoma cells, are injected into immunocompromised mice, either subcutaneously, orthotopically or systemically. To avoid a rejection of the implanted human cells by the host immune system the use of immunocompromised mice, usually athymic nude or severe-compromised immunodeficient mice, is required (118). The use of allografts supersedes this requirement. In the syngeneic tumor model cancer cells from a mouse are isolated, immortalized, cultured and expanded *in vitro* and injected into a mouse of the same inbred strain. Common injection methods to study primary tumor growth or metastasis are intravenous, intraperitoneal or subcutaneous injection. In 1973, the first syngeneic mouse model for metastasis was described using B16 melanoma cells (119). By now, cell lines for syngeneic tumor models are derived from tumors in a variety of organs. They differ in tumor growth, proliferation, immunogenicity, morbidity, mortality and metastatic capacity. Widely used are lines from murine colon carcinoma (CT26.WT and MC38), breast carcinoma (4T1 and EMT6), lung carcinoma (LLC1 and KLN205) and melanoma (B16). A different model allowing to study tumor development and especially initiation is the carcinogen-inducible model. Here, carcinogenic chemical substances are administered and induce specific mutations that cause spontaneous transformation events. Well-known examples are the application of urethane in order to induce lung tumorigenesis and the application of azoxymethane (AOM) in order to induce colorectal carcinomas (120, 121). Another approach to investigate *de novo* tumor progression is the utilization of genetically engineered or transgenic tumor models. In a similar manner to the carcinogen-inducible model they offer the possibility to elucidate the interplay between the tumor and an immunocompetent tumor microenvironment (122). Commonly used are the Mouse mammary tumor virus Polyoma Virus middle T antigen (MMTV-PyMT) model and the MMTV-Neu model for the initiation of breast cancer (123). Genetically engineered and syngeneic tumor models are also capable to display the formation of metastasis. We incorporated the LLC1 syngeneic tumor model, the AOM-Dextran sulfate (DSS) colorectal cancer model and the MMTV-PyMT breast cancer model into our study. In this way, we exclusively utilize immunocompetent mice while exerting diverse mechanisms of tumor initiation.

### 2.3.1 Syngeneic tumor model

The syngeneic tumor model offers invaluable advantages compared to other tumor models. Simple application and fast tumor growth rates ensure a short experiment duration. Intravenous and intraperitoneal injection are stable models to study metastasis, and subcutaneous injection can as well be used for this application although a dissection of the primary tumor may be required. The main advantage over especially the xenograft model is the prevention of graft versus host



reactions when working with fully immunocompetent mice, because the tumor cells are immunologically compatible with the acceptor animal. In that way, it is possible to study the tumor microenvironment and immune response. Nevertheless, a syngeneic model represents a completely murine model and results might not be fully transferable to human applications. The examination of metastases in a syngeneic model can be compromised by mortality or morbidity caused by the primary tumor especially in a subcutaneous model.

LLC1 cells are derived from a Lewis lung carcinoma of a mouse with C57/BL6 background (124). They are characterized by a fast and homogeneous growth rate but weak immunogenicity (125, 126). Either if the cells are injected intravenously or subcutaneously, they are highly tumorigenic and the tumor incidence reaches 100% (126). In the intravenous model, the metastases are homogeneously distributed over the lung and same is true for the subcutaneous model (126). However, the study of metastases in the subcutaneous model has the fault of morbidity of the primary tumor, which is with increasing tumor volume regularly affected by ulceration (126). In summary, the LLC1 syngeneic tumor model is a valuable model to investigate tumor growth and metastasis as well as the effects of chemotherapeutic agents.

### **2.3.2 AOM-DSS colorectal cancer model**

The AOM-DSS colorectal cancer model is a chemically induced cancer model in which DNA damage is induced followed by multiple cycles of colitis. AOM is a procarcinogenic agent that is metabolized by enzyme CYP2E1 to methylazoxymethanol that is then secreted by the bile and taken up by the epithelial cells of the colon. There, the highly reactive substance induces O<sup>6</sup> methylguanine adducts in the DNA leading to transitions from guanine to adenosine bases, thus inducing mutagenesis (127, 128). DSS is a polysaccharide with structural similarities to heparin and the ability to impair the colon epithelium (128). The treatment of animals with DSS provokes a severe colitis, hence the initiation of inflammation-related colon cancer (121). The developing carcinomas are mostly adenocarcinomas located in the distal colon (129). It is recommended to perform the AOM-DSS model with littermates housed under the same conditions to ensure a similar microbiome and little genetic variation (121, 130).

Several vital advantages distinguish the AOM-DSS model as a very popular one to study colorectal cancer. It is relatively affordable and takes only little time in preparation as time-consuming genetically modifications can be omitted. Furthermore, it is a powerful and reproducible tool with a tumor incidence of up to 100% (121, 131). The histology of the tumors and aberrant crypts depicts the human colorectal cancer development to a high degree and similarities in

mutations such as  $\beta$ -catenin and KRAS mutations can be observed (129). But the main advantage is the endogenous origin of the tumor cells themselves making them accessible for genetic alterations and providing insights in close to praxis tumor initiation. Moreover, the use of fully immunocompetent mice provides a good basis to study immune response and tumor stroma.

However, the AOM-DSS model is not free of faults. Reported hepatotoxicity of AOM dependent on mouse strain and facility environment requires trial experiments for the finding of the correct dose (121, 132). The overall tumor development can vary between different mouse strains (129). Additionally, the experimental procedure is time-consuming with an approximate duration of 12 weeks and frequent monitoring of the mice particularly after DSS treatment is inevitable (121). A recent study questions the use of the model to elucidate colorectal cancer in humans. A cross-species comparison demonstrated divergent variable sites, mutated genes and altered pathways between humans and mice (133). Nevertheless, the AOM-DSS colorectal cancer model remains a reliable and powerful tool that can display many features of human colorectal cancer and is therefore used to investigate tumor initiation, diagnosis and prognosis (134-136).

### **2.3.3 MMTV-PyMT breast cancer model**

The MMTV-PyMT breast cancer model is a murine genetically engineered tumor model to mimic human ductal breast carcinomas. MMTV-PyMT transgenic animals express the Polyoma Virus middle T antigen under the control of the mouse mammary tumor virus promoter (137). This mammary gland specific expression allows to study every aspect from *de novo* tumor development to metastasis. The model displays initial lesions, EMT, the development of mammary adenocarcinomas and in the last stage the formation of pulmonary metastases (137). Commonly used are female virgin mice developing the first palpable tumors with a latency of 8 weeks (138).

The model bears various benefits. The incidence for tumors and metastases is immense (139). Moreover, the MMTV-PyMT model is a suitable tool to study human breast cancer. Its stage for development that are hyperplasia, adenoma, early and late carcinoma resemble human breast cancer development (140). Several other features like ErbB2 overexpression add to a good cross-species comparability (141). A main advantage of the model is the endogenous origin of the tumor cells, which allows genetic alterations in order to provide insights in the earliest stages of tumor initiation, EMT and fibroblast recruitment (142-145). Furthermore, the use of fully immunocompetent mice offers a chance to study immune response and tumor cell and stroma interactions (146-148).

One of the few drawbacks of the model is the duration of the animal experiments conditioned on latency and tumor growth rate. Another one can be the morbidity caused by a high primary tumor burden which encumbers the investigation of metastases (149, 150). A removal of primary tumors is however impeded because of the multiplicity of tumor sites. Additionally, there is data indicating a lower metastasis incidence as compared to human breast cancer (122). Nevertheless, the MMTV-PyMT tumor model offers a shorter latency and better metastasis incidence than other breast cancer models available making it a highly valuable, stable and reproducible tool to study to obtain insights into breast cancer development and progression.

### 3 AIM OF THIS STUDY

Metabolites such as lactic acid, acetate or free fatty acids are found at high concentrations in tumors. Although data indicate metabolites having functions in tumor metabolism, immune system modulation and metastasis formation, the role of metabolites as signaling molecules is poorly understood. I hypothesize that metabolites are able to use the respective metabolite receptors to modulate tumor growth and progression in an autocrine or paracrine manner. My aim was to analyze the expression of metabolites in tumor cells as well as in tumor stroma cells and to test whether loss of any of the receptors affects the tumor growth, progression and metastasis. Moreover, another aim was the generation of mice with a conditional knockout of the *Ffar4* gene in order to elucidate the function of the receptor and its downstream signaling pathways in tumor and immune cells.



Na <sub>2</sub> HPO <sub>4</sub> (10 mM)	-	1.44 g
KH <sub>2</sub> PO <sub>4</sub> (2 mM)	-	0.24 g
KCl (2.7 mM)	-	0.20 g

Distilled water was added to the final volume of 1000 ml. pH was adjusted to 7.4 using HCl.

#### Phosphate- buffered saline with Tween-20 (PBST)

Tween-20	-	1 ml
PBS	-	1000 ml

#### TAE Buffer (1x)

Tris-acetate	-	40 mM
EDTA	-	1 mM

Distilled water was added to the final volume

#### Polymerase chain reaction (PCR)

PCR buffer 10X: 200mM Tris, 500mM KCl. pH was adjusted to 8.4.

dNTPs: dATP+dGTP+dCTP+dTTP (25 µmol)

MgCl<sub>2</sub>: 50 mM

#### DNA loading dye

Glycerol	-	30%
Bromophenol blue	-	0.25%

Dissolved in distilled water

#### X-Gal staining solution A

NaH <sub>2</sub> PO <sub>4</sub> x H <sub>2</sub> O	-	27.6 g
H <sub>2</sub> O	-	up to 1000 ml

#### X-Gal staining solution B

Na <sub>2</sub> HPO <sub>4</sub> x 7 H <sub>2</sub> O	-	53.65 g
H <sub>2</sub> O	-	up to 1000 ml

#### X-Gal staining PBS 0.1 M

Solution A	-	115 ml
Solution B	-	385 ml
H <sub>2</sub> O	-	500 ml

pH adjusted to 7.3

X-Gal staining intermediate solution

EGTA	-	1.91 g
MgCl <sub>2</sub>	-	0.41 g
PBS 0.1 M	-	1000 ml

X-Gal staining fixative solution

Glutaraldehyde 25%	-	1.6 ml
Intermediate solution	-	200 ml

X-Gal staining washing solution

Sodium deoxycholate	-	0.08 g
NP-40	-	160 µl
Intermediate solution	-	800 ml

X-Gal staining solution

K <sub>3</sub> [Fe(III)(CN) <sub>6</sub> ]	-	0.659 g
K <sub>4</sub> [Fe(II)(CN) <sub>6</sub> ]	-	0.844 g
X-Gal	-	0.1 g in 2 ml DMF
Washing solution	-	200 ml

Fat buffer

NaCl	-	125 mM
KCl	-	5 mM
CaCl <sub>2</sub>	-	1 mM
Tris (pH 8)	-	25 mM
MgCl <sub>2</sub>	-	2.5 mM
KH <sub>2</sub> PO <sub>4</sub>	-	1 mM
H <sub>2</sub> O	-	up to 1000 ml
Adjust pH to 7.4.		
Glucose	-	4 mM
BSA (Fraction V)	-	2%

**4.3 Enzymes**

Restriction enzymes and Phusion® HF DNA Polymerase were purchased from New England BioLabs (NEB). Proteinase K was purchased from Roth (Cat. No. 7528.2).

#### 4.4 Primers

##### RT-PCR primers (human)

Gene name	Sequence	Probe
GAPDH	GGGAAACTGTGGCGTGAT AGCTCAGGGATGACCTTGC	34
Ffar1	CAGCTTCCTGTACCCCAATC CGGATTAAGCACCACACTCC	45
Ffar2	CGGCCTCTGTATGGAGTGAT TGATCACGATGGTGCAGTG	49
Ffar3	CACCCACTGTGGTACAAGACC GGCCACACTCACCAGACC	43
Ffar4	GCGTCTTCTTCCGAGTCGT CAAAAGAGACATCCCACGAGA	80
Hcar1	GGTGCTGAGGGATCTGTTTC GCAATTGTATTGGACTCAGCAC	37
Hcar2	TGTGGGGCATCACTATTGG TTCTGGATCGGCATCTTCTT	10
Hcar3	TTCTGTGGGGCATCACTGT GCCATTCTGGATCAGCAACT	10

##### RT-Primers (mouse)

Gene name	Sequence	Probe
GAPDH	AGCTTGTCATCAACGGGAAG TTTGATGTTAGTGGGGTCTCG	9
Ffar4	CCCAACCGCATAGGAGAAAT TATGCCAAGCTCAGCGTAAG	IDT individual



#### 4.5 Plasmids

Gene name	Company: catalogue number
PX459v2	Addgene: 62988

#### 4.6 Antibodies

Name	Company: catalogue number	Dilution	Application
RFP antibody [5f8]	Chromotek: 5f8-100	1:500	IF
RFP antibody Pre-adsorbed	Rockland: 600-401-379	1:1000	IF
Mouse CD45 FITC conjugate	Invitrogen: MCD4501	1:100	IF
Rat anti mouse CD68:Biotin	Bio-Rad: MCA1957BT	1:100	IF
Alexa Fluor® 488 anti-mouse F4/80	Biologend: 123119	1:100	IF
Biotin anti-BrdU mouse	Biologend: 339810	1:50	IHC
Streptavidin, Alexa Fluor™ 488 conjugate	Invitrogen: S11223	1:300	IF
Alexa Fluor™ 594 donkey anti-rabbit IgG	Invitrogen: A21207	1:100	IF
AlexaFluor™ 594 donkey anti rat	Invitrogen: A21209	1:100	IF

#### 4.7 Cell lines

Name	Origin	Source
B16F10	Mouse melanoma	American Type Culture Collection (ATCC)
MC-38	Mouse colon adenocarcinoma	Kerafast
CT26.WT	Mouse colon carcinoma	Sigma-Aldrich

LLC1	Mouse Lewis lung carcinoma	American Type Culture Collection (ATCC)
T47D	Human breast carcinoma	Deutsche Sammlung von Mikroorganismen und Zellkulturen GmbH (DSMZ)
BT-474	Human breast carcinoma	Sigma-Aldrich
MDA-MB-361	Human breast carcinoma	Sigma-Aldrich
SW403	Human colorectal carcinoma	Deutsche Sammlung von Mikroorganismen und Zellkulturen GmbH (DSMZ)
T84	Human colorectal carcinoma	Sigma-Aldrich

#### **4.8 Bacterial strains**

XL1-Blue competent cells (Cat.nr: 200249) were obtained from Agilent technologies.

#### **4.9 Medium**

##### Bacterial growth medium

Luria-Bertani (LB) medium

Bacto-Tryptone	-	10 g
Bacto-Yeast extracts	-	5 g
NaCl	-	5 g

Dissolved in 950 ml distilled water. pH was adjusted to 7.0 using 5 N NaOH. The volume to 1000 ml was adjusted with distilled water and autoclaved.

##### Bacterial LB-Agar medium

Bacto-Tryptone	-	10 g
Bacto-Yeast extracts	-	5 g
NaCl	-	5 g
Bacto Agar	-	7 g

Dissolved in 1000 ml distilled water and sterilized by autoclaving.

##### Antibiotics 1000x

Different antibiotics were dissolved as mentioned below:

Ampicillin, 50 mg/ml in distilled water.

Kanamycin monosulfate, 10 mg/ml in distilled water.

Antibiotics were sterilized using 0.22 µm filters and stored at -20 °C.

Complete DMEM growth medium

DMEM (Gibco:10938-025)	-	500.0 ml
Fetal bovine serum (Gibco: 10270106)	-	55.0 ml (10%)
L-Glutamine (100X) (Gibco: 25030-081)	-	5.5 ml
Penicillin-streptomycin (100X) (Gibco: 15140-122)	-	5.5 ml

Complete RPMI growth media

RPMI (Gibco: 21875091)	-	500.0 ml
Fetal bovine serum (Gibco: 10270106)	-	55.0 ml (10%)
Penicillin-streptomycin (100X) (Gibco: 15140-122)	-	5.5 ml (1%)
L-Glutamine (100X) (Gibco: 25030-081)	-	5.5 ml (1%)

Complete F12:DMEM growth media

F12:DMEM 1:1 (Gibco: 11320-033)	-	500.0 ml
Fetal bovine serum (Gibco: 10270106)	-	55.0 ml (10%)
Penicillin-streptomycin (100X) (Gibco: 15140-122)	-	5.5 ml (1%)
L-Glutamine (100X) (Gibco: 25030-081)	-	5.5 ml (1%)

Complete Leibovitz's L15 growth media

Leibovitz's L15 (Gibco: 11415-049)	-	500.0 ml
Fetal bovine serum (Gibco: 10270106)	-	55.0 ml (10%)
Penicillin-streptomycin	-	5.5 ml (1%)

(100X) (Gibco: 15140-122)

L-Glutamine (100X) - 5.5 ml (1%)  
(Gibco: 25030-081)

ES cell medium

DMEM - 500.0 ml  
(Gibco:10938-025)

Fetal bovine serum - 55.0 ml (10%)  
(Gibco: 10270106)

L-Glutamine (100X) - 5.5 ml  
(Gibco: 25030-081)

Penicillin-streptomycin - 5.5 ml  
(100X) (Gibco: 15140-122)

MEM NEAA - 5.5 ml  
(100x) (Invitrogen: 11140)

LIF - 1 ml  
(10<sup>7</sup> units) (Millipore: ESG1107)

GSKβ-inhibitor CHIR99021 - 0.5 ml  
(Stemgent: 04-0004)

β-Mercaptoethanol - 0.6 ml  
(Life Technologies: 31350010)

Feeder cell medium

DMEM - 500.0 ml  
(Gibco:10938-025)

Fetal bovine serum - 55.0 ml (10%)  
(Gibco: 10270106)

L-Glutamine (100X) - 5.5 ml  
(Gibco: 25030-081)

Penicillin-streptomycin - 5.5 ml  
(100X) (Gibco: 15140-122)

MEM NEAA - 5.5 ml  
(100x) (Invitrogen: 11140)

PBS (CaCl<sub>2</sub><sup>-</sup>, MgCl<sub>2</sub><sup>-</sup>) (Gibco: 14190-094)

Trypsin, 0.25% (1X) with EDTA x 4 Na, Liquid (Gibco: 25200056)

#### **4.10 Kits**

NucleoSpin® Plasmid kit (Machery-Nagel: 740588.250)

NucleoBond® Xtra Maxi kit (Machery-Nagel: 740414.100)

NucleoSpin® Gel and PCR Clean-up kit (Macherey-Nagel: 740609-250)

Quick-RNA™ Prep Kit Micro (Zymo: R1051), Mini (Zymo: R1055)

Rneasy Lipid Tissue Mini Kit (Qiagen: 74804)

DNeasy® Blood & Tissue Kit (Qiagen: 69506)

ProtoScript® II First Strand cDNA Synthesis Kit (NEB: E6560L)

CloneJET PCR Cloning Kit (Thermo Scientific: K1232)

MEGAscript™ Transcription Kit (Invitrogen: AM1354)

MEGAclear™ Transcription Clean-Up Kit (Invitrogen: AM1908)

TaqMan Probe Master

Lightcycler 480 Probe Master (Roche)

Universal probe library set (Roche)

Vectastain® Elite® ABC Kit, Peroxidase (Standard) (Vector Laboratories: PK-6100)

DAB Peroxidase Substrate Kit (Vector Laboratories: SK-4100)

Glycerol assay kit (Randox: GY 105)

Non Esterified Fatty Acid assay kit (Randox: FA 115)

#### **4.11 Genetic mouse models**

Control C57BL/6J animals were purchased from Charles River. HCA1<sup>mRFP</sup> animals were generated in-house and kindly provided by Kashan Ahmed (34). HCA2<sup>mRFP</sup> were generated in-house and kindly provided by Julien Hanson (151). HCA1<sup>-/-</sup> animals were provided by the Texas

Institute of Genomic Medicine (Houston, TX). HCA2<sup>-/-</sup> animals were generated and kindly provided by Sorin Tunaru (35). FFA2<sup>mRFP</sup>, FFA2<sup>-/-</sup> and FFA3<sup>mRFP</sup> animals were generated in-house and kindly provided by Cong Tang (40). FFA4<sup>-/-</sup> (Ffar4<sup>tm1(KOMP)VICg</sup>) sperm was purchased from the UC Davis KOMP Repository Knockout Mouse Project. Mice were created with *in-vitro*-fertilization by our transgenic service team. FFA4<sup>flox/flox</sup> animals were created with the CRISPR/Cas9 system. MMTV-PyMT mice (FVB/N-Tg(MMTV-PyVT)634Mul/J) were purchased from Jackson Laboratories (137). Animals were backcrossed to a C57BL/6 background and crossed with HCA1<sup>mRFP</sup>, HCA2<sup>mRFP</sup>, FFA2<sup>mRFP</sup>, HCA1<sup>-/-</sup>, HCA2<sup>-/-</sup> or FFA2<sup>-/-</sup> animals to obtain MMTV-PyMT<sup>+</sup>;HCA1<sup>mRFP</sup>, MMTV-PyMT<sup>+</sup>;HCA2<sup>mRFP</sup>, MMTV-PyMT<sup>+</sup>;FFA2<sup>mRFP</sup>, MMTV-PyMT<sup>+</sup>;HCA1<sup>-/-</sup>, MMTV-PyMT<sup>+</sup>;HCA2<sup>-/-</sup> or MMTV-PyMT<sup>+</sup>;FFA2<sup>-/-</sup> animals. Mice were maintained under specific pathogen free conditions. Protocols were performed according to institutional and national guidelines.

## 5 METHODS

### 5.1 CRISPR/Cas

The CRISPR.MIT.EDU online tool was used to identify guide and protospacer adjacent motif (PAM) sequences. Guides with least off-targets were chosen. BLAT search with the USCS and BLAST search with NIH online tools have been performed to assure the absence of off-targets. Reverse complements of guide sequences have been designed. The bases CACCG- have been added to the 5' end of each forward sequence and AAAC- have been added to each reverse sequence as an extension for cloning. Sequences without the PAM sequence were provided by Sigma-Aldrich.

#### Cloning guide oligos in the sgRNA-Cas-Puro expression vector (PX459v2, Addgene)

Linearization:

NEB buffer 2.1	3 $\mu$ l
PX459v2	3 $\mu$ g
BbsI	2 $\mu$ l
H <sub>2</sub> O	up to 30 $\mu$ l

Digestion was incubated for 3 h at 37°C and then loaded to a 0.8% agarose gel. Gel extraction was performed using the NucleoSpin® kit (Machery-Nagel).

Oligo Annealing:

NEB buffer 2.1	2 $\mu$ l
Guide oligo top 100 $\mu$ M	3 $\mu$ g
Guide oligo bottom 100 $\mu$ M	2 $\mu$ l
H <sub>2</sub> O	14 $\mu$ l

Annealing mixes for each oligo pairs were incubated at 95°C for 5 min and the cooled down to room temperature for 1 h.

Ligation:

Buffer T4DNA Ligase 10x	1 $\mu$ l
T4DNA Ligase	1 $\mu$ g
Linearized PX459v2	50 ng

Annealed Oligos	5 $\mu$ l
H <sub>2</sub> O	up to 10 $\mu$ l

Ligation mixture was incubated for 20 min at room temperature.

#### Transformation:

The heat shock method was used. 5  $\mu$ l of ligation were added to chemo competent XL-1 blue cells and incubated for 10 min on ice. The tubes were then incubated at 42°C for 45 sec and immediately put on ice for 2 min. 500  $\mu$ l of LB growth medium without antibiotic were added and the mixture was incubated at 37°C for 1 h shaking at 900 rpm. Next, 200  $\mu$ l of the mixture were plated on LB agar plates containing 100  $\mu$ g/ml Ampicillin and incubated overnight at 37°C. The next day colonies were picked and cultures with 5 ml LB growth medium containing 100  $\mu$ g/ml Ampicillin were incubated on a shaker overnight at 37°C. Then, miniprep was performed using the NucleoSpin® Plasmid kit (Machery-Nagel).

#### Digestion:

Cutsmart® buffer	5 $\mu$ l
EcoRI-HF®	2 $\mu$ l
Plasmid containing guide	1 $\mu$ g
H <sub>2</sub> O	up to 30 $\mu$ l

The mixture was incubated at 37°C for 3 h and then loaded on a 0.8% agarose gel. A fragment of 669 bp should be obtained to prove the presence of the Puromycin resistance gene of the plasmid.

Sequencing of the clones was carried out at Microsynth Seqlab using the U6-Fwd primer 5'-GAGGGCCTATTTCCCATGATTCC-3'. For positive clones, the plasmid containing the guide was used to perform a maxiprep using the NucleoBond® Xtra Maxi kit (Machery-Nagel).

#### Guide testing in embryonal stem (ES) cells:

##### Transfection:

The day before transfection, 6-well plates with inactivated feeder cells were prepared. On the day of transfection, medium was changed on v6.5 ES cells 2h before trypsination. For transfection, cells were washed with PBS, trypsinated and separated. Medium was added and cells were centrifuged and counted. In each well of the 6-well plate with feeder cells 300 000 ES cells were plated in 2 ml medium. DNA premix and Lipofectamine premix were prepared.



**DNA premix per well**

PX459v2 with guide (1 µg/µl)	1 µl
Optimem	147 µl

**Lipofectamine premix per well**

Lipofectamine 2000	15 µl
Optimem	142.5 µl

Each premix was mixed well and then added to 150 µl of Lipofectamine premix were added to each tube with DNA premix, mixed well and incubated for 5 min at room temperature. 300 µl of DNA-Lipofectamine mix were added to each well. Cells were incubated for 24 h.

**Puromycin selection:**

Medium was changed to medium containing 1.5 µg/ml Puromycin. Cells were incubated for 24 h and then medium was changed to medium containing 1.5 µg/ml Puromycin. Cells were incubated for 24 h. Medium was changed to normal ES cell medium. Cells were incubated for 3-4 days.

**ES cell gDNA extraction:**

gDNA extraction was carried out using the DNeasy® Blood & Tissue Kit (Qiagen). Concentration of samples was measured with the Nanodrop ND-100 Spectrophotometer. Samples were diluted to 20 ng/µL.

**CRISPR PCR screening:**

10x buffer	5 µl
dNTPs	0.4 µl
Forward primer 10 µM	2 µl
Reverse primer 10 µM	2 µl
MgCl <sub>2</sub>	1.5 µl
Taq	0.3 µl
H <sub>2</sub> O	33.8 µl
Template DNA	5 µl

1	98°C	30 sec	
2	98°C	20 sec	
3	58°C	20 sec	35 cycles
4	72°C	30 sec	
5	72°C	60 sec	
6	4°C	∞	

The PCR product was loaded on a 2% agarose gel and the 50 bp ladder was used. A smeary band should be visible to ensure high efficiency of insertions and deletions.

#### *In vivo* CRISPR/Cas9 gene editing

Single stranded repair template (ssODN) design:

For designing the ssODN a sequence of the guide including the PAM sequence was complemented with homology arm of 60 nucleotides on each end. A loxP sequence was added at the Cas9 cutting site three nucleotides from the PAM sequence. Orientation of guide and loxP sequences were considered. HPCL-purified ssODNs were obtained from Sigma-Aldrich.

ssDNA sequencing:

5x GC buffer (NEB)	10 µl
dNTPs 10mM	1 µl
primer 1 10 µM	1 µl
primer 2 10 µM	1 µl
Phusion® HF Taq (NEB)	0.5 µl
DMSO	1.5 µl
H <sub>2</sub> O	33 µl
Plasmid with guide 5 ng/µl	2 µl

To obtain the ssDNA sequence the PX459v2 plasmid containing the guide sequence was used as the PCR template. Primer 1 was designed by connecting the T7 promoter 5'-TTAATACGACTCACTATAGG-3' to the guide sequence. Primer 2 was identical to the last nucleotides of the forward tracrRNA sequence in the plasmid 5'-AAAAGCACCGACTCGGTGCC-3'. The PCR product was loaded on a 0.8% agarose gel, the band of 154 bp size was cut out and the ssDNA was purified using the NucleoSpin® Gel and PCR Clean-up kit (Macherey-Nagel). The

resulting ssDNA composed of the tracrRNA, the reverse complement of the guide sequence and the reverse complement of the T7 promoter was used for following steps.

Annealing:

T7 promoter 100 $\mu$ M	1 $\mu$ l
ssDNA 100 $\mu$ M	1 $\mu$ l
T4 Ligase buffer	1 $\mu$ l
H <sub>2</sub> O	7 $\mu$ l

Mixture was incubated at 95°C and then cooled down by 0.5°C per sec to 4°C.

*In vitro* transcription:

5  $\mu$ l of the annealed template were used to perform *in vitro* transcription following the MEGAscript™ protocol (Invitrogen). The transcription mixture was incubated overnight at 37°C and treated with TURBO DNase. Subsequently the MEGAclean™ kit (Invitrogen) was used to purify the resulting gRNA. 50 $\mu$ l of H<sub>2</sub>O were used for elution. Quality of the gRNA was controlled by loading 2.5 $\mu$ l of the sample on a 2% agarose gel.

Injection:

	Stock concentration	Final concentration	Volume
gRNA1	250 ng/ $\mu$ l	20 ng/ $\mu$ l	2.4 $\mu$ l
gRNA2	250 ng/ $\mu$ l	20 ng/ $\mu$ l	2.4 $\mu$ l
Cas9 mRNA	1 $\mu$ g/ $\mu$ l	50 ng/ $\mu$ l	1.5 $\mu$ l
ssODN1	10 $\mu$ M	100 ng/ $\mu$ l	6.4 $\mu$ l
ssODN2	10 $\mu$ M	100 ng/ $\mu$ l	6.4 $\mu$ l
H <sub>2</sub> O			10.9 $\mu$ l

The injection mixture was freshly prepared at every day of injection. Injection was performed by the in-house transgenic service unit on C57BL/6 blastocysts which were transferred to pseudo-pregnant female animals in order to generate chimeric offspring.

Analysis of offspring:

CRISPR PCR screening strategy was used to identify founder animals with successful hetero- or homozygous insertion of loxP sites. In addition, a PCR strategy spanning both loxP sites was

used. PCR products were loaded onto a 4% agarose gel, cut out and treated with the NucleoSpin® Gel and PCR Clean-up kit (Macherey-Nagel). Then, sequences were cloned into XL-1 blue chemocompetent cells using the CloneJET PCR Cloning Kit (ThermoScientific) and the heat shock method. The bacteria were plated on LB agar plates containing 100 µg/ml Ampicillin and incubated overnight at 37°C. The next day, colonies were picked and cultures with 5 ml LB growth medium containing 100 µg/ml Ampicillin were incubated on a shaker overnight at 37°C. Colony PCR according to the protocol was performed to control the successful transformation. Then, miniprep was performed using the NucleoSpin® Plasmid kit (Macherey-Nagel). Sequencing of the plasmid DNA was carried out at Microsynth Seqlab using the respective PCR primers. Founders with correct insertion of the lox P sites were bred to C57BL/6 mice to verify germ line transmission. All animal procedures were approved by the Hessian Regional Board Regierungspräsidium Darmstadt.

## 5.2 Cell culture

B16 F10 and LLC1 cells were cultured in complete DMEM growth medium at 5% CO<sub>2</sub>. BT-474 and T47D cells were cultured in RPMI complete growth medium at 5% CO<sub>2</sub>. T84 cells were cultured in F12:DMEM complete growth medium at 5% CO<sub>2</sub>. SW403 and MDA-MB-361 cells were cultured in Leibovitz's L15 complete growth medium at 0.1% CO<sub>2</sub>. Cells were tested negative for mycoplasma contamination before experiments. All cells were incubated at 37°. Confluent cells were washed with PBS once and treated with 0.25% Trypsin-EDTA solution for 1 to 3 min until the cells were dissociated. Then, complete growth medium was added and resuspended cells were centrifuged for 3 min at 900 rpm and seeded onto the new cell culture dish.

## 5.3 Expression analysis

For expression analysis of the Origene Cancer Survey array cDNA from the original plates was dissolved and distributed to LightCycler plates to a concentration of 0.75 ng per reaction. For expression analysis in human cell lines, cells from 10 cm plates were harvested and RNA isolation was carried out according to the manufacturer's protocol (Zymo MicroPrep). The Nanodrop ND-100 Spectrophotometer was used for quality control of the samples. RNA was reverse transcribed using the ProtoScript® II kit (NEB) following the manufacturer's protocol. Quantitative RT-PCR was performed using the Roche Light cycler480 Probes Master System. Primers were designed with the Universal Probes Library online tool provided by Roche. To normalize the relative expression to GAPDH the following formula was used:

$$\Delta CP = 2^{CP_{(GAPDH)} - CP_{(gene\ of\ interest)}}$$

For expression analysis in murine adipose tissue, AdipoqCre<sup>+</sup>;FFA4<sup>flox/flox</sup> and AdipoqCre<sup>-</sup>;FFA4<sup>flox/flox</sup> animals were sacrificed using CO<sub>2</sub>. Epididymal white adipose tissue was collected and immediately frozen on dry ice, then tissue was lysed following the Qiagen RNeasy Lipid protocol. RNA isolation, quality control and transcription were carried out as mentioned above. Intron-spanning primers and an individual probe for murine *Ffar4* were designed using the Integrated DNA Technologies (IDT) online tool. For both the Roche LightCycler480 Probes Master System and the IDT system concentrations of 30 ng per reaction were used. Relative expression was normalized to GAPDH.

#### 5.4 Adipocyte isolation

To obtain gDNA from adipocytes and for the lipolysis assay, adipocyte isolation was necessary. First, the fat buffer was prepared and stored at 37°C in a water bath. Then, animals were sacrificed using CO<sub>2</sub> and the epididymal fat pads were dissected and stored in PBS. The fat tissue was sheared with a scalpel and mixed with 5 ml fat buffer and Collagenase II 0.25mg/ml. The mixture was shaken at 37°C in a water bath for 45 min. The lysed tissue was filtered and washed with fat buffer. Next, the adipocytes floating on the surface of the mixture were collected. For gDNA extraction the adipocytes were treated according to the Direct PCR (tail) solution (Viagen). For the lipolysis assay, the adipocytes were stimulated with the respective reagents and the assay was carried out following the protocols of the Glycerol assay kit (Randox) or the Non Esterified Fatty Acid assay kit (Randox).

#### 5.5 BrdU and H&E staining

Tissues or organs were fixed in 4% PFA overnight at 4°C and dehydrated in 30% sucrose for one day. Samples were prepared with the following treatments:

1	70% Ethanol for 2 hours
2	80% Ethanol for 2 hours
3	95% Ethanol for 2 hours
4	100% Ethanol for 2 hours
5	Xylol for 2 hours
6	Paraffin I for 2 hours
7	Paraffin II overnight

Samples were then embedded in paraffin and dried overnight at room temperature before sectioning. To count tumors or metastasis 5 μM sections every 200μM were taken through the

whole tissue. Sections were dried overnight. For deparaffinization, section were incubated at 60°C for 20 min.

Rehydration treatments are as follows:

1	Xylol	5 min
2	Xylol	5 min
3	100% Ethanol	5 min
4	95% Ethanol	5 min
5	80% Ethanol	5 min
6	70% Ethanol	5 min
7	Distilled water	5 min

BrdU staining day 1:

1	Wash with PBS	2 x 5 min
2	Incubation with 0.3% H <sub>2</sub> O <sub>2</sub> in Methanol	20 min
3	Wash with PBS	2 x 5 min
4	Incubation with 4M HCl	30 min at 37°C
5	Wash with PBST	3 x 5 min
6	Incubation in PBST	25 min
7	Incubation with anti BrdU Biotin antibody	Overnight at 4°C

BrdU staining day 2:

1	Preparation of Vectastain Reagent by diluting Reagent A and B together in PBS 1:50 each, incubation at RT	30 min
2	Wash sections with PBST	3 x 5 min
3	Incubation with Vectastain Reagent	30 min
4	Wash with PBS	2 x 5 min

5	Preparation of DAB solution	5 ml distilled water + 2 drops buffer + 4 drops DAB stock solution + 2 drops H <sub>2</sub> O <sub>2</sub>
6	Incubation with DAB solution	15 min and visual control
7	Stop reaction in tap water	5 min
8	Wash in PBS	5 sec
9	Wash in distilled water	5 sec

H&E staining:

1	Hematoxilin	4 min
2	Wash with tap water	10 min
3	Eosin	5 sec
4	70% Ethanol	2 min
5	80% Ethanol	2 min
6	95% Ethanol	2 min
7	100% Ethanol	2 min
8	Xylol	5 min
9	Xylol	5 min
10	Dried and mounted with Pertex.	

### 5.6 X-Gal staining

Tissues or organs were fixed in 0.2 % PFA overnight at 4°C and put in 30% sucrose for one day. Samples were embedded in O.C.T. Tissue Tec solution (Sakura Finetechnical) and frozen on dry ice. 20 µm cryo-sections were prepared and frozen.

X-Gal staining protocol as follows:

1	Fixing solution	5 min
2	Washing solution shaking on ice	3 x 5 min
3	Staining solution	37°C, overnight

4	Wash in PBS	5 sec
5	Wash in distilled water	5 sec

H&E staining was performed afterwards.

### 5.7 Immunofluorescence

Tissues or organs were fixed in 4% PFA overnight at 4°C and put in 30% sucrose for one day. Samples were embedded in O.C.T. Tissue Tec solution (Sakura Finetechnical) and frozen on dry ice. 20 µm cryo-sections were fixed in ice cold acetone for 10 min, washed three times in PBS, incubated for 1 h with 5% horse serum, 0.1% NaN<sub>3</sub> and 0.1% Triton-X in PBS for blocking and permeabilization, and sections were then incubated overnight with primary antibodies. Sections were washed four times in PBS for 15 min and then incubated for 2 h at room temperature with secondary antibodies and Hoechst 33342. After washing four times in PBS for 15 min, slices were mounted and analyzed using the Leica TCS SP5.

For IF staining of samples from FFA4<sup>lacZ</sup> reporter animal tissues or organs were fixed in 0.2 % PFA overnight at 4°C and put in 30% sucrose for one day. Samples were embedded in O.C.T. Tissue Tec solution (Sakura Finetechnical) and frozen on dry ice. 20 µm cryo-sections were fixed in ice cold acetone for 10 min, washed three times in PBS. Then, samples were incubated with SPiDER βGal for 3 h at 37°C and washed with PBS three times for 5 min. Subsequently blocking and staining was performed as described above.

### 5.8 Syngeneic tumor model

50 µl containing 3x10<sup>5</sup> B16F10 melanoma, MC-38 colon adenocarcinoma, CT26 colon carcinoma or LLC1 lung carcinoma cells were injected s.c. into the right flank of the mouse. Animals were sacrificed using CO<sub>2</sub> either after 21 days or at a tumor volume of 1.7 cm<sup>3</sup>. Next, animals were perfused with PBS followed by PFA. Tumors and lungs of reporter animals were collected and analyzed according to the Immunofluorescence protocol. Histological analysis for metabolite receptor expression in the tumor stroma and possible lung metastases was performed. Tissues of receptor deficient animals and their littermate controls were treated according to the BrdU and H&E staining protocol. Tumor volume and weight were analyzed as well as tumor growth and number of lung metastases. Tumor volume was calculated by the use of the formula

$$V = 0.5 \times d^2 \times D,$$



where d is the minor and D is the major tumor axis. Only male animals were used, and mice were 10-20 weeks of age. A minimum of 5 animals per group was used.

### 5.9 Colorectal cancer model

Animals were injected with 10 mg/kg bodyweight AOM 1 mg/ml in 0.9% physiologic salt solution at day zero. From day 5-10, 26-31 and 47-52 animals received drinking water with 1.8% DSS, in between the cycles normal drinking water was provided. Animals were sacrificed at day 84 using CO<sub>2</sub>. Colons were dissected and flushed with PBS, cut open longitudinal and pictures were taken. Next, colons were rolled up in a swiss roll and colons of reporter animals were treated following the Immunofluorescence protocol in order to analyze expression of metabolite receptors histologically. Colons of receptor deficient animals and their littermate controls were treated according to the BrdU and H&E staining protocol. Only male animals were used, and mice were 8-15 weeks of age. A minimum of 5 animals per group was used.

### 5.10 Breast cancer model

Female mice carrying the MMTV-PyMT transgene were frequently scored from an age of 6 weeks on. Upon reaching a maximal total tumor volume of 1.7 cm<sup>3</sup> animals were sacrificed using CO<sub>2</sub>. Then, animals were perfused with PBS followed by PFA. For reporter animals, tumors and lungs were collected and treated according to the Immunofluorescence protocol. Tumors and lungs of receptor deficient animals and their littermate controls were treated following to the BrdU and H&E staining protocol. Scoring included record of the timepoint of the onset of the first palpable tumor, of the timepoint the maximal tumor volume was reached as well as the volume of the tumors at all scoring timepoints. Lungs were analyzed for the number of metastases. Tumor volume was calculated by the use of the formula

$$V = 0.5 \times d^2 \times D,$$

where d is the minor and D is the major tumor axis. Single tumor volumes were added up to a total tumor volume. Only female mice were used, and a minimum of 4 animals per group was included. The Hessian Regional Board Regierungspräsidium Darmstadt approved all experimental animal procedures.

### 5.11 Statistical analysis

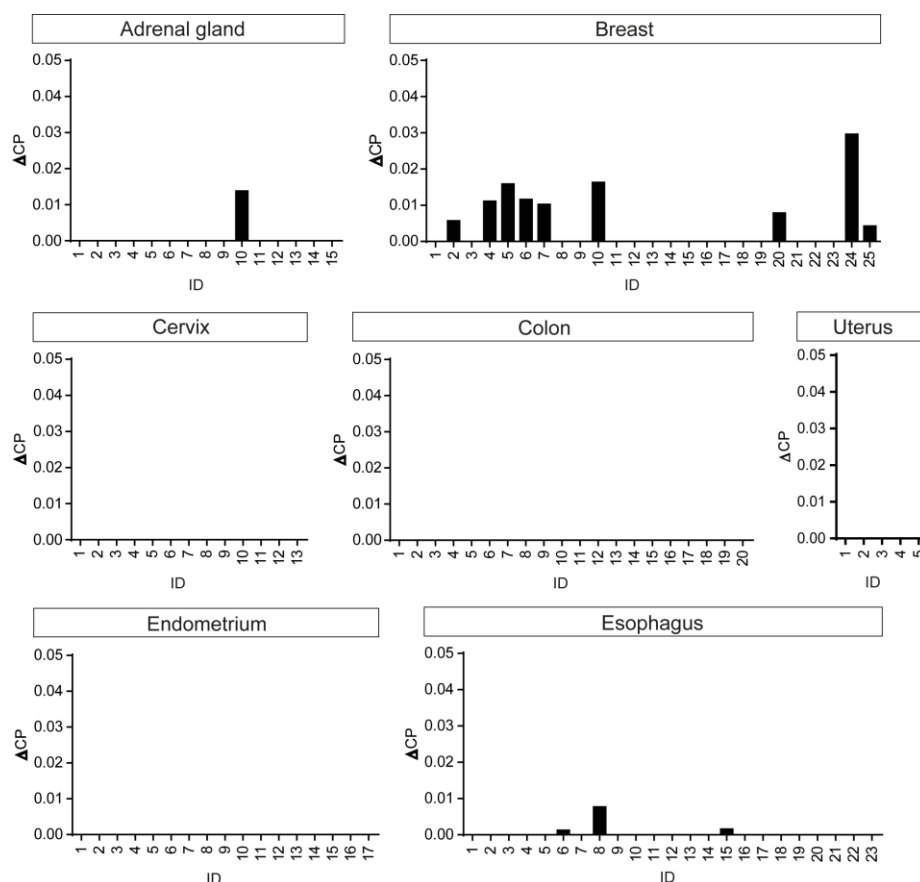
All raw data was analyzed with Student's t-test. Depicted are mean values  $\pm$  SD or  $\pm$  SEM as indicated in the figure legends. Statistical significance was defined as \*P < 0.05; \*\*P < 0.01; \*\*\*P < 0.001, \*\*\*\*P < 0.0001; n.s., not significant.

## 6 RESULTS

### 6.1 Metabolite receptor expression in human solid tumors

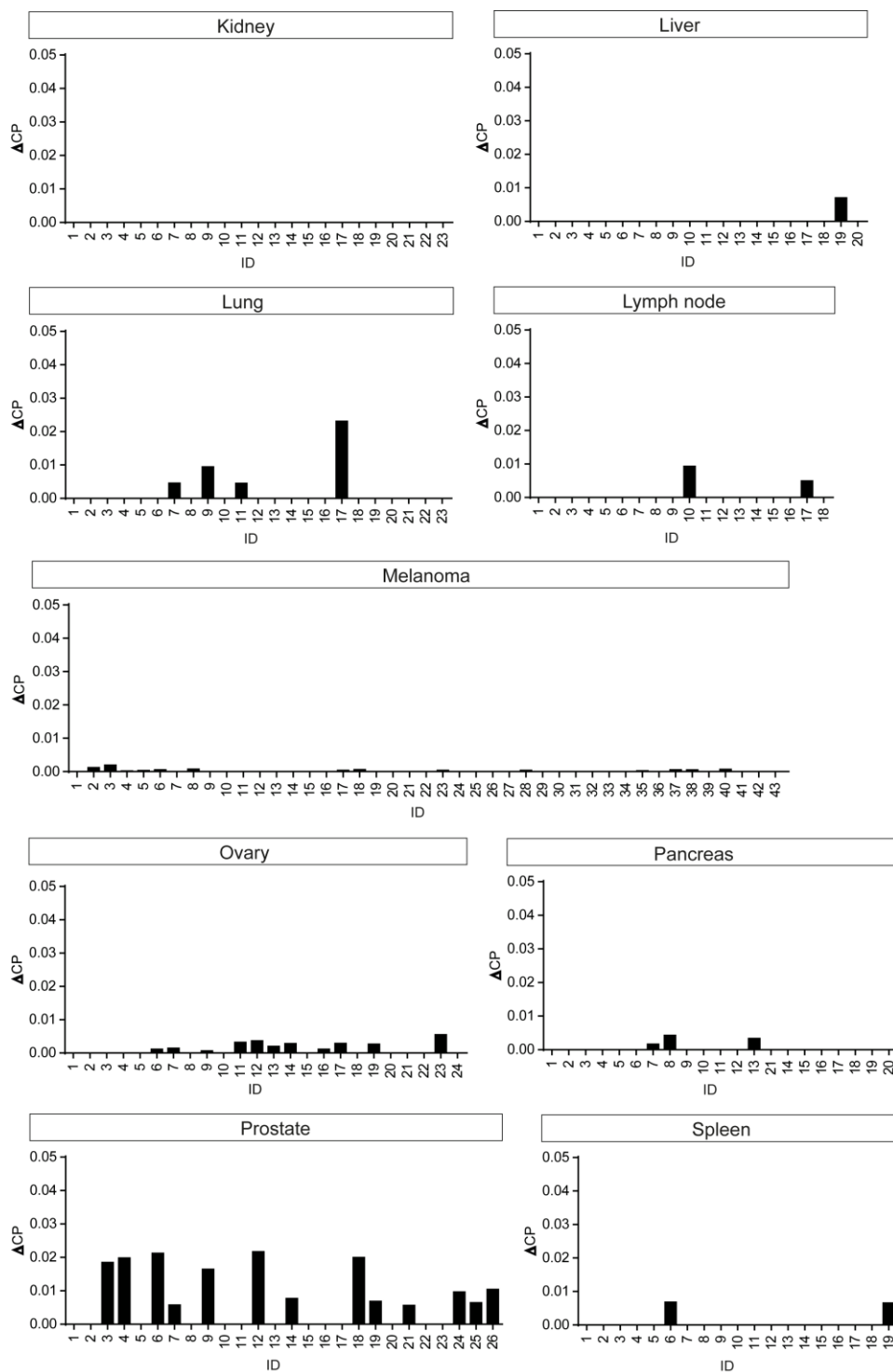
#### 6.1.1 HCA1 is expressed in breast tumor samples

We performed a RT-qPCR assay on 425 cDNAs from human solid tumors. The cDNA array consisted of a variety of tumor entities. We analyzed the expression of HCA1-3 and FFA1-4 in relation to the expression of the housekeeping gene GAPDH. We found an elevated expression of HCA1 in many of the breast tumor samples (Figure 2). In these samples, the expression of HCA1 was around one to three percent of the GAPDH expression. We also detected HCA1 expression in prostate and urinary bladder samples (Figure 2) but refrained from following up on these results because HCA2 and HCA3 were expressed in the prostate samples too. In addition, HCA2, HCA3 and FFA2 were expressed in urinary bladder samples too (data not shown). Hence, HCA1 expression in prostate and urinary bladder tumors appears comparatively unspecific. We could not detect a remarkable HCA1, HCA2 or HCA3 expression in other tumor entities.



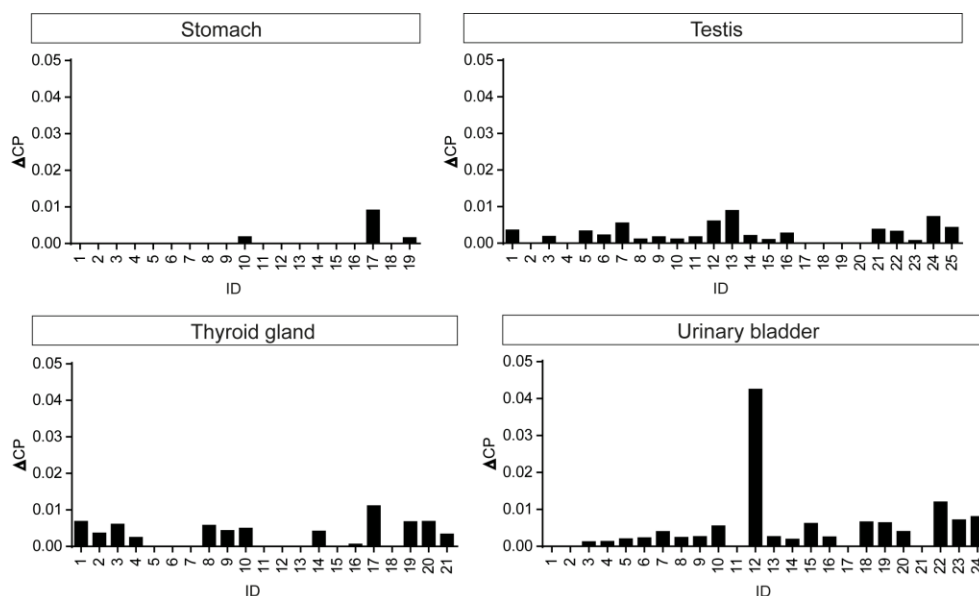
**Figure 2: HCA1 is expressed in human solid breast tumors.** RT-qPCR analysis of HCA1 expression in cDNA of human solid tumor samples, GAPDH served as a house keeping gene,  $\Delta CP = 2^{CP(GAPDH) - CP(\text{gene of interest})}$

Figure 2 continued:



**Figure 2: HCA1 is expressed in human solid breast tumors.** RT-qPCR analysis of HCA1 expression in cDNA of human solid tumor samples, GAPDH served as a house keeping gene,  $\Delta CP = 2^{CP(GAPDH) - CP(\text{gene of interest})}$

Figure 2 continued:



**Figure 2: HCA1 is expressed in human solid breast tumors.** RT-qPCR analysis of HCA1 expression in cDNA of human solid tumor samples, GAPDH served as a house keeping gene,  $\Delta CP = 2^{CP(GAPDH) - CP(\text{gene of interest})}$

### 6.1.2 FFA4 is expressed in colon tumor samples

FFA4 showed an elevated expression of around one percent of the GAPDH expression in nearly all of the colon tumor samples (Figure 3). Remarkably, the expression in other tumor entities was very low leaving the expression in colon cancer samples highly specific. The overall expression of FFA1-3 was either low or inconsistent (data not shown).

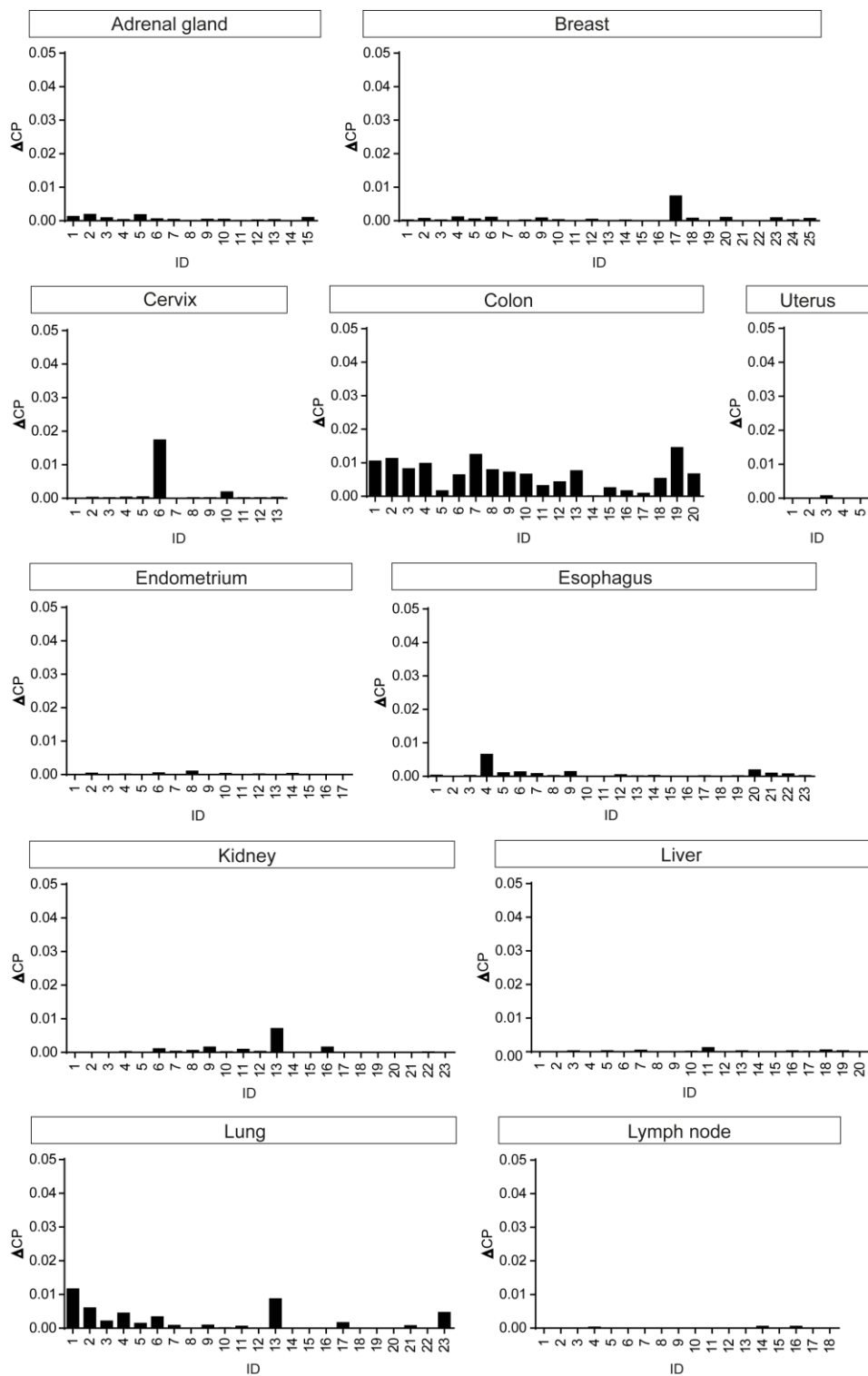


**Figure 3: FFA4 is expressed in human solid colon tumors.** RT-qPCR analysis of FFA4 expression in cDNA of human solid tumor samples, GAPDH served as a house keeping gene,  $\Delta CP = 2^{CP(GAPDH) - CP(\text{gene of interest})}$

Figure 3 continued:

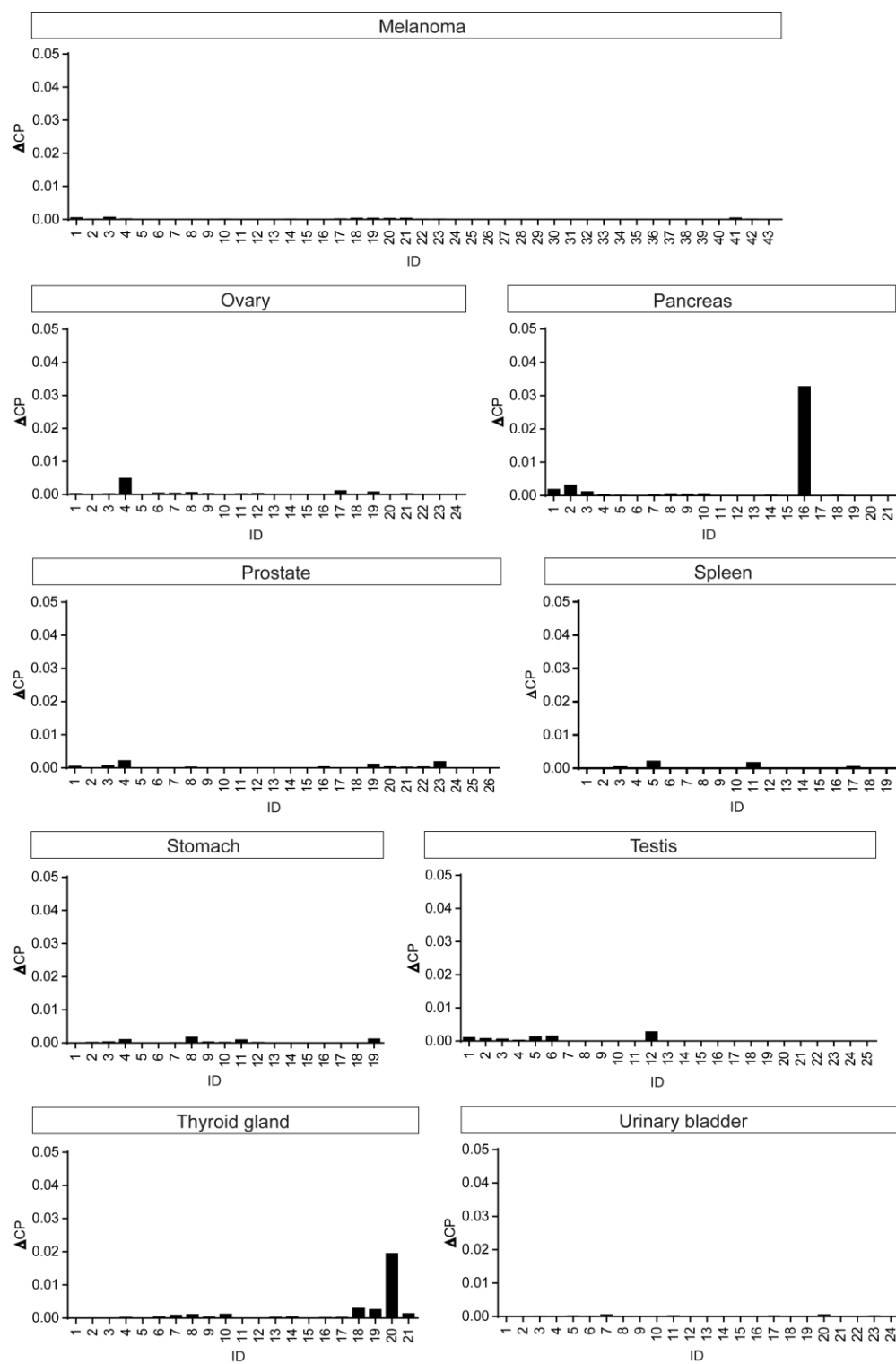


**Figure 3: FFA4 is expressed in human solid colon tumors.** RT-qPCR analysis of FFA4 expression in cDNA of human solid tumor samples, GAPDH served as a house keeping gene,  $\Delta CP = 2^{CP(GAPDH) - CP(\text{gene of interest})}$

## 6.2 Metabolite receptor expression in tumor cell lines

To confirm the data we obtained from the RT-qPCR assay on human tumor cDNAs, we analyzed the expression of HCA1 in human breast cancer cell lines and the expression of FFA4 in human colon cancer cell lines. The RT-qPCR analysis of the breast cancer cell lines T47D, BT-474 and MDA-MB-361 showed expression of HCA1 of around one percent compared to GAPDH, which is similar to the expression in the human cancer cDNA samples (compare Figure 2 and Figure 4A). The analysis of FFA4 in the colon cancer cell lines T84 and SW403 showed expression of FFA4 although it was minor compared to the human cancer samples (compare Figure 3 and Figure 4B).

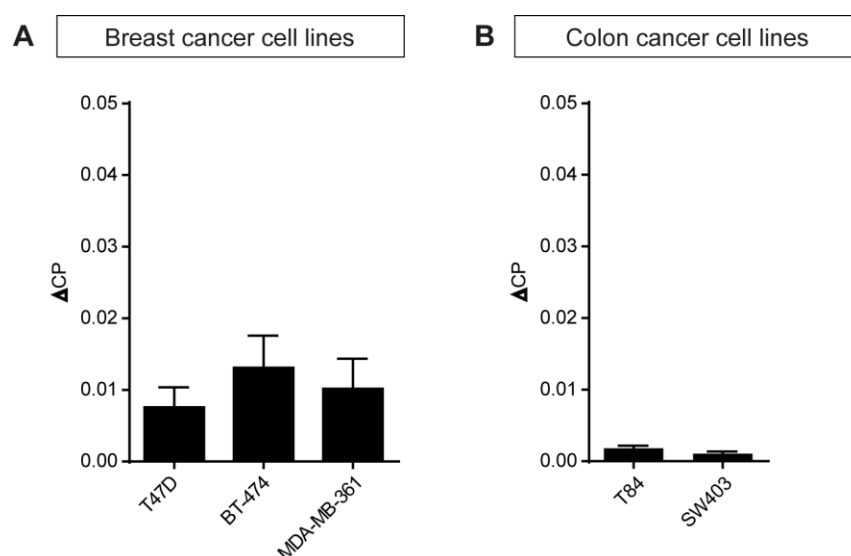


**Figure 4: HCA1 expression in human breast cancer cell lines and FFA4 expression in human colon cancer cell lines.** (A) RT-qPCR analysis of HCA1 expression in cDNA of human breast cancer cell lines. (B) RT-qPCR analysis of FFA4 expression in cDNA of human colon cancer cell lines. GAPDH served as a house keeping gene,  $\Delta CP = 2^{CP(GAPDH) - CP(\text{gene of interest})}$ . Shown are representative data of five independent experiments with mean  $\pm$  SD.

### 6.3 Generation of *Ffar4*<sup>lox</sup> mice

Since FFA4 is expressed in human colorectal carcinomas and in human colon cancer cell lines, we performed  $\beta$ -gal staining and IF staining for FFA4 in small intestines and colons of untreated mice expressing lacZ under the control of the *Ffar4* promoter (FFA4lacZ reporter mice). In both the small intestine and the colon, we observed epithelial cells expressing FFA4 (Figure 5A, B). To gain insights in the function of FFA4 in cancer and metabolism we generated FFA4<sup>loxP/loxP</sup> mice with the CRISPR/Cas9 system. *Ffar4* comprises three exons of which the second exon is coding for the transmembrane domain 5 of the receptor. We inserted loxP sites 66 bp upstream and 136 bp downstream of the exon 2 (Figure 5C). Therefore, we cloned the 5'- and the 3'-guide sequences (Table 1) into PX459v2 plasmids and transfected them to v6.5 ES cells. PCR on gDNA of the transfected ES cells presented diffuse bands at the desired heights (Figure 5D). The presence of the diffuse bands resulted from PCR amplicons of different lengths, thus indicated a high frequency of deletions and insertions at the prospective insertion sites for the loxP sites. A mixture of guide RNAs, Cas9 mRNA and the ssODNs (Table 1) was injected into C57BL/6 zygotes, which were then transferred to pseudo-pregnant female animals. The PCR analysis of the offspring revealed one male animal which had a heterozygous insertion of the 5'-loxP site and homozygous insertion of the 3'-loxP site. (Figure 5E). The prospective founder animal was bred to C57BL/6J females to generate F1 heterozygous offspring. The offspring was crossed to either LysM-Cre (152), Adipoq-Cre (153) or Villin-Cre (154) transgenic mice to generate either monocyte and macrophage, adipocyte or epithelial cell specific FFA4 knockout animals.

**Table 1: Guide and ssODN sequences for CRISPR/Cas9 gene editing of *Ffar4*.**

5'-guide	5'- ATTGTTCCAGGGGTTAGCAG-3'
3'-guide	5'-TGTAGCCCACAAACGAGGGC-3'
5'-ssODN	5'-CTTCCTGTCACAACAGCTTGTAACACACAGTGTACAGTGTCTCCTGTA GCCCACAAACGAGATAACTTCGTATAATGTATGCTATACGAAGTTATGG CTGGGCTAAAGGCCAAGGAAGAAGCCAGGCATTTAAGTGATGTTGTTT TCTCTTTTGC-3'
3'-ssODN	5'-CTTAGAAAACAAAAGGCCAAAATAAATATACAAACTCACCCCTCATTGT TCCAGGGGTTAGATAACTTCGTATAGCATAACATTATACGGAGTTATCAG AGGATCTGCCAGTGAGTTAGGATTGTAAGTGTACTGTTAGGACCCCAAAGTGT CCTCTGACT-3'



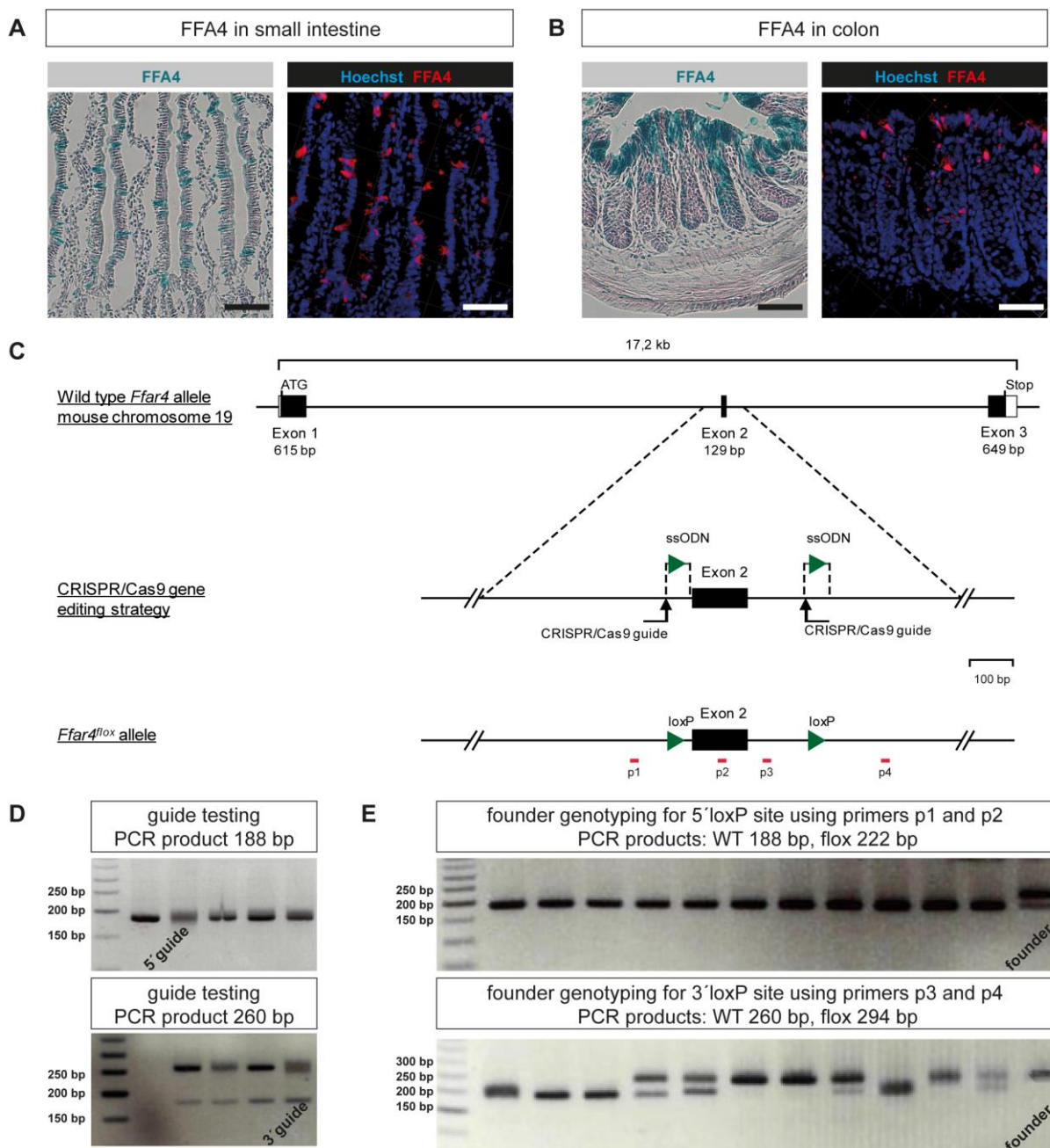


**Figure 5: Targeting strategy for the generation of mice with loxP-flanked (floxed (fl)) *FFA4* alleles.** (A) Representative images of FFA4 expression in small intestine. Left panel: lacZ and H&E staining, right panel: SPiDER  $\beta$ -gal staining, scale bars 50 $\mu$ m. (B) Representative images of FFA4 expression in colon. Left panel: lacZ and H&E staining, right panel: SPiDER  $\beta$ -gal staining, scale bars 50 $\mu$ m. (C) Targeting scheme for generation of floxed FFA4 including primers for guide testing and genotyping. (D) Upper panel: PCR screening for 5' guide insertion-deletion activity. Primers p1 and p2 were used. Lower panel: PCR screening for 3' guide insertion-deletion activity. Primers p3 and p4 were used. Smear bands on gel indicating high insertion-deletion activity. (E) PCR screening for loxP site insertion in potential founder animals. Upper panel: 5' loxP site is inserted in one allele of the founder. Lower panel: 3' loxP sites are inserted in both alleles of the founder.

Recombination on DNA level was analyzed by PCR analysis of gDNA from AdipoqCre<sup>+</sup>;FFA4<sup>loxP/loxP</sup> epididymal white adipocytes (Figure 6A). We used the primers p1 and p4 (Figure 6C) to detect either a band representing the recombined allele (275 bp) or the corresponding amplificate of the floxed allele (640 bp) or a band representing the wild type allele (572 bp). The PCR on gDNA of an AdipoqCre<sup>+</sup>;FFA4<sup>loxP/loxP</sup> animal delivered a band of 275 bp indicating recombinatory activity. However, a band representing the floxed allele was obtained as well indicating either incomplete recombination or imperfect adipocyte isolation. To test for recombination on RNA level RT-qPCR on cDNA from AdipoqCre<sup>+</sup>;FFA4<sup>loxP/loxP</sup> epididymal white adipocytes was carried out showing a reduction of *Ffar4* mRNA by 96% (Figure 6B). As a functional proof of recombination, Sabrina Sapski performed a lipolysis assay. Lipolysis in isolated adipocytes was induced by isoproterenol. While addition of FFA4 agonists TUG-891 and Compound A reduced lipolysis significantly in AdipoqCre<sup>+</sup>;FFA4<sup>loxP/loxP</sup> animals, lipolysis in AdipoqCre<sup>+</sup>;FFA4<sup>loxP/loxP</sup> animals was hardly affected upon addition of FFA4 agonists (Figure 6C). Hence, an adipocyte specific deletion of FFA4 was achieved.

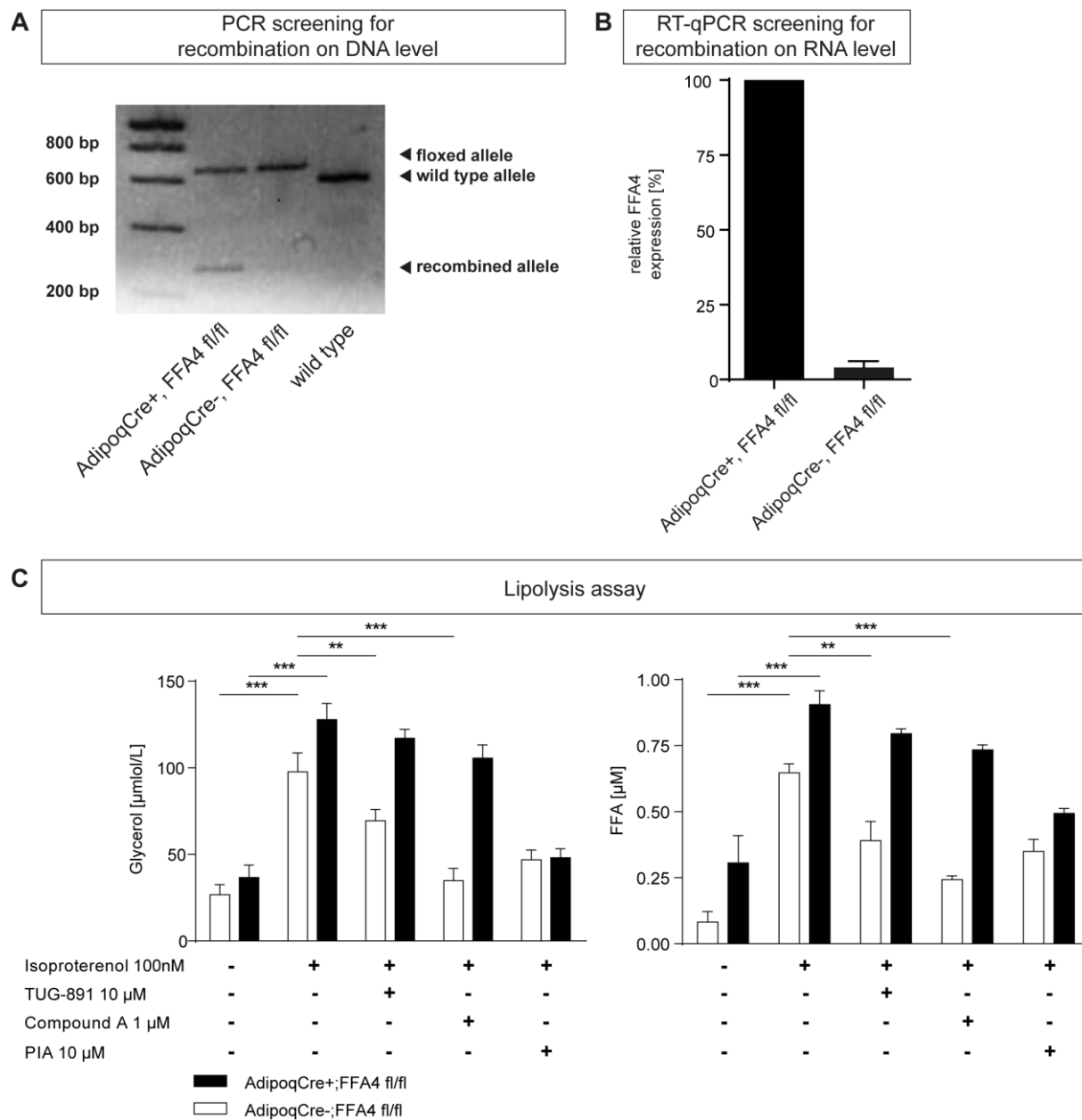


**Figure 6: Recombination of AdipoqCre in FFA4<sup>loxP/loxP</sup> animals.** (A) PCR screening for recombination in genomic DNA of AdipoqCre+; FFA4<sup>loxP/loxP</sup> and AdipoqCre-; FFA4<sup>loxP/loxP</sup> animals. Band of recombined allele: 275 bp, band of wild type allele: 572 bp, band of floxed allele: 640 bp. (B) RT-qPCR screening for recombination on mRNA level in AdipoqCre+; FFA4<sup>loxP/loxP</sup> and AdipoqCre-; FFA4<sup>loxP/loxP</sup> animals. Shown is the relative expression, results of three individual experiments each in duplicates, mean±SD. (C) Lipolysis assay for white epididymal adipocytes of AdipoqCre+; FFA4<sup>loxP/loxP</sup> and AdipoqCre-; FFA4<sup>loxP/loxP</sup> animals. Shown are the released glycerol and free fatty acids. Lipolysis was induced with Isoproterenol, FFA4 agonists TUG-891 and Compound A were used to block lipolysis. Addition of (R)-N<sup>6</sup>-(2-Phenylisopropyl) adenosine (PIA) inhibits lipolysis in AdipoqCre+; FFA4<sup>loxP/loxP</sup> animals indicating responsiveness of adipocytes to antilipolytic signaling via GPCRs in general. Results are from three individual experiments, \*\* P < 0.01, \*\*\* P < 0.001, mean±SD. One-way ANOVA and Tukey's Multiple Comparison Test. Lipolysis assay performed by Sabrina Sapski.

## 6.4 Syngeneic LLC1 tumor model

### 6.4.1 HCA2, FFA2 and FFA4 are expressed in tumor stroma of LLC1 tumors

In preliminary experiments, we compared tumor stroma formation and the presence of immune cells in syngeneic tumors resulting from subcutaneous injection of B16 F10, MC-38, CT26.WT or LLC1 cells in HCA1<sup>mRFP</sup>, HCA2<sup>mRFP</sup>, FFA2<sup>mRFP</sup>, FFA3<sup>mRFP</sup> or FFA4<sup>lacZ</sup> reporter mice. IF staining with pan leukocyte marker CD45 proved LLC1 cells to be more suitable for this model than the other cell lines tested as the resulting LLC1 tumors had noticeable compartments of tumor stroma represented by CD45 positive cells. Table 2 shows for which of the cell lines a co-localization of CD45 positive cells and cells expressing mRFP or lacZ could be observed. In the LLC1 tumors, a co-localization between immune cells and receptor positive cells was found for three out of five reporter lines. This result outnumbered the other tumor cell lines tested.

**Table 2: Comparison of colocalization between CD45 and metabolite receptors reporter in different syngeneic tumor models**

	LLC1	B16 F10	MC-38	CT-26.WT
<b>HCA1<sup>mRFP</sup></b>	–	–	–	–
<b>HCA2<sup>mRFP</sup></b>	✓	✓	–	✓
<b>FFA2<sup>mRFP</sup></b>	✓	–	–	✓
<b>FFA3<sup>mRFP</sup></b>	–	–	–	–
<b>FFA4<sup>lacZ</sup></b>	✓	–	–	–

We continued in order to identify cells of the tumor stroma that express metabolite receptors and injected LLC1 cells subcutaneously into either HCA2<sup>mRFP</sup>, FFA2<sup>mRFP</sup> or FFA4<sup>lacZ</sup> reporter mice. In all the tumors we performed IF staining for CAFs and immune cells. The fibroblast markers PDGFR $\alpha$  and  $\alpha$ -SMA did not stain any cells with metabolite receptors expression (data not shown). However, IF staining with CD45 revealed co-localization of CD45 and metabolite receptor expression for all three receptors. In the LLC1 tumors in HCA2<sup>mRFP</sup> animals, more than 10% of cells could be identified as immune cells expressing CD45. Around 58% of these cells also expressed HCA2 (Figure 7A, B). To further elucidate the type of immune cells, we used CD68 and F4/80 antibodies as markers for macrophages. We identified 8% of cells being F4/80 positive and 8.5% of cells being CD68 positive but the fractions of double-positive cell were very small with 2.7% respective 1.4% of cells (Figure 7C-F). As some cells can be stained with both macrophage markers, there is a certain overlap and both fractions do not need to add up to the percentage of CD45 positive cells.

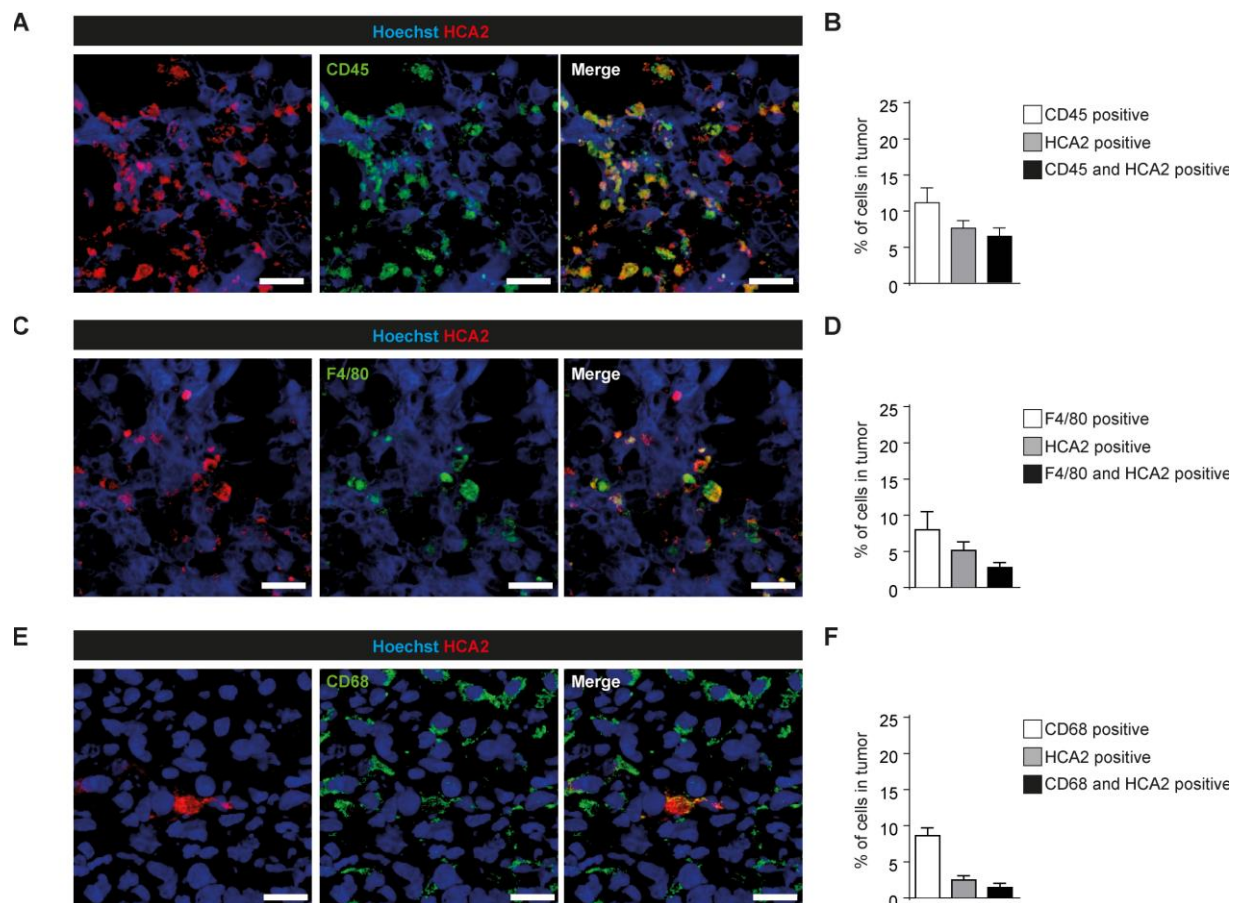


**Figure 7: Expression of HCA2 and immune markers in LLC1 tumors.** (A, C, E) Representative confocal images of LLC1 primary tumors. Staining for HCA2 and the indicated markers, all scale bars 20  $\mu$ M. (B, D, F) Quantification of staining, shown is the percentage of stained cell per tumor. For each condition four fields of view from  $n=3$  animals were analyzed. Shown are mean $\pm$ SD.

The LLC1 tumors of FFA2<sup>mRFP</sup> animals presented 10.4% of CD45 positive cells and 4.4% of CD45 and FFA2 positive cells (Figure 8A, B). The staining with macrophage markers revealed F4/80 respective CD68 positive fractions of 6.9% respective 5.8%. Similar to the results for HCA2<sup>mRFP</sup> animals, the percentage of FFA2 and macrophage marker double-positive cells is minor (Figure 8C-F).



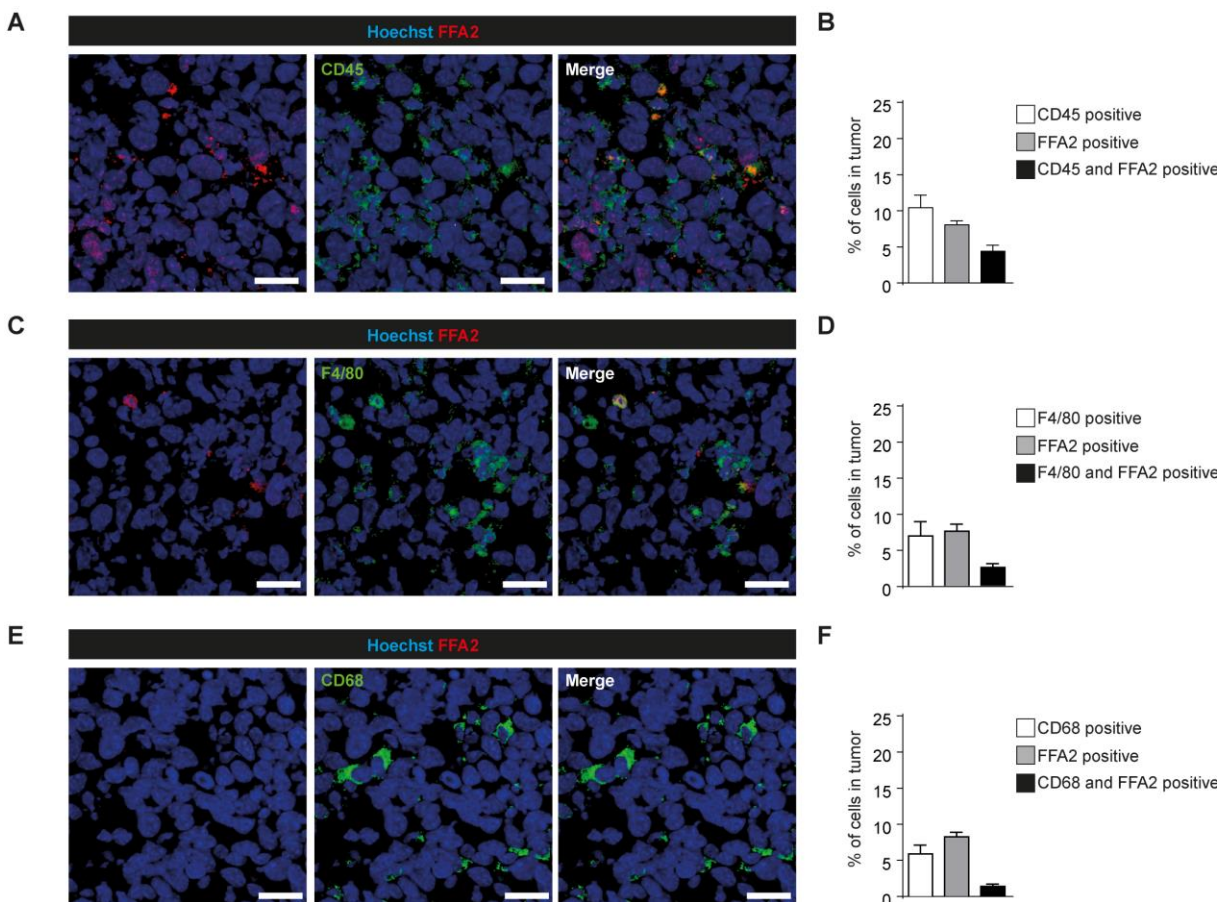


**Figure 8: Expression of FFA2 and immune markers in LLC1 tumors.** (A, C, E) Representative confocal images of LLC1 primary tumors. Staining for FFA2 and the indicated markers, all scale bars 20  $\mu$ M. (B, D, F) Quantification of staining, shown is the percentage of stained cell per tumor. For each condition four fields of view from  $n=3$  animals were analyzed. Shown are mean $\pm$ SD.

In LLC1 tumors of FFA4<sup>lacZ</sup> reporter mice we recognized a FFA4 expression in only 3.2 - 3.6% of the cells. Leukocytes in general, stained with CD45, formed a fraction of 7.2% of the cells while macrophage markers stained fractions of 6.2% F4/80 positive cells and 4.5% CD68 positive cells. The fractions of macrophages also expressing FFA4 were limited to 1.7% for F4/80 respective 2.2% for CD68 (Figure 9). Despite only small fractions of TAMs expressing the metabolite receptors tested, we determined to test the influence of the loss of the receptors on the LLC1 tumor model.

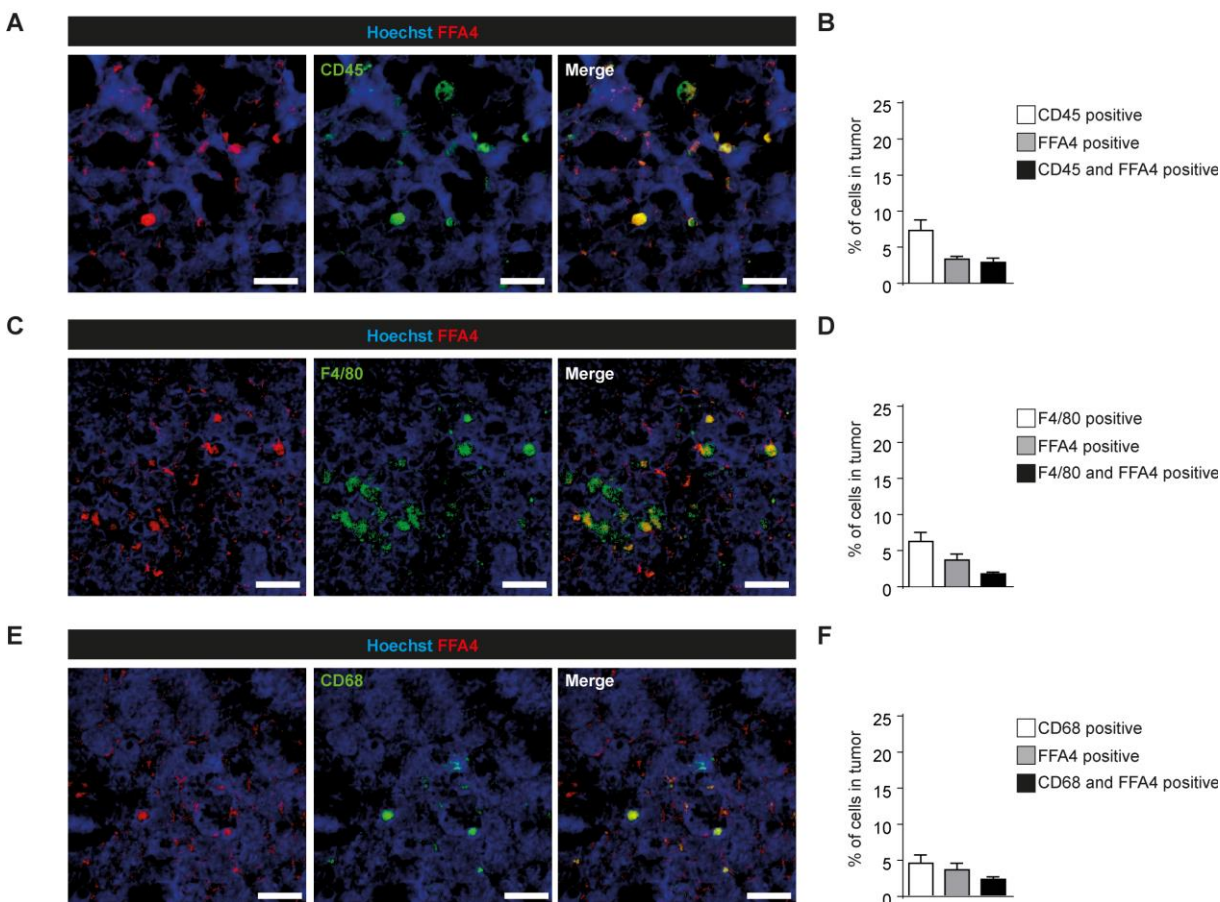


**Figure 9: Expression of FFA4 and immune markers in LLC1 tumors.** (A, C, E) Representative confocal images of LLC1 primary tumors. Staining for FFA4 and the indicated markers, all scale bars 20  $\mu$ M. (B, D, F) Quantification of staining, shown is the percentage of stained cell per tumor. For each condition four fields of view from  $n=3$  animals were analyzed. Shown are mean $\pm$ SD.

#### 6.4.2 Knockout of HCA2, FFA2 or FFA4 does not cause change of volume and weight of LLC1 tumors

To further test whether the loss of HCA2, FFA2 or FFA4 has an impact on tumor growth, LLC1 cells were injected s.c. into HCA2<sup>-/-</sup>, FFA2<sup>-/-</sup> and FFA4<sup>-/-</sup> animals as well as their wild type littermates. Animals were sacrificed either after 21 days or upon reach of a maximal tumor volume of 1.7 cm<sup>3</sup>. Tumor development was monitored by measuring tumor size and calculating the resulting tumor volume. None of the knockout groups showed a significantly altered tumor growth during the experiment (Figure 10). Likewise, when we sacrificed the mice and dissected the tumors no significant difference in tumor volume and weight between knockout and wild type animals could be observed (Figure 10). Tumor growth as well as size of the dissected tumors are underlying a large variance although nearly all the experiments had to be ended after the same time period. Comparing the mean weight and volume of dissected tumors in the wild type groups,

the mean weight and volume of tumors in the FFA2<sup>+/+</sup> groups is more than 50% higher than the mean weight and volume of tumors in the HCA2<sup>+/+</sup> group. Concluding, this syngeneic tumor model is affected by large variance and the obtained data shows LLC1 tumor growth not being changed by the loss of any of the metabolic receptors tested.

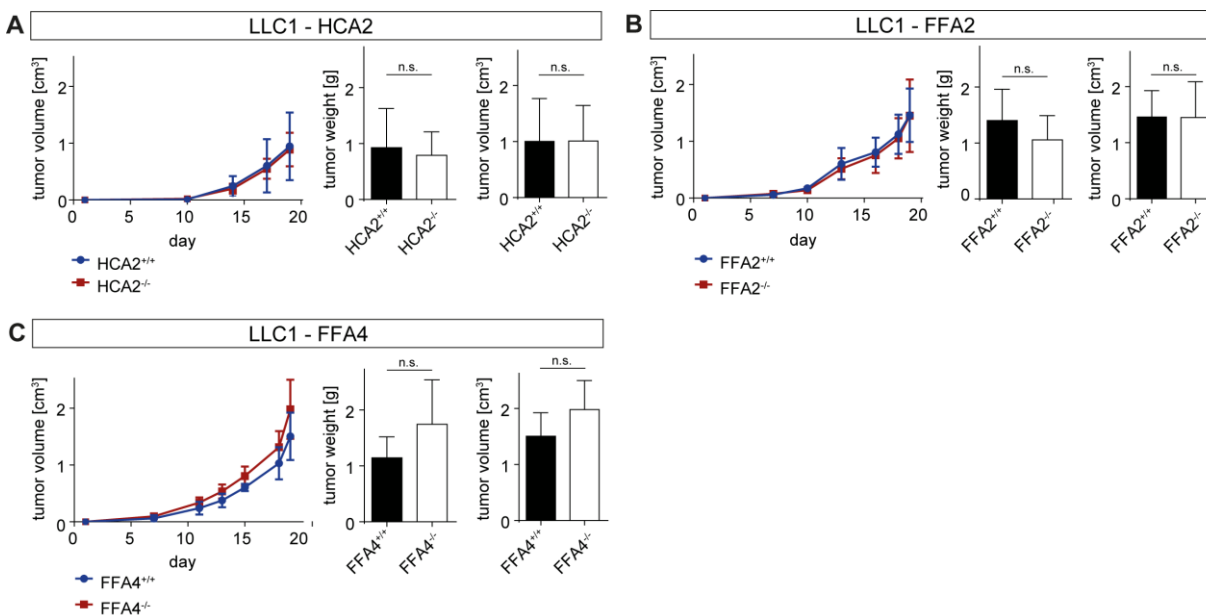


**Figure 10: Syngeneic LLC1 tumor model.** (A) LLC1 tumors in HCA2<sup>+/+</sup> (n=5) and HCA2<sup>-/-</sup> (n=6), Left panel: tumor growth over the course of the time, middle panel: weight of dissected tumors, right panel: volume of dissected tumors. (B) LLC1 tumors in FFA2<sup>+/+</sup> (n=6) and FFA2<sup>-/-</sup> (n=5), Left panel: tumor growth over the course of the time, middle panel: weight of dissected tumors, right panel: volume of dissected tumors. (C) LLC1 tumors in FFA4<sup>+/+</sup> (n=5) and FFA4<sup>-/-</sup> (n=5), Left panel: tumor growth over the course of the time, middle panel: weight of dissected tumors, right panel: volume of dissected tumors. n.s. not significant, mean±SD; unpaired, two-tailed Student's *t*-test.

#### 6.4.3 Knockout of HCA2, FFA2 or FFA4 does not change metastasis in the LLC1 syngeneic tumor model

Subcutaneous LLC1 cell tumors have the ability to develop lung metastasis (155, 156). Therefore, we histologically analyzed the lungs of the knockout and wild type animals using the proliferation marker BrdU as well as Hematoxylin and Eosin staining. In none of the wild type and knockout groups we could identify metastatic growth in any of the lungs (data not shown).



## 6.5 AOM-DSS colorectal cancer model

### 6.5.1 HCA2, FFA2 and FFA4 are expressed in tumor stroma of colorectal tumors

Considering the results of the expression analysis of metabolite receptors in human solid tumors showing FFA4 expression primarily in colorectal carcinomas, we decided to use FFA4<sup>lacZ</sup> reporter animals to determine FFA4 expression in AOM-DSS colorectal carcinoma tumor stroma. Furthermore, literature suggesting the expression of HCA2, FFA2 and to a certain degree also of FFA4 on immune cells (36) as well as the results from the LLC1 syngeneic tumor model confirming these suggestions led us to also include HCA2<sup>mRFP</sup> and FFA2<sup>mRFP</sup> reporter animals. After i.p. injection of AOM, mice were kept for 12 weeks with three cycles of DSS administration. Colons of the sacrificed mice were used to carry out IF staining for CAFs and immune cells. No co-expression was found for any of the metabolite receptors and the fibroblast markers PDGFR $\alpha$  and  $\alpha$ -SMA. Next, we performed staining for immune markers beginning with leukocyte marker CD45. In the colon tumors of HCA2<sup>mRFP</sup> animals, the population of CD45 positive cells was 8.9%. Of these cells, 67% also expressed HCA2 (Figure 11A, B). The fraction of F4/80 positive macrophages was 7.8% but only 2.3% of cells were double positive for both F4/80 and HCA2 (Figure 11C, D). We could identify only a small fraction of macrophages expressing CD68 with a low percentage of CD68 and HCA2 double positive cells (Figure 11E, F).

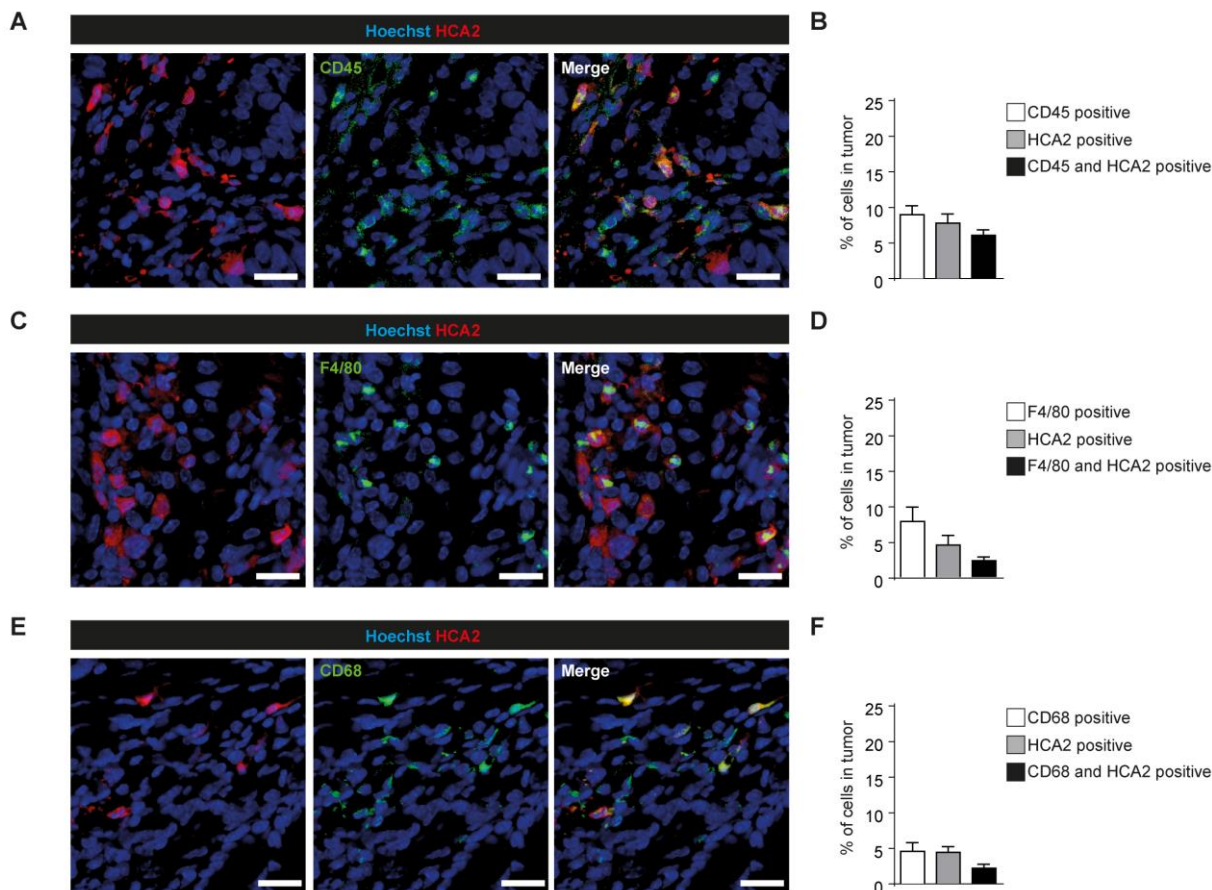


**Figure 11: Expression of HCA2 and immune markers in AOM-DSS colorectal carcinomas.** (A, C, E) Representative confocal images of colon compromising AOM-DSS-induced tumors. Staining for HCA2 and the indicated markers, all scale bars 20  $\mu$ M. (B, D, F) Quantification of staining, shown is the percentage of stained cell per colon tumor. For each condition four fields of view from  $n=3$  animals were analyzed. Shown are mean $\pm$ SD.

In the colon tumors of FFA2<sup>mRFP</sup> animals, we detected 9.7% of the cells expressing CD45 but only 30% of them were also stained FFA2 positive (Figure 12A, B). In addition, the macrophage fractions stained with F4/80 respective CD68 were of a low number of 7.8% respective 4.5% of cells in the tumors and the corresponding fractions of double positive cells were small as well with 2.3% and 2.1% (Figure 12C-F).

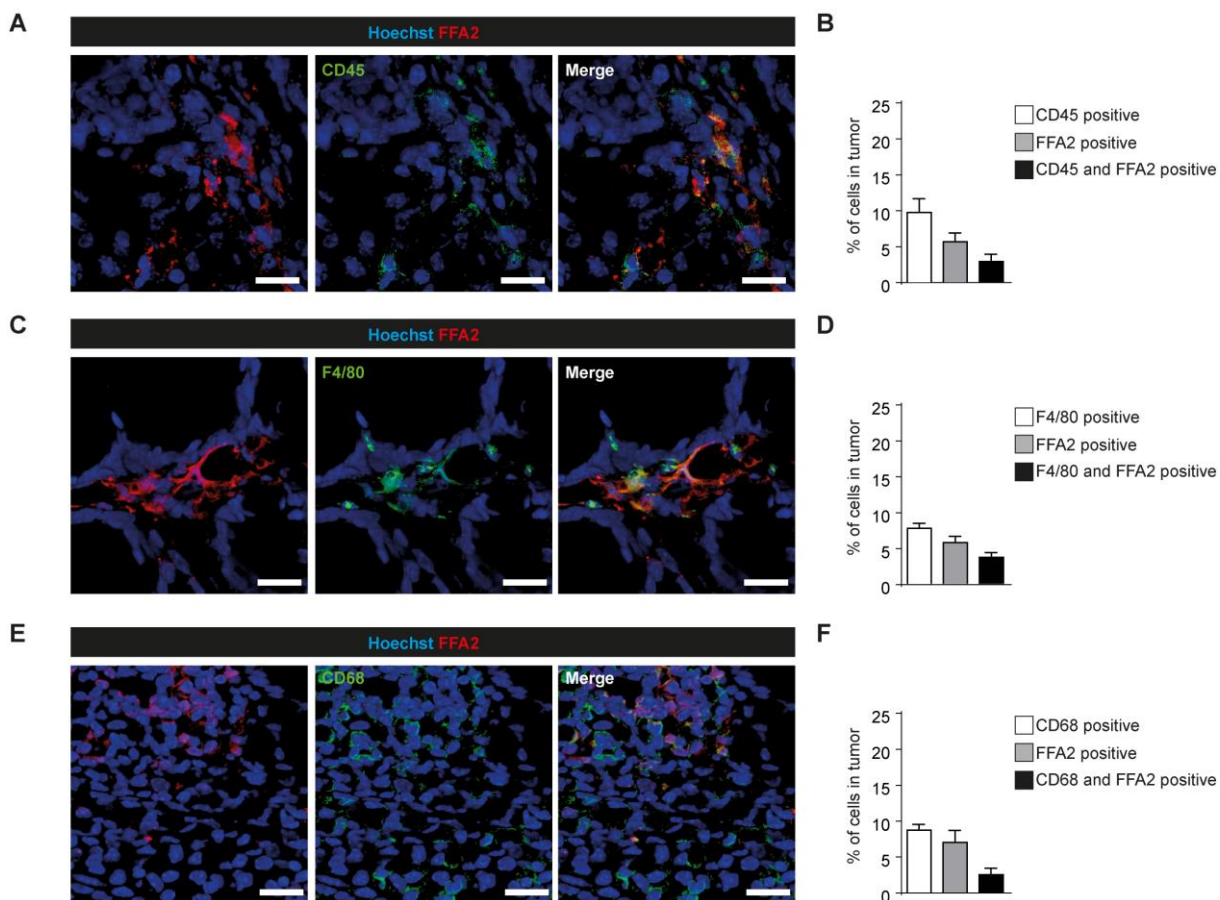


**Figure 12: Expression of FFA2 and immune markers in AOM-DSS colorectal carcinomas.** (A, C, E) Representative confocal images of colon comprising AOM-DSS-induced tumors. Staining for FFA2 and the indicated markers, all scale bars 20  $\mu$ M. (B, D, F) Quantification of staining, shown is the percentage of stained cell per colon tumor. For each condition four fields of view from  $n=3$  animals were analyzed. Shown are mean $\pm$ SD.

In the AOM-DSS experiment, the FFA4<sup>lacZ</sup> animals showed very little colocalization for the reporter and any of the immune markers. We could identify cell populations of CD45 positive leukocytes, F4/80 positive macrophages and CD68 positive macrophages accounting 7.3%, 8.6% and 8.6% of the colon tumor cells. The corresponding fractions of double positive cells amounted to 2.1%, 1.3% and 2% of cells (Figure 13).

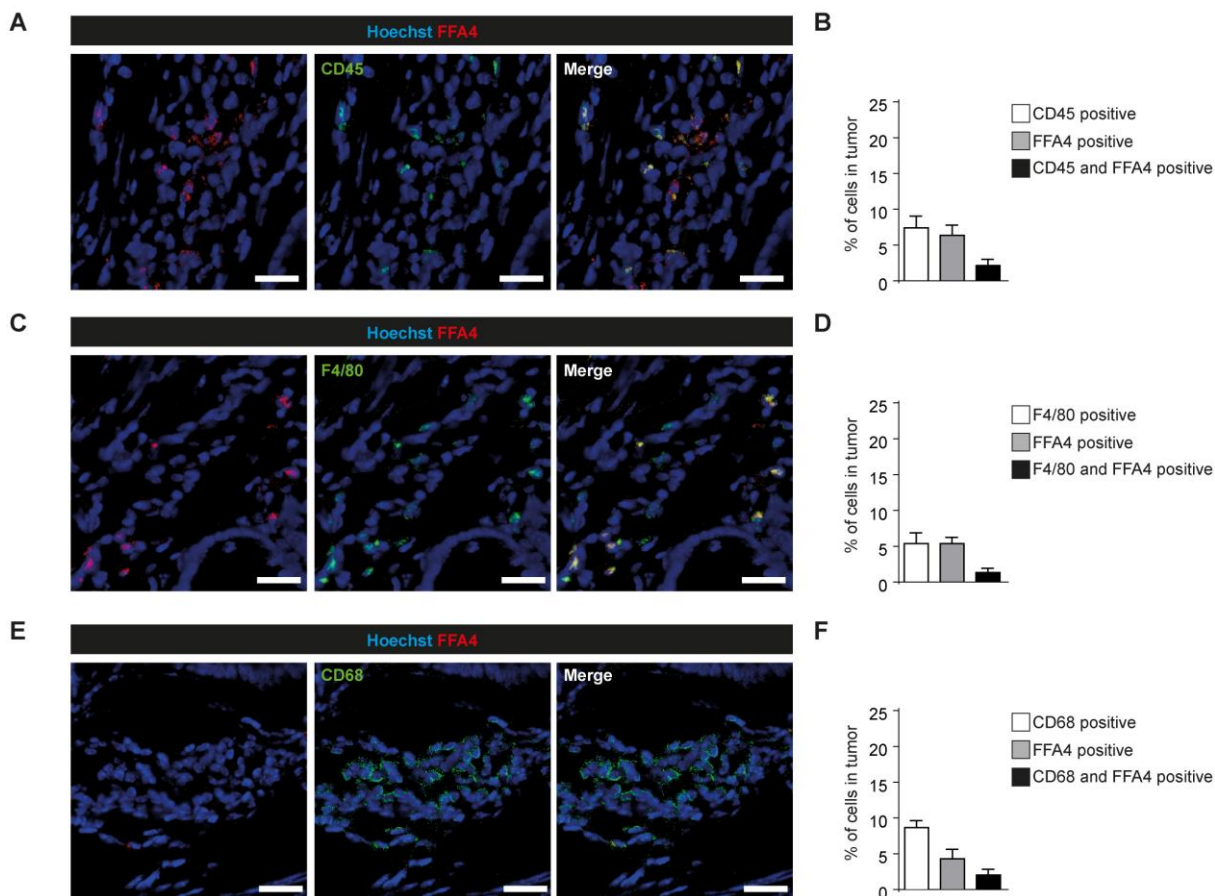


**Figure 13: Expression of FFA4 and immune markers in AOM-DSS colorectal carcinomas.** (A, C, E) Representative confocal images of colon comprising AOM-DSS-induced tumors. Staining for FFA4 and the indicated markers, all scale bars 20  $\mu$ M. (B, D, F) Quantification of staining, shown is the percentage of stained cell per colon tumor. For each condition four fields of view from  $n=3$  animals were analyzed. Shown are mean $\pm$ SD.

### 6.5.2 Knockout of HCA2 or FFA4 does not change tumor growth of colorectal tumors

To evaluate if loss of any of the receptors has an impact on number or area of the developing colorectal carcinomas, we used HCA2<sup>-/-</sup>, FFA2<sup>-/-</sup> and FFA4<sup>-/-</sup> animals as well as their wild type littermates. Tumor growth was induced by i.p. injection of the cancerogenic agent AOM and three cycles of administration of DSS in the animals' drinking water. The weight loss after the DSS cycles is considered a predictor of the final tumor burden (157). We did not observe significant differences in the animals' weight development (Figure 14A, E). From the trend of HCA2<sup>-/-</sup> animals recovering not as well as their wild type littermates from the DSS cycles (Figure 14A) we could not deviate a higher tumor burden. For HCA2<sup>-/-</sup> and FFA4<sup>-/-</sup> animals and their respective wild type littermates, no significant difference in the number of tumors per colon could be observed (Figure 14B, F). The mean values are very similar and vary from 6.5 to 8.2 tumors per colon. Same is true for the area of the colons which is covered by the carcinomas (Figure 14C, G). Here, the mean values vary from 0.31 to 0.45 cm<sup>2</sup> tumor area. Moreover, histologic analysis did not reveal differences in tumor structure (Figure 14D, H). In summary, the loss of HCA2 or FFA4 did not result in an alteration of AOM-DSS colon tumor progression.



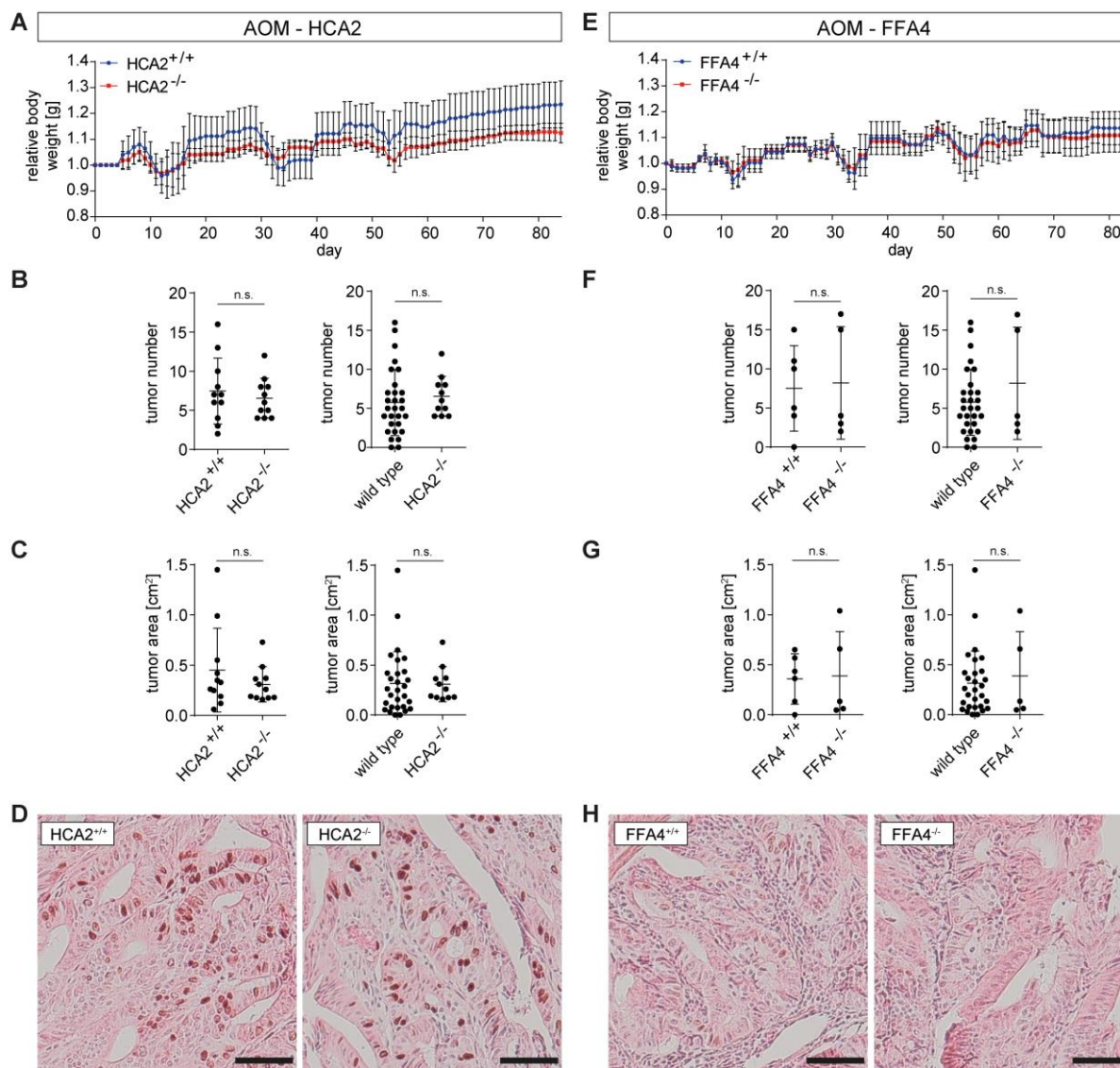


**Figure 14: AOM-DSS colorectal cancer model.** (A-D) HCA2<sup>+/+</sup> (n=11) and HCA2<sup>-/-</sup> (n=11), (A) Relative weight of experimental animals over the course of the time. (B, C) n.s. not significant, mean±SD; unpaired, two-tailed Student's *t*-test. (B) Left panel: tumor number at day of sacrifice HCA2<sup>+/+</sup> vs HCA2<sup>-/-</sup>, right panel: tumor number at day of sacrifice all wild type animals vs HCA2<sup>-/-</sup>, (C) Left panel: tumor area in cm<sup>2</sup> at day of sacrifice HCA2<sup>+/+</sup> vs HCA2<sup>-/-</sup>, right panel: tumor area in cm<sup>2</sup> at day of sacrifice all wild type animals vs HCA2<sup>-/-</sup>. (D) Representative images of colon, BrdU and H&E used. Left panel: tumor in HCA2<sup>+/+</sup> animal, right panel: tumor in HCA2<sup>-/-</sup> animal, scale bars 50μM. (E-H) FFA4<sup>+/+</sup> (n=6) and FFA4<sup>-/-</sup> (n=5), (E) Relative weight of experimental animals over the course of the time. (F, G) n.s. not significant, mean±SD; unpaired, two-tailed Student's *t*-test. (F) Left panel: tumor number at day of sacrifice FFA4<sup>+/+</sup> vs FFA4<sup>-/-</sup>, right panel: tumor number at day of sacrifice all wild type animals vs FFA4<sup>-/-</sup>, (G) Left panel: tumor area in cm<sup>2</sup> at day of sacrifice FFA4<sup>+/+</sup> vs FFA4<sup>-/-</sup>, right panel: tumor area in cm<sup>2</sup> at day of sacrifice all wild type animals vs FFA4<sup>-/-</sup>. (H) Representative images of colon, BrdU and H&E used. Left panel: tumor in FFA4<sup>+/+</sup> animal, right panel: tumor in FFA4<sup>-/-</sup> animal, scale bars 50μM.

### 6.5.3 Knockout of FFA2 increases tumor number but not area in the AOM-DSS model

In contrast to the findings for HCA2 and FFA4 knockouts, the knockout of FFA2 turned out to promote tumor progression. Although the weight curves for knockout and wild type animals did not differ significantly (Figure 15A), the number of tumors per colon was significantly increased for

FFA2<sup>-/-</sup> animals compared to their wild type littermates (Figure 15C). Colons of knockout animals had a significantly higher mean tumor count of 6.8 tumors compared to colons of wild type animal with a mean tumor count of 3.3 tumors. Anyhow, the total area covered by the tumors was increased by 106% in the group of knockout animals, but no significance was achieved (Figure 15D). In addition to these data, we asserted that tumor number and area was generally lower in FFA2 knockout and wild type animals. When tumor number and area of FFA2<sup>-/-</sup> animals was compared to those of all wild type animals, no difference could be observed (Figure 15C, D right panel). To diminish the influence of different microbiomes of the mice we used animals bred in the same room under same conditions and we pooled and redistributed their litter multiple times during the course of the experiment. Nevertheless, our findings indicate that the loss of FFA2 can have a protumoral outcome in the AOM-DSS colon cancer model.

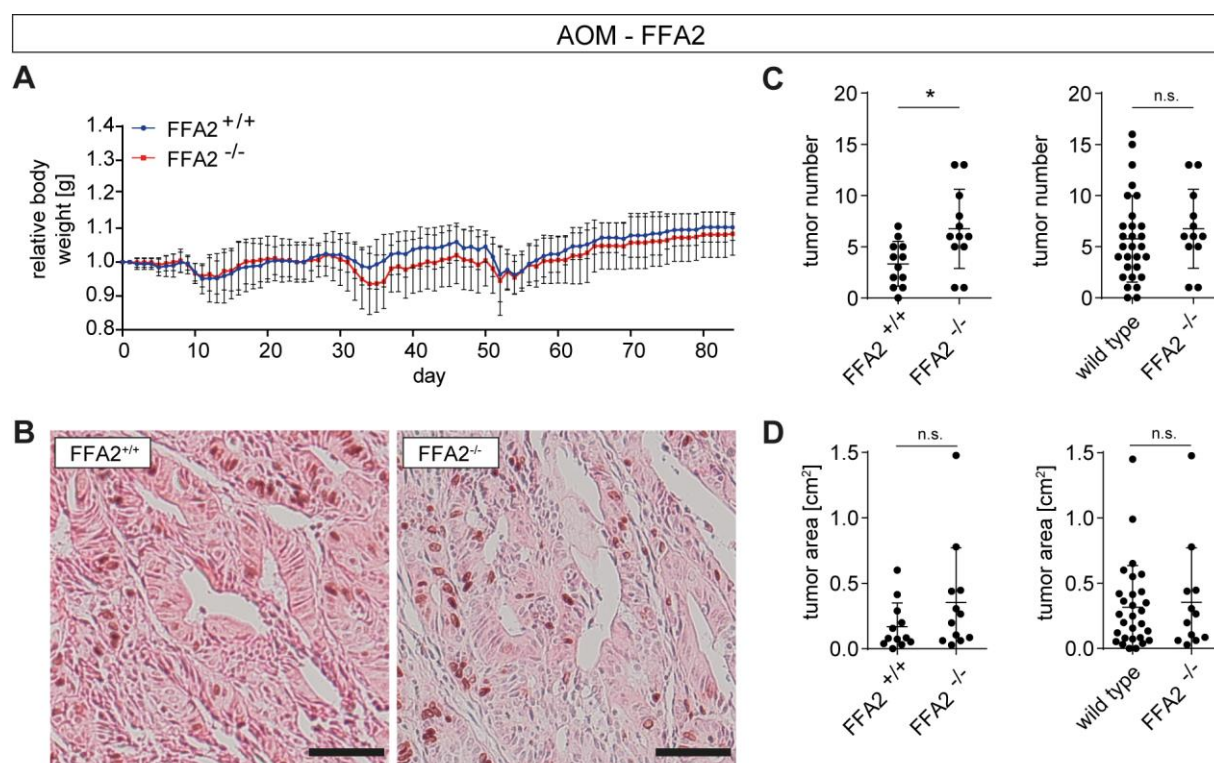


**Figure 15: AOM-DSS colorectal cancer model.** (A-D) FFA2<sup>+/+</sup> (n=12) and FFA2<sup>-/-</sup> (n=12), (A) Relative weight of experimental animals over the course of the time. (B) Representative images of colon, BrdU and H&E used. Left panel: tumor in FFA2<sup>+/+</sup> animal, right panel: tumor in FFA2<sup>-/-</sup> animal, scale bars 50 $\mu$ M. (C, D) \*P < 0.05, n.s. not significant, mean $\pm$ SD; unpaired, two-tailed Student's *t*-test. (C) Left panel: tumor number at day of sacrifice FFA2<sup>+/+</sup> vs FFA2<sup>-/-</sup>, right panel: tumor number at day of sacrifice all wild type animals vs FFA2<sup>-/-</sup>, (D) Left panel: tumor area in cm<sup>2</sup> at day of sacrifice FFA2<sup>+/+</sup> vs FFA2<sup>-/-</sup>, right panel: tumor area in cm<sup>2</sup> at day of sacrifice all wild type animals vs FFA2<sup>-/-</sup>.

## 6.6 MMTV-PyMT breast cancer model

### 6.6.1 HCA1, HCA2 and FFA2 are expressed in the stroma of MMTV-PyMT tumors

The stroma of MMTV-PyMT tumors is not only composed of immune cells, fibroblasts, pericytes, endothelial and epithelial cells but also a large number of adipocytes is enclosed. Since it is well known that HCA1 is expressed on white adipocytes (34), we bred HCA1<sup>mRFP</sup> animals with animals carrying the MMTV-PyMT transgene. The mammary tumors of the MMTV-PyMT<sup>+</sup>;HCA1<sup>mRFP</sup> animals contained a large number of adipocyte shaped cells expressing HCA1 (Figure 16). None of the cells expressing immune cell markers did as well express HCA1. Likewise, staining with the fibroblast markers PDGFR $\alpha$  and  $\alpha$ -SMA did not achieve any co-expression with HCA1 nor with HCA2 or FFA2. The F4/80 positive macrophages and the cells expressing HCA1 were located next to each other with hardly any overlap.

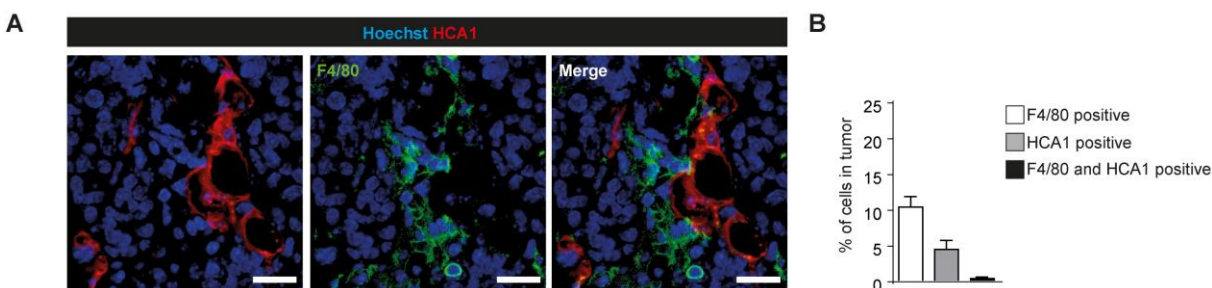


**Figure 16: Expression of HCA1 and F4/80 in MMTV-PyMT breast carcinomas.** (A) Representative confocal image of MMTV-PyMT tumor. Staining for HCA1 and F4/80, all scale bars 20  $\mu$ M. (B) Quantification of staining, shown is the percentage of stained cell per tumor. For each condition four fields of view from n=3 animals were analyzed. Shown are mean $\pm$ SD.

In the breast tumors of MMTV-PyMT<sup>+</sup>;HCA2<sup>mRFP</sup> animals, 7.3% of cells could be identified as immune cells expressing CD45. Around 82% of these cells also expressed HCA2 (Figure 17A, B). To further elucidate the type of immune cells we used F4/80 and CD68 antibodies as markers for macrophages. We identified 13.1% of cells being F4/80 positive and 5.6% of cells being CD68 positive. Furthermore, the fractions of double-positive cell were 5.4% respective 4.1% of cells (Figure 17C-F).



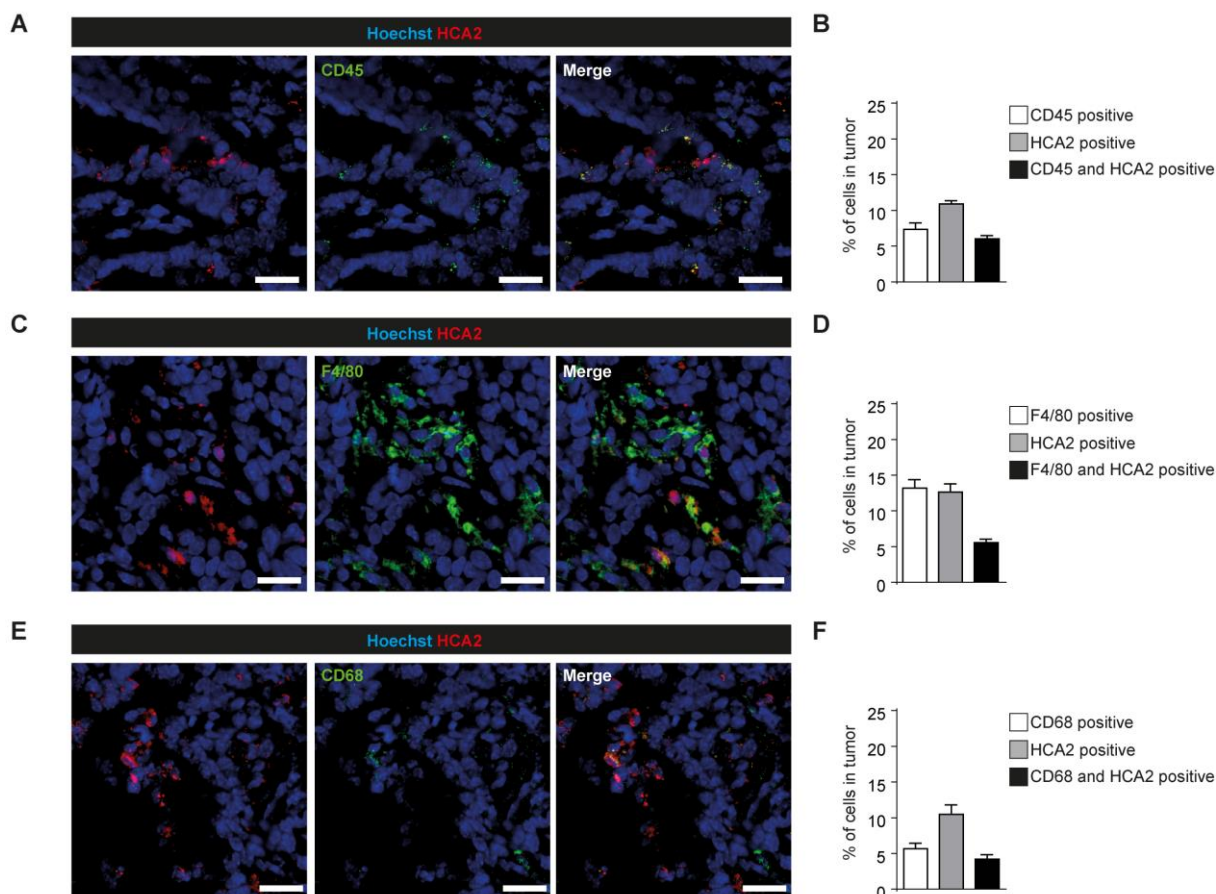


**Figure 17: Expression of HCA2 and immune markers in MMTV-PyMT breast carcinomas.** (A, C, E) Representative confocal images of MMTV-PyMT tumors. Staining for HCA2 and the indicated markers, all scale bars 20  $\mu$ M. (B, D, F) Quantification of staining, shown is the percentage of stained cell per tumor. For each condition four fields of view from  $n=3$  animals were analyzed. Shown are mean $\pm$ SD.

The breast tumors of MMTV-PyMT<sup>+</sup>;FFA2<sup>mRFP</sup> contained a high number of immune cells. A remarkable percentage of 21.1% of cells could be stained with CD45. Moreover, nearly all of the FFA2 positive cells (6.5%) expressed CD45 (6.1%) thus were immune cells (Figure 18A, B). To analyze if the cells were TAMs we used F4/80 and CD68. The F4/80 positive cell population was 4.6% with 85% of the cells also expressing FFA2 (Figure 18C, D). The CD68 positive cell population was 4.1% with 51% of the cells also expressing FFA2 (Figure 18E, F). The fraction of FFA2 positive cells was larger than the two macrophage fractions indicating that FFA2 is as well expressed in other types of immune cells. Further histological analysis revealed that markers for neutrophils, B-cells and T-cells sporadically stained FFA2 positive cells (data not shown). The main fraction of FFA2 positive cells however was characterized as macrophages.

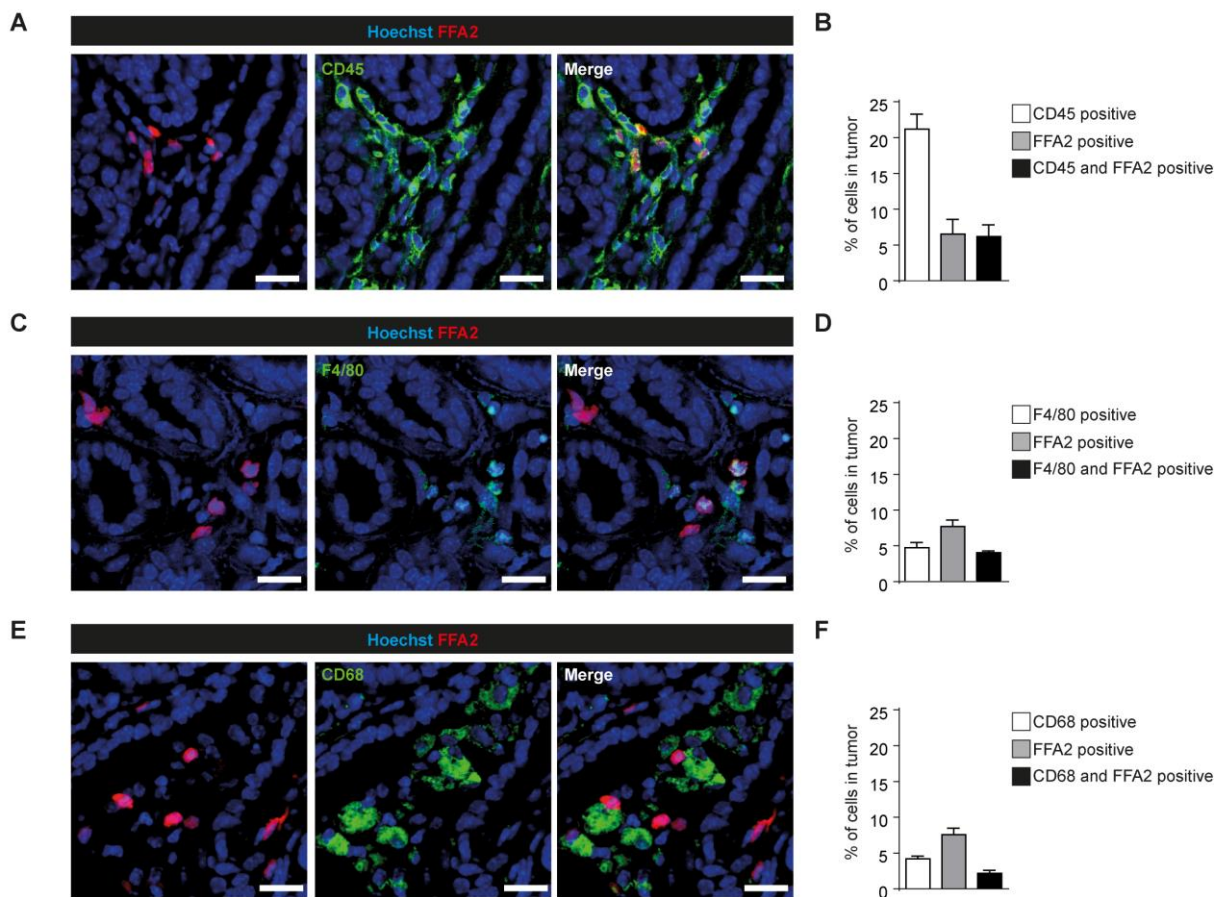


**Figure 18: Expression of FFA2 and immune markers in MMTV-PyMT breast carcinomas.** (A, C, E) Representative confocal images of MMTV-PyMT tumors. Staining for FFA2 and the indicated markers, all scale bars 20  $\mu$ m. (B, D, F) Quantification of staining, shown is the percentage of stained cell per tumor. For each condition four fields of view from n=3 animals were analyzed. Shown are mean $\pm$ SD.

### 6.6.2 Knockout of HCA1 or HCA2 does not influence onset and growth of MMTV-PyMT tumors significantly

To further test whether the loss of any of the receptors affects tumor progression we bred HCA1<sup>-/-</sup>, HCA2<sup>-/-</sup> and FFA2<sup>-/-</sup> animals with animals carrying the MMTV-PyMT transgene that develop breast tumors spontaneously (137). Regular scoring including palpation of potential tumor sites was performed. For MMTV-PyMT<sup>+</sup>;HCA2<sup>-/-</sup> animals and their MMTV-PyMT<sup>+</sup>;HCA2<sup>+/+</sup> littermates no difference in tumor onset could be observed, the age of mice when the first palpable tumor developed did not differ significantly (Figure 19A). On average the first tumor of MMTV-PyMT<sup>+</sup>;HCA2<sup>-/-</sup> animals was palpable on day 81. The first palpable tumor of MMTV-PyMT<sup>+</sup>;HCA2<sup>+/+</sup> or all wild type animals pooled together could be found on average at day 85 respective day 76.5. Likewise, the growth curves showing the tumor volume in relation to time showed no significant difference in their growth rates (Figure 19C). In addition to that the knockout of HCA2 had no impact on the age of animals upon achieving the maximal total tumor volume of 1.7 cm<sup>3</sup> (Figure 19B). MMTV-PyMT<sup>+</sup>;HCA2<sup>-/-</sup> animals had to be sacrificed on average at day 119 while MMTV-PyMT<sup>+</sup>;HCA2<sup>+/+</sup> or all wild type animals pooled together had to be sacrificed at day 117 respective at day 120. In summary, the loss of HCA2 had no impact on growth and progression of MMTV-PyMT mammary tumors although their tumor stroma contained immune cells expressing HCA2.

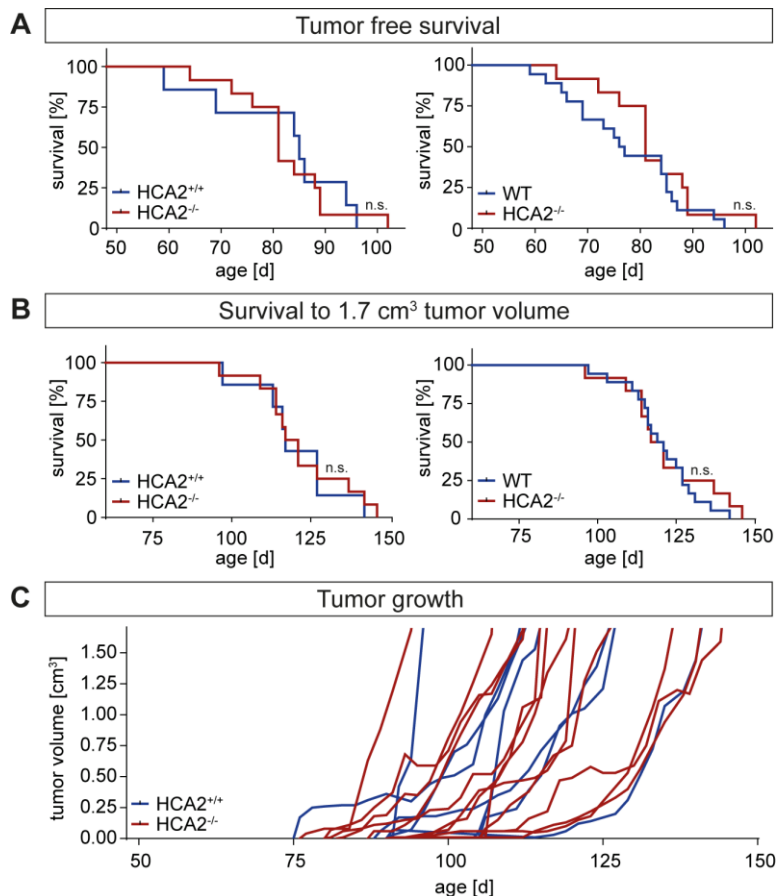


**Figure 19: MMTV-PyMT breast cancer model in HCA2<sup>-/-</sup> and HCA2<sup>+/+</sup> animals.** (A) Kaplan-Meier-curve of tumor free survival. Left panel HCA2<sup>+/+</sup> vs HCA2<sup>-/-</sup>, right panel all WT animals vs HCA2<sup>-/-</sup>. (B) Kaplan-Meier-curve of survival up to achieving the maximal tumor volume of 1.7 cm<sup>3</sup>. Left panel HCA2<sup>+/+</sup> vs HCA2<sup>-/-</sup>, right panel all WT animals vs HCA2<sup>-/-</sup>. (A,B) HCA2<sup>-/-</sup> n=12, HCA2<sup>+/+</sup> n=7, WT n=18; n.s. not significant, Log-rank-test. (C) Development of tumor volume over the course of the time. Each graph representing an individual.

The knockout of HCA1 in animals carrying the MMTV-PyMT transgene led to a slightly earlier onset of tumors on average on day 67.5 compared to average tumor onset for MMTV-PyMT<sup>+</sup>;HCA1<sup>+/+</sup> animals or all wild type animals pooled on day 80 respective on day 76.5. However, no significance was achieved (Figure 20A). The growth curves depicting the tumor volume in relation to time are generally steeper for MMTV-PyMT<sup>+</sup>;HCA1<sup>-/-</sup> animals and they were also shifted to the left which goes in line with the earlier tumor onset (Figure 20C). The combination of earlier onset of tumors and steeper growth curves resulted in a slightly but not significantly younger age when MMTV-PyMT<sup>+</sup>;HCA1<sup>-/-</sup> animals reached the maximal total tumor volume of 1.7 cm<sup>3</sup> compared to their MMTV-PyMT<sup>+</sup>;HCA1<sup>+/+</sup> littermates (Figure 20B, left panel). The experiment was impaired by a low animal number for the MMTV-PyMT<sup>+</sup>;HCA1<sup>+/+</sup> group. To mend this fact we compared the age of animals upon achieving the maximal total tumor volume of 1.7 cm<sup>3</sup> between the MMTV-PyMT<sup>+</sup>;HCA1<sup>-/-</sup> group and all wild type animals pooled together (Figure 20B, right

panel). HCA1 knockout mice carrying the MMTV-PyMT transgene had to be sacrificed at a significantly younger age (day 93.5) the wild type mice carrying the MMTV-PyMT transgene (day 115.5). These data imply that the loss of HCA1, which is primarily expressed in adipocytes of the MMTV-PyMT tumor stroma, can accelerate the onset of the tumors to a certain degree and the improvement in tumor growth can cause an earlier achievement of the finishing criteria, which is a total tumor volume of 1.7 cm<sup>3</sup>.

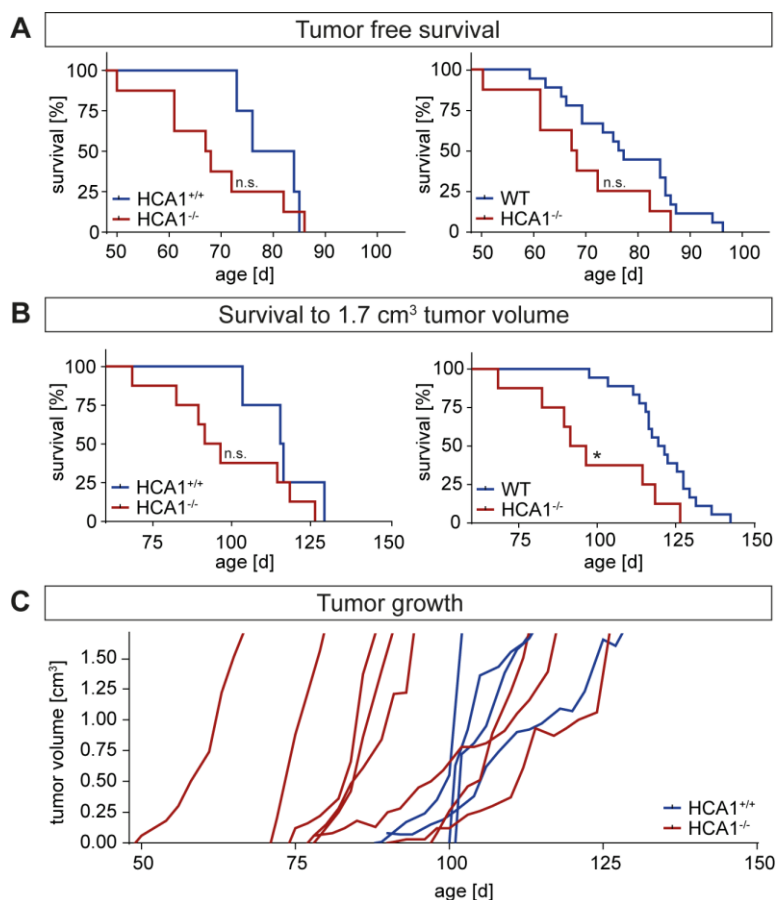


**Figure 20: MMTV-PyMT breast cancer model in HCA1<sup>-/-</sup> and HCA1<sup>+/+</sup> animals.** (A) Kaplan-Meier-curve of tumor free survival. Left panel HCA1<sup>+/+</sup> vs HCA1<sup>-/-</sup>, right panel all WT animals vs HCA1<sup>-/-</sup>. (B) Kaplan-Meier-curve of survival up to achieving the maximal tumor volume of 1.7 cm<sup>3</sup>. Left panel HCA1<sup>+/+</sup> vs HCA1<sup>-/-</sup>, right panel all WT animals vs HCA1<sup>-/-</sup>. (A, B) HCA1<sup>-/-</sup> n=8, HCA1<sup>+/+</sup> n=4, WT n=18; \*P < 0.05, n.s. not significant, Log-rank-test. (C) Development of tumor volume over the course of the time. Each graph representing an individual.

### 6.6.3 Knockout of FFA2 leads to earlier onset of MMTV-PyMT tumors

In FFA2 deficient mice carrying the MMTV-PyMT transgene, animals were significantly younger than their wild type littermates when the first palpable tumor occurred (Figure 21A left panel). The first tumor for MMTV-PyMT<sup>+</sup>;FFA2<sup>-/-</sup> animals was palpable on average at day 58.5. In contrast the

MMTV-PyMT<sup>+</sup>;FFA2<sup>+/+</sup> group and the group of all wild type animals showed their first palpable tumor on average at day 69 respective at day 76.5 (Figure 21A right panel). However, the tumors of MMTV-PyMT<sup>+</sup>;FFA2<sup>-/-</sup> animals grew at a rate comparable to those of the MMTV-PyMT<sup>+</sup>;FFA2<sup>+/+</sup> littermate animals (Figure 21C). The outcome of these two factors was a significantly younger age of MMTV-PyMT<sup>+</sup>;FFA2<sup>-/-</sup> animals upon achieving the maximal total tumor volume of 1.7 cm<sup>3</sup> (Figure 21) regardless if they are compared to the MMTV-PyMT<sup>+</sup>;FFA2<sup>+/+</sup> group or all wild type animals. On average MMTV-PyMT<sup>+</sup>;FFA2<sup>-/-</sup> animals had to be sacrificed at day 106.5; MMTV-PyMT<sup>+</sup>;FFA2<sup>+/+</sup> animals had to be sacrificed at day 122 and the group of all wild type animals had to be sacrificed at day 120. All together, the loss of FFA2 resulted in an earlier onset of MMTV-PyMT tumors and likewise in an earlier achieving of the maximal tumor volume.

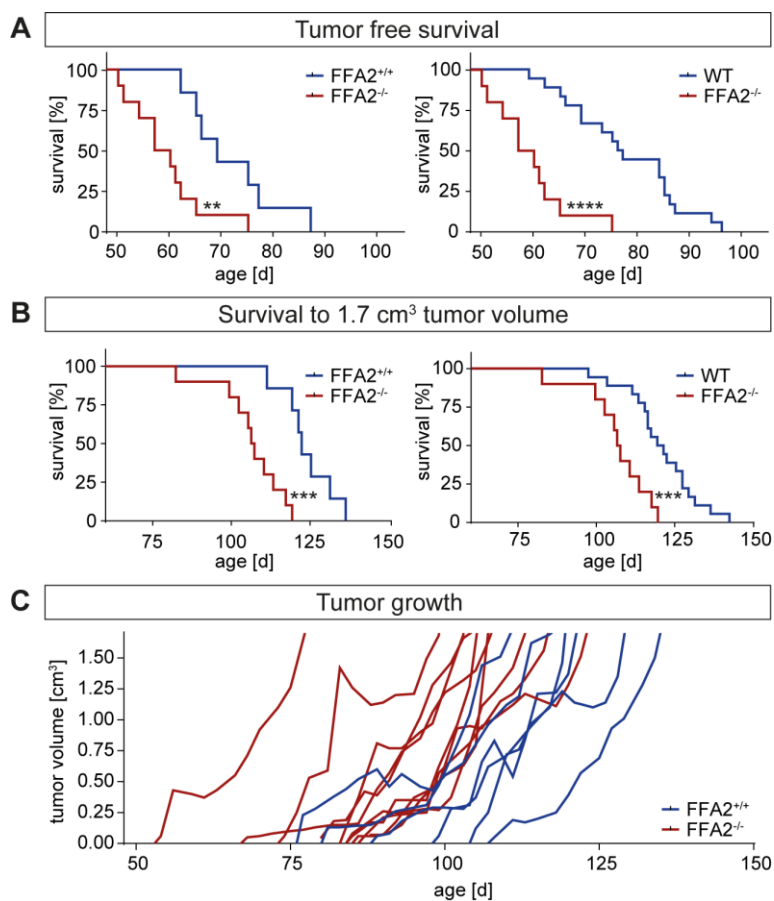


**Figure 21: MMTV-PyMT breast cancer model in FFA2<sup>-/-</sup> and FFA2<sup>+/+</sup> animals.** (A) Kaplan-Meier-curve of tumor free survival. Left panel FFA2<sup>+/+</sup> vs FFA2<sup>-/-</sup>, right panel all WT animals vs FFA2<sup>-/-</sup>. (B) Kaplan-Meier-curve of survival up to achieving the maximal tumor volume of 1.7 cm<sup>3</sup>. Left panel FFA2<sup>+/+</sup> vs FFA2<sup>-/-</sup>, right panel all WT animals vs FFA2<sup>-/-</sup>. (A, B) FFA2<sup>-/-</sup> n=10, FFA2<sup>+/+</sup> n=7, WT n=18; \*\* P < 0.01, \*\*\* P < 0.001, \*\*\*\* P < 0.0001, n.s. not significant, Log-rank-test. (C) Development of tumor volume over the course of the time. Each graph representing an individual.



#### 6.6.4 Knockout of HCA1, HCA2 or FFA2 does not change metastasis in MMTV-PyMT breast cancer model

The MMTV-PyMT breast cancer model is a very common model to study metastasis (123). In this connection, the lung is known as the main metastatic site (138). Therefore, we studied the lungs of experimental animals for metastatic growth by histologically analyzing the lungs of MMTV-PyMT positive knockout and wild type animals using the proliferation marker BrdU as well as Hematoxylin and Eosin staining. We analyzed sections of 5  $\mu$ M thickness every 600  $\mu$ M from ventral to dorsal orientation of the lungs. Number and area of metastases from the sections were added up. For MMTV-PyMT positive animals lacking HCA1, HCA2 or FFA2 and their respective littermates, frequent presence of metastases could be observed. However, number and area of metastases was not changed significantly (Figure 22). Metastases were found in all analyzed animals but one confirming a high metastases incidence (139). We found differences in metastasis for all the receptors. The deletion of HCA1 led to an increase in metastases number from 10 in the MMTV-PyMT<sup>+</sup>;HCA1<sup>+/+</sup> animals to 17 in the MMTV-PyMT<sup>+</sup>;HCA1<sup>-/-</sup> animals but it did not alter the metastatic area (Figure 22A, B). The deletion of HCA2 on the other hand caused a decrease of metastases along with an unchanged metastatic area (Figure 22C, D). The MMTV-PyMT<sup>+</sup>;FFA2<sup>+/+</sup> animals presented on average 8.2 metastases per lung compared to 5.1 metastases per MMTV-PyMT<sup>+</sup>;FFA2<sup>-/-</sup> lung (Figure 22 E). The metastatic area in MMTV-PyMT<sup>+</sup>;FFA2<sup>-/-</sup> lungs is also decreased compared to lungs of their wild type littermates (Figure 22 F). All the data have a considerable variation in common. Therefore, we compared the mice lacking the metabolite receptors to all pooled wild type mice (Figure 22). Nevertheless, no significance was obtained. The data from this setup of the model does not indicate an influence of the loss of any of the receptors on the formation of metastases.

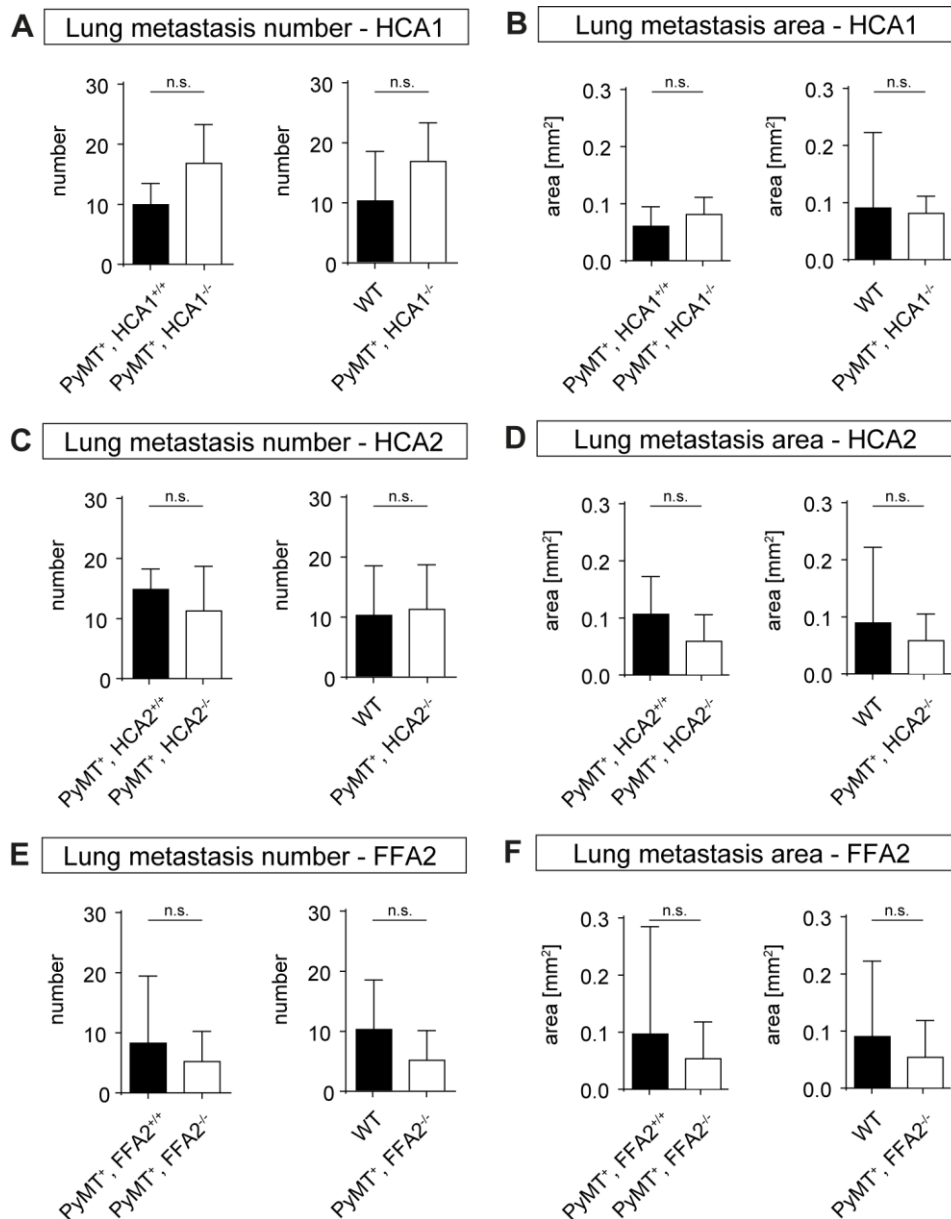


**Figure 22: Lung metastasis in the MMTV-PyMT model.** Lungs were stained with BrdU, Hematoxylin and Eosin. Sections of 5  $\mu\text{m}$  thickness every 600  $\mu\text{m}$  from ventral to dorsal orientation of the lungs were analyzed. Number and area of metastases from the sections were added up. n.s. not significant, mean $\pm$ SD; unpaired, two-tailed Student's *t*-test. (A) Metastases number at day of sacrifice. Left panel: MMTV-PyMT<sup>+</sup>;HCA1<sup>+/+</sup> (n=3) vs. MMTV-PyMT<sup>+</sup>;HCA1<sup>-/-</sup> (n=3), right panel: all wild type animals (n=12) vs. MMTV-PyMT<sup>+</sup>;HCA1<sup>-/-</sup>. (B) Metastases area in mm<sup>2</sup> at day of sacrifice. Left panel: MMTV-PyMT<sup>+</sup>;HCA1<sup>+/+</sup> vs. MMTV-PyMT<sup>+</sup>;HCA1<sup>-/-</sup>, right panel: all wild type animals vs. MMTV-PyMT<sup>+</sup>;HCA1<sup>-/-</sup>. (C) Metastases number at day of sacrifice. Left panel: MMTV-PyMT<sup>+</sup>;HCA2<sup>+/+</sup> (n=3) vs. MMTV-PyMT<sup>+</sup>;HCA2<sup>-/-</sup> (n=3), right panel: all wild type animals (n=12) vs. MMTV-PyMT<sup>+</sup>;HCA2<sup>-/-</sup>. (D) Metastases area in mm<sup>2</sup> at day of sacrifice. Left panel: MMTV-PyMT<sup>+</sup>;HCA2<sup>+/+</sup> vs. MMTV-PyMT<sup>+</sup>;HCA2<sup>-/-</sup>, right panel: all wild type animals vs. MMTV-PyMT<sup>+</sup>;HCA2<sup>-/-</sup>. (E) Metastases number at day of sacrifice. Left panel: MMTV-PyMT<sup>+</sup>;FFA2<sup>+/+</sup> (n=6) vs. MMTV-PyMT<sup>+</sup>;FFA2<sup>-/-</sup> (n=8), right panel: all wild type animals (n=12) vs. MMTV-PyMT<sup>+</sup>;FFA2<sup>-/-</sup>. (F) Metastases area in mm<sup>2</sup> at day of sacrifice. Left panel: MMTV-PyMT<sup>+</sup>;FFA2<sup>+/+</sup> vs. MMTV-PyMT<sup>+</sup>;FFA2<sup>-/-</sup>, right panel: all wild type animals vs. MMTV-PyMT<sup>+</sup>;FFA2<sup>-/-</sup>.



## 7 DISCUSSION

Our study showed the expression of HCA1 in solid human breast tumors and the expression of FFA4 in solid human colorectal tumors. In addition, the expression of HCA1 in human breast cancer cell lines as well as the expression of FFA4 in human colorectal cancer cell lines was confirmed (158, 159). Data indicating HCA2, FFA2 and FFA4 expression in macrophages was also confirmed by our study as we found the expression of these metabolite receptors in TAMs in all three tumor models (38, 47, 160). Surprisingly, the loss of HCA2 did not alter tumor growth and progression in any of the models. We also did not foresee that deletion of FFA4 had no impact on the LLC1 syngeneic tumor model and particularly on the AOM-DSS colorectal cancer model. The influence of HCA1 deletion was investigated in the MMTV-PyMT breast cancer model and revealed a moderately improved tumor growth. The absence of FFA2 did not affect tumor growth in the LLC1 model but led to an increased number of colorectal tumors in the AOM-DSS model while the tumor area remained unchanged. The most conclusive results were obtained with the deletion of FFA2 in the MMTV-PyMT model. Here, we demonstrate that the loss of FFA2 significantly reduces tumor latency and also significantly improves tumor growth. However, the formation of metastases in the LLC1 model and the MMTV-PyMT model did not show any changes upon the loss of any of the metabolite receptors. Together, our results describe a tumor protective effect of FFA2 with an unclear impact on metastatic processes.

### 7.1 The role of HCA1 in breast cancer

Many studies showed the expression of the lactate receptor HCA1 in different human tumor cell lines and human patient tumor samples (158, 159). High lactate concentrations in tumors correlate with poor patient prognosis (63-65). Therefore, it is widely perceived that HCA1 signaling is connected with enhanced tumor growth and survival, which differs from our findings. *Stäubert et al.* show *in vitro* data indicating that a siRNA mediated knockdown of HCA1 in human MCF7 breast cancer cells is able to decrease cell viability and mildly induces apoptosis (158). In the same manner *Lee et al.* suggest that an impaired growth as well as a slight increase in apoptosis of HCA1 silenced tumor cell lines might be a result of suppressed angiogenesis through the PI3K/AKT-cAMP response element binding protein (CREB) pathway (159). Both studies additionally utilize a xenograft model in which HCA1 silenced MCF7 cells are implanted orthotopically to immunodeficient mice. They observe a significantly decreased tumor growth and angiogenesis in HCA1 deficient tumors compared to the tumors of mice that received MCF7 cells treated with scrambled siRNA. These results may support the hypothesis that activation of HCA1 with lactate and the downstream signaling promote angiogenesis and rescue tumor cells from

apoptosis. However, the use of cell lines is afflicted with the absence of stromal cells. It is not possible to mimic the crucial effects of the tumor microenvironment on the investigated processes. The influence of stromal adipocytes and particularly the interactions between lactate and TAMs and T-cells, which is not necessarily HCA1 mediated, do not find access into a cell line-based model. In the xenograft model the recruitment of CAFs and vessel formation might be possible, but mechanisms will differ from the physiologic state. Animals used in a xenograft model are obligatory immunodeficient, thus no macrophage mediated vessel formation or T-cell recruitment can take place.

Our dissenting findings could result from the fact that we did not observe HCA1 expression on MMTV-PyMT tumor cells and also from effects of the microenvironment on tumor growth. It is known that lactate inhibits lipolysis in adipocytes via HCA1 receptor signaling in an insulin dependent manner (34). The antilipolytic effect upon application of glucose is conditioned on the one hand by HCA1 mediated inhibition of cAMP formation and on the other hand by the insulin receptor mediated cAMP degradation. In HCA1 deficient mice, the application of glucose resulted in a strongly decreased antilipolysis, hence to availability of FFAs and glycerol (34). The presence of adipocytes in the tumor stroma of MMTV-PyMT breast carcinomas could offer an explanation for the improved tumor growth in the absence of HCA1, because consistent lipolysis would offer increased FFAs level. As mentioned before FFAs serve as invaluable nutrients for tumor cells. The uptake of exogenous FFAs contributes to cover the tumor cells' high demand in lipids which can be used as intermediates in the production of ATP, as building blocks or as signaling molecules (91). Lactate in the tumor microenvironment is also used to promote tumor growth in a HCA1-independent manner. It polarizes TAMs from the antitumoral M1 type to the protumoral M2 type and it can inhibit the pro-inflammatory response of macrophages and T-cells in the tumor stroma (161, 162). The abrogation of lipolysis in adipocytes and a constant aerobic glycolysis may yield lactate levels which are high enough modulate the immune response. Recent research in human lung cancer also suggested that HCA1 receptor signaling in tumor cells decreasing cAMP levels and inhibiting PKA causes activation of the transcriptional coactivator TAZ that interacts with the transcription factor TEAD and so induces the expression of programmed cell death protein 1 ligand (PD-L1) (163). PD-L1 leads to a reduction in interferon- $\gamma$  (IFN- $\gamma$ ) production and the induction of apoptosis in T-cells. These tumor-promoting consequences of HCA1 deletion might outweigh the effects observed in the *in vitro* studies. In summary, we observed a tumor promoting effect of HCA1 deletion in MMTV-PyMT positive animals. As this is contradictory to some existing studies, the role of HCA1 in breast cancer remains elusive. The adipocyte-specific deletion of

HCA1 in the MMTV-PyMT breast cancer model could offer insights in the absence of antilipolysis and the resulting availability of FFAs as a putative mechanism for enhanced tumor growth.

## 7.2 Expression of HCA2 in tumor-associated macrophages and its role in tumor development

We found HCA2 expression in immune cells particularly macrophages what is in line with existing studies (160, 164). Only little is known about the function of HCA2 signaling in macrophages. *Shi et al.* suggest inhibition of chemoattractant-mediated macrophage migration and a resulting downregulation of inflammation as a possible result of HCA2 activation (160). A recent study demonstrated that activation of HCA2 in bone marrow derived macrophages suppresses a pro-inflammatory macrophage function by inhibiting the production of pro-inflammatory cytokines, the uptake of low-density lipoprotein and by impairing chemotaxis (44). In all tumor models, the expression of HCA2 in TAMs apparently did not play a substantial role as tumor development in HCA2 deficient mice remained unchanged. The LLC1 model showed a rather small population of HCA2<sup>mRFP</sup> positive TAMs. Herein the missing effect of HCA2 deletion in LLC1 tumor bearing mice can be reasoned.

The role of HCA2 in breast cancer is likewise poorly investigated. *Elangovan et al.* discovered expression of HCA2 in human mammary tissue whereas HCA2 expression was undetectable in malignant mammary tissue as well as in human breast cancer cell lines (165). Moreover, they deleted HCA2 in mice carrying the MMTV-Neu transgene and observed enhanced tumor growth and declined survival asserting a tumor-protective effect of HCA2 (165). In our study, similarly negative results for HCA2 expression in human patient samples were obtained. The genetically engineered model for murine breast cancer generated divergent insights. We could not detect a change in tumor latency, animal survival and metastasis formation. Possible reasons therefore can be found when comparing the models. Although the rat homolog of ErbB2 (Neu) and PyMT are both expressed under the control of the MMTV promoter there are considerable differences. MMTV-Neu positive female animals develop palpable breast carcinomas not before the age of five months (166), whereas in the MMTV-PyMT model less than half the time is required. Additionally, the MMTV-Neu model shows a minor tumor incidence leading to a decreased aggressiveness of tumors compared to the MMTV-PyMT model where an effect of the deletion of HCA2 perhaps did not appear within the experiment period. Another discrepancy lies in the experimental setup. In the existing study, the animals were monitored until they had to be euthanized because of tumor or metastasis related morbidity. A difference in survival was only demonstrated after 275 days (165). However, in our study, the animals were sacrificed at a total

tumor volume of 1.7 cm<sup>3</sup> and none of the animals showed any interference of tumors and metastases with normal healthy behavior. In summary, an impact of HCA2 signaling on the development of breast cancer remains unclear. Further research has to be conducted in order to elucidate the role of HCA2.

In the investigation of HCA2 related effects in the context of colon cancer, a study by *Singh et al.* received plenty of attention. They claim HCA2 is expressed in monocytes and dendritic cells orchestrating the differentiation of T-reg cells and the production of the pro-inflammatory cytokine IL-17 and the anti-inflammatory cytokine IL-10 in the lamina propria of the colon (157). Furthermore, the authors suggest that butyrate or niacin can activate HCA2 in order to impart the anti-inflammatory cascade. The knockout of HCA2 in animals treated with AOM and DSS led to a more severe weight loss, increased diarrhea, rectal bleeding and polyp development as well as decreased IL-10 and increased IL-17 levels compared to wild type animals (157). Reciprocal transplantations of bone marrow between HCA2 deficient animals to wild type animals showed that both hematopoietic and non-hematopoietic cells contribute to the discovered phenotype. The role of gut microbiota that are known to produce butyrate was investigated by the use of antibiotics. Antibiotic treatment before AOM application in wild type animals resulted in increased inflammation and polyp formation whereas the AOM-DSS effect in HCA2 deficient mice was ameliorated (157). These data deviate certainly from our findings, as we could not detect a significant impact of HCA2 knockout on weight development, diarrhea, rectal bleeding and polyp formation. We could confirm HCA2 expression in TAM but did not detect it in dendritic cells. However, HCA2 deficient mice showed impaired weight recovery from the DSS treatment but this did not affect other factors. In general, we observed more polyps in the wild type mice and a larger variance of the results. We used a sufficient animal number of 12 animals per group whereas *Singh et al.* used only 6 animals per group what even emphasizes the occurred variance of our findings. Another difference in the experimental setup lies in the use of DSS. They applied two cycles of 6 days of 2% DSS and one cycle of 2 days of 1% DSS. We identified a concentration of 1.8% in 3 cycles of 5 days each as the most viable experimental setup in order to generate weight loss and diarrhea as a reaction to the DSS but not to lose animals because they underwent a weight loss of 20%. AOM dose did not differ between the studies. As *Singh et al.* proved with the use of antibiotics, the gut microbiome plays an essential role in the AOM-DSS colorectal cancer model. The study remains inconclusive about the background of the HCA2 deficient and the wild type animals and moreover, it is not stated whether littermates were utilized. The use of littermates is crucial as we can assume that littermates share a similar microbiome (167). Strain dependent differences can be eliminated as well as differences arising from separated housing. As *Singh et*

*al.* do not testify about background and housing conditions these factors cannot be excluded as explanations for divergent results. Together, our results do not indicate a role of HCA2 in the tumor models tested. Whether the expression of HCA2 in macrophages can affect other inflammatory or malignant diseases and which mechanistic cascades regulate a possible function of HCA2 in inflammatory colon cancer shall be the subject of more extensive research.

### **7.3 FFA4 effects in tumor growth remain unclear**

Our findings revealed FFA4 expression in human solid colon tumors and in human tumor cell lines as well as in murine TAMs and in the murine colonic epithelium. However, a knockout of FFA4 did not cause any alteration in primary tumor growth and metastasis in any of the tumor models. Previous studies demonstrated an anti-inflammatory effect of FFA4 signaling in macrophages via  $\beta$ -arrestin recruitment of the receptor that blocks interaction of TGF- $\beta$ -activated kinase 1 binding protein (TAB-1) with TGF- $\beta$ -activated kinase 1 (TAK1) and downregulates the production and release of pro-inflammatory mediators (38). Nevertheless, little research about the role of FFA4 in tumors has been conducted. FFA4 expression was detected in human colorectal carcinoma cell lines and patient samples (168, 169). *Wu et al.* point out that FFA4 signaling activates the PI3K/AKT-NF- $\kappa$ B pathway with following release of VEGF, IL-8 and PGE<sub>2</sub> (168). In addition to the angiogenetic switch, hints for FFA4 promoting EMT were given. In a xenograft model, the knockdown of FFA4 in HCT-116 colorectal carcinoma cells that were implanted to immunodeficient mice did not lead to an altered tumor growth. The utilization of cell lines and a xenograft model does not display the crucial effects of the tumor microenvironment particularly the effect of FFA4 deficiency in TAMs. In summary, present data are inconclusive about the physiological and pathophysiological function of FFA4 in colorectal tumor cells, TAMs and stromal adipocytes.

### **7.4 The tumor-protective effect of FFA2**

The knockout of FFA2 in the LLC1 syngeneic tumor model did not alter primary tumor growth. Present data indicate controversial roles of FFA2 signaling in different immune cells. We detected FFA2 in CD45 positive cells in LLC1 tumor primarily in macrophages. Therefore, we expected either delayed or enhanced tumor growth. The reason for the absence of any effect might be the relatively small fraction of FFA2 positive cells.

We identified only small fractions of immune cells in the AOM-DSS colorectal cancer model as FFA2 positive, and the deletion of FFA2 did not affect weight development. However, a significantly increased tumor number compared to littermates but not compared to all wild type

animals points towards an anti-inflammatory function of FFA2. *Sivaprakasam et al.* obtained similar results in an AOM-DSS model and showed a beneficial influence of FFA2 signaling on the growth of bacteria that are essential for a healthy gut microbiome (170). Earlier studies already discovered possible mechanisms of FFA2 involvement in colitis and colon cancer formation. It was shown that germ-free mice possess lower amounts of SCFA in their gut and have a greater suffering in DSS colitis experiment which was ameliorated by the application of SCFAs. In FFA2 deficient mice, a similar suffering was observed but application of SCFAs was ineffective (171, 172). Acetate mediated FFA2 signaling in neutrophils caused release of ROS and phagocytic activity in wild type animals but not in FFA2 deficient mice (171). To prove that immune cells are responsible for the phenotype *Maslowski et al.* used bone marrow chimeras and implanted bone marrow from FFA2 deficient mice to wild type mice which resulted in the same phenotype as in globally FFA2 deficient animals (171). Later *Smith et al.* revealed SCFAs regulating T-reg cells in colonic inflammation in a FFA2-dependant manner in order to attenuate colitis (172). The application of SCFAs to germ-free mice significantly increased the number of colonic T-reg cells and the expression of transcription factor *Foxp3* and IL-10 on the T-reg cells indicating anti-inflammatory effects (172). FFA2 expression in T-reg cells was significantly elevated and the ligand propionate could only stimulate *Foxp3* and IL-10p production in wild type but not in FFA2 knockout animals. A reduced expression of histone deacetylases (HDACs) and enhanced acetylation were demonstrated to be additional FFA2 dependent consequences of propionate application (172). To link their findings to colitis the group used a T cell transfer colitis model. Either naïve T cells only or naïve T cells in combination with T-reg cells were injected to lymphopenic mice causing colitis in the T cell only group. T cell transfer to wild type and FFA2 deficient animals in combination with propionate administration revealed significantly reduced inflammatory parameters in propionate treated wild type animals compared to their FFA2 deficient counterparts (172). A recent study of Pan et al. contains results similar to our findings whereby they used a modified AOM-DSS model (114). The data support the idea that loss of FFA2 causes an overexpression of its downstream cAMP-PKA-CREB-HDAC signaling with following dysregulation of inflammation suppressor genes (114). Additionally to the role of FFA2 as an epigenetic regulator for the suppression of tumorigenesis, the importance of FFA2 in colonic neutrophil homeostasis is highlighted. FFA2 deficiency resulted in infiltration of neutrophils into the lamina propria and enhanced cancer formation in AOM-DSS treated colons. Moreover, the study confirmed the correlation between HDAC overexpression and FFA2 deficiency (114).

Nevertheless, studies offering contradictory data for the role of FFA2 in inflammation and colon cancer do exist. *Sina et al.* also detect FFA2 expression on neutrophils in the colon but upon DSS



treatment of FFA2 deficient animals, the neutrophil migration and inflammatory tissue destruction decrease compared to wild type animals (49). *Ex vivo* experiments present FFA2 as a mediator inducing neutrophil chemotaxis via p38 MAPK signaling. However, DSS treatment in this study results in increased morbidity of FFA2 knockout animals (49). The use of scores and indices with unclear explanation of composition complicate comparison to other studies of the subject. Further research indicating pro-inflammatory function of FFA2 was conducted by *Kim et al.* showing a reduced response on chemically induced inflammation or bacterial infection in the colon (173). Application of SCFAs promoted the production of cytokines and chemokines under inflammatory conditions. In the following, leukocyte recruitment and T cell activation was mediated by FFA2 and FFA3 in an ERK1/2 and p38 MAPK dependent manner (173). Recently, the same group published data showing increased severity and morbidity in FFA2 deficient mice in a DSS colitis model. They now highlight FFA2 as a mediator of epithelial barrier immunity and suppressor of inflammation and colon carcinogenesis (174). All the studies include considerations about varying results in other research. Possible reasons named are for example differences in the genetic background of the mice, housing conditions, experimental models and different functions of FFA2 in different stages of inflammation, hyperplasia and carcinogenesis. To obtain reliable insights in the role of FFA2 in colon cancer progression assimilation of inflammation and carcinogenesis models and experimental conditions are of crucial importance.

Putative functions of FFA2 in breast cancer progression are poorly understood. The effects of FFA2 and FFA3 signaling were investigated by *Thirunavukkarasan et al.* and they showed that FFA2 overexpression in MCF7 and MDA-MB-231 human breast cancer cell lines inhibits the Hippo-YAP pathway and increases the expression of the adhesion protein E-cadherin (175). The authors deduct that FFA2 and FFA3 drive tumor cells from the mesenchymal to the epithelial phenotype, thus reduce inflammation and potentially hinder metastasis (175). In the MMTV-PyMT breast cancer model, we could not detect tumor cells expressing FFA2. Hence, we cannot confirm or disprove their conclusions. Immune cells and white adipocytes express relevant levels of FFA2. We detected that nearly all FFA2 positive cells in MMTV-PyMT are also positive for CD45, marking them as immune cells. The largest fraction of FFA2 positive immune cells was formed by macrophages. Little is known about the specific function of FFA2 in macrophages. Interestingly, a study conducted by *Nakajima et al.* demonstrates that FFA2 overexpression in adipocytes results in the release of TNA- $\alpha$  from M2 type macrophages (176). The tumor stroma is predominantly populated with macrophages of the M2 type (177). As FFA2 expressing white adipocytes are also a part of the tumor stroma the described mechanism might be transmissible to the situation in the MMTV-PyMT tumor stroma. A knockout of FFA2 would sequentially lead to a decreased TNF- $\alpha$

level. The binding of TNF- $\alpha$  to its receptor promotes Caspase-8 mediated cell death in form of apoptosis or necroptosis (178). A reduction in apoptosis or necroptosis can enhance tumor growth and progression as observed in the MMTV-PyMT<sup>+</sup>;FFA2<sup>-/-</sup> animals. Because of the abundance of adipocytes in the mammary fat pad, the described mechanism can already come into force when the first aberrant cells develop resulting in a protumoral effect of FFA2 deficiency.

Several other functions of TAMs have been described whereas none of them is linked to FFA2 signaling yet. The activation or mutation of KRAS in TAMs promotes NF- $\kappa$ B mediated transcription of epidermal growth factor (EGF) and EGF receptor activation resulting in improved migration of MMTV-PyMT tumor cells (179). EGF activation affects CAFs and the extracellular matrix in order to facilitate migration that can cause infiltration of tumor cells into neighboring tissues as well as metastasis formation. In human breast cancers, the expression of human epidermal growth factor receptor 2 (HER2) correlates with a poor prognosis (180). If FFA2 was involved in these signaling processes it would presumably suppress the KRAS signaling pathway. Therefore, uncoupling of FFA2 signaling might result in increased transcription of EGF and improved tumor progression. *DeNardo et al.* propose that regulatory factors such as IL-4, IL-13 and possibly IFN- $\gamma$  mediate the expression of EGF in TAMs and hence promote infiltration and metastasis (181). Furthermore, in a mouse model of HER2 positive breast cancer (MMTV-HER2) a subpopulation of cancer cells requires TAMs for their early dissemination (182). The tumor cells and TAMs release cytokine CCL2 in order to attract CD206 positive macrophages. Consequently, Wnt-1 is upregulated and E-cadherin junctions in tumor cells are downregulated pushing the tumor cells to a pro-inflammatory mesenchymal phenotype. FFA2 would have a suppressive function in this mechanism as, according to our findings, FFA2 deficiency leads to a shorter tumor latency and enhanced tumor growth. Further research is required to elucidate the role of FFA2 in the breast cancer microenvironment and also its downstream signaling pathways. Our findings indicate that antagonism of FFA2 can impede the development of aberrant cells and following breast tumor formation in the MMTV-PyMT model. As a GPCR FFA2 is easily accessible for pharmacological interventions and might offer new therapeutic approaches to treat mammary tumors.

### **7.5 Studying metastases formation in the LLC1 syngeneic tumor model and the MMTV-PyMT breast cancer model**

In our study, the focus was put on primary tumor growth and metastasis formation was only a secondary read-out. This reflects in the experimental design of the LLC1 syngeneic and the MMTV-PyMT breast cancer model. In the LLC1 model, we sacrificed each animal group when the primary tumor size reached the endpoint or when morbidity required the end of the experiment.



We did not observe lung metastases at all. As the LLC1 model is often used to study lung metastases we can suggest that time for sufficient metastasis formation was too short. Indeed, other variants of the LLC1 model are preferred for this application. Intravenous injection of tumor cells is the most straightforward approach. Two weeks after injection metastatic nodules in the lung can be analyzed (126). Another approach is the subcutaneous injection of tumor cells with following dissection of the primary tumor. Here, two weeks after injection of the tumor cells the newly developed primary tumor is surgically removed. Afterwards, the animals are kept for two more weeks before lung metastasis analysis is carried out (183). As our findings did not indicate a change in primary tumor growth upon metabolite receptor deficiency, we resigned from performing a study focusing on the influence of metabolite receptor deficiency on metastasis formation.

The MMTV-PyMT breast cancer model is known as a strong tool to study lung metastasis formation in mammary tumor bearing mice. As described above, our focus lay on primary tumor development, thus we sacrificed the animals when the total tumor volume reached the endpoint. No animal showed signs of tumor or metastasis related morbidity. We detected lung metastases in nearly all animals, but no significance was achieved and variance was high. The absent significance might relate to the different time points of sacrificing. Because of comparable growth rates and only different tumor latency, the period for metastasis formation in all animals remained similar. To create a robust setup for the investigation of metastatic processes a fixed time point for sacrificing should be set. In that way the earlier onset e.g. in MMTV-PyMT<sup>+</sup>;FFA2<sup>-/-</sup> animals compared to their wild type counterparts would also result in a prolonged period of metastasis and presumably in an increase of metastases number and area. These investigations are a central jigsaw piece of further research on the topic in order to elucidate the function and downstream signaling pathways of FFA2 in breast cancer. In clinical patients, the circumvention of metastasis can determine patient survival and is therefore an attractive target of pharmacological intervention.

## 8 REFERENCES

1. Bray F, Ferlay J, Soerjomataram I, Siegel RL, Torre LA, Jemal A. Global cancer statistics 2018: GLOBOCAN estimates of incidence and mortality worldwide for 36 cancers in 185 countries. *CA: a cancer journal for clinicians*. 2018;68(6):394-424.
2. Hanahan D, Weinberg RA. The hallmarks of cancer. *Cell*. 2000;100(1):57-70.
3. Hanahan D, Weinberg RA. Hallmarks of cancer: the next generation. *Cell*. 2011;144(5):646-74.
4. Pavlova NN, Thompson CB. The Emerging Hallmarks of Cancer Metabolism. *Cell metabolism*. 2016;23(1):27-47.
5. DeBerardinis RJ, Chandel NS. Fundamentals of cancer metabolism. *Science advances*. 2016;2(5):e1600200.
6. Kruiswijk F, Labuschagne CF, Vousden KH. p53 in survival, death and metabolic health: a lifeguard with a licence to kill. *Nature reviews Molecular cell biology*. 2015;16(7):393-405.
7. Stine ZE, Walton ZE, Altman BJ, Hsieh AL, Dang CV. MYC, Metabolism, and Cancer. *Cancer discovery*. 2015;5(10):1024-39.
8. Barthel A, Okino ST, Liao J, Nakatani K, Li J, Whitlock JP, Jr., et al. Regulation of GLUT1 gene transcription by the serine/threonine kinase Akt1. *The Journal of biological chemistry*. 1999;274(29):20281-6.
9. Dibble CC, Manning BD. Signal integration by mTORC1 coordinates nutrient input with biosynthetic output. *Nature cell biology*. 2013;15(6):555-64.
10. Vogelstein B, Kinzler KW. Cancer genes and the pathways they control. *Nature medicine*. 2004;10(8):789-99.
11. Yuan TL, Cantley LC. PI3K pathway alterations in cancer: variations on a theme. *Oncogene*. 2008;27(41):5497-510.
12. Wieman HL, Wofford JA, Rathmell JC. Cytokine stimulation promotes glucose uptake via phosphatidylinositol-3 kinase/Akt regulation of Glut1 activity and trafficking. *Molecular biology of the cell*. 2007;18(4):1437-46.
13. Warburg O, Wind F, Negelein E. The Metabolism of Tumors in the Body. *J Gen Physiol*. 1927;8(6):519-30.
14. Warburg O. Über den Stoffwechsel der Carcinomzelle. *Naturwissenschaften*. 1924;12(50):1131-7.
15. Eagle H. The minimum vitamin requirements of the L and HeLa cells in tissue culture, the production of specific vitamin deficiencies, and their cure. *The Journal of experimental medicine*. 1955;102(5):595-600.
16. Vander Heiden MG, Cantley LC, Thompson CB. Understanding the Warburg effect: the metabolic requirements of cell proliferation. *Science (New York, NY)*. 2009;324(5930):1029-33.

17. Boroughs LK, DeBerardinis RJ. Metabolic pathways promoting cancer cell survival and growth. *Nature cell biology*. 2015;17(4):351-9.
18. Vaupel P, Kallinowski F, Okunieff P. Blood flow, oxygen and nutrient supply, and metabolic microenvironment of human tumors: a review. *Cancer research*. 1989;49(23):6449-65.
19. Commisso C, Davidson SM, Soydaner-Azeloglu RG, Parker SJ, Kamphorst JJ, Hackett S, et al. Macropinocytosis of protein is an amino acid supply route in Ras-transformed cells. *Nature*. 2013;497(7451):633-7.
20. Krajcovic M, Krishna S, Akkari L, Joyce JA, Overholtzer M. mTOR regulates phagosome and entotic vacuole fission. *Molecular biology of the cell*. 2013;24(23):3736-45.
21. Stolzing A, Grune T. Neuronal apoptotic bodies: phagocytosis and degradation by primary microglial cells. *FASEB journal : official publication of the Federation of American Societies for Experimental Biology*. 2004;18(6):743-5.
22. Kerr MC, Teasdale RD. Defining macropinocytosis. *Traffic (Copenhagen, Denmark)*. 2009;10(4):364-71.
23. Kamphorst JJ, Cross JR, Fan J, de Stanchina E, Mathew R, White EP, et al. Hypoxic and Ras-transformed cells support growth by scavenging unsaturated fatty acids from lysophospholipids. *Proceedings of the National Academy of Sciences of the United States of America*. 2013;110(22):8882-7.
24. Cheung EC, Lee P, Ceteci F, Nixon C, Blyth K, Sansom OJ, et al. Opposing effects of TIGAR- and RAC1-derived ROS on Wnt-driven proliferation in the mouse intestine. *Genes & development*. 2016;30(1):52-63.
25. Chandel NS, Tuveson DA. The promise and perils of antioxidants for cancer patients. *The New England journal of medicine*. 2014;371(2):177-8.
26. Gorrini C, Harris IS, Mak TW. Modulation of oxidative stress as an anticancer strategy. *Nature reviews Drug discovery*. 2013;12(12):931-47.
27. Wang R, Dillon CP, Shi LZ, Milasta S, Carter R, Finkelstein D, et al. The transcription factor Myc controls metabolic reprogramming upon T lymphocyte activation. *Immunity*. 2011;35(6):871-82.
28. Eberhardy SR, Farnham PJ. c-Myc mediates activation of the cad promoter via a post-RNA polymerase II recruitment mechanism. *The Journal of biological chemistry*. 2001;276(51):48562-71.
29. Cunningham JT, Moreno MV, Lodi A, Ronen SM, Ruggero D. Protein and nucleotide biosynthesis are coupled by a single rate-limiting enzyme, PRPS2, to drive cancer. *Cell*. 2014;157(5):1088-103.
30. Mannava S, Grachtchouk V, Wheeler LJ, Im M, Zhuang D, Slavina EG, et al. Direct role of nucleotide metabolism in C-MYC-dependent proliferation of melanoma cells. *Cell cycle (Georgetown, Tex)*. 2008;7(15):2392-400.
31. Ahn CS, Metallo CM. Mitochondria as biosynthetic factories for cancer proliferation. *Cancer & metabolism*. 2015;3(1):1.

32. Lee JV, Carrer A, Shah S, Snyder NW, Wei S, Venneti S, et al. Akt-dependent metabolic reprogramming regulates tumor cell histone acetylation. *Cell metabolism*. 2014;20(2):306-19.
33. Sabari BR, Tang Z, Huang H, Yong-Gonzalez V, Molina H, Kong HE, et al. Intracellular crotonyl-CoA stimulates transcription through p300-catalyzed histone crotonylation. *Molecular cell*. 2015;58(2):203-15.
34. Ahmed K, Tunaru S, Tang C, Muller M, Gille A, Sassmann A, et al. An autocrine lactate loop mediates insulin-dependent inhibition of lipolysis through GPR81. *Cell metabolism*. 2010;11(4):311-9.
35. Tunaru S, Kero J, Schaub A, Wufka C, Blaukat A, Pfeffer K, et al. PUMA-G and HM74 are receptors for nicotinic acid and mediate its anti-lipolytic effect. *Nature medicine*. 2003;9(3):352-5.
36. Offermanns S. Free fatty acid (FFA) and hydroxy carboxylic acid (HCA) receptors. *Annu Rev Pharmacol Toxicol*. 2014;54:407-34.
37. Hirasawa A, Tsumaya K, Awaji T, Katsuma S, Adachi T, Yamada M, et al. Free fatty acids regulate gut incretin glucagon-like peptide-1 secretion through GPR120. *Nature medicine*. 2005;11(1):90-4.
38. Oh DY, Talukdar S, Bae EJ, Imamura T, Morinaga H, Fan W, et al. GPR120 is an omega-3 fatty acid receptor mediating potent anti-inflammatory and insulin-sensitizing effects. *Cell*. 2010;142(5):687-98.
39. Brown AJ, Goldsworthy SM, Barnes AA, Eilert MM, Tcheang L, Daniels D, et al. The Orphan G protein-coupled receptors GPR41 and GPR43 are activated by propionate and other short chain carboxylic acids. *The Journal of biological chemistry*. 2003;278(13):11312-9.
40. Tang C, Ahmed K, Gille A, Lu S, Grone HJ, Tunaru S, et al. Loss of FFA2 and FFA3 increases insulin secretion and improves glucose tolerance in type 2 diabetes. *Nature medicine*. 2015;21(2):173-7.
41. Cai TQ, Ren N, Jin L, Cheng K, Kash S, Chen R, et al. Role of GPR81 in lactate-mediated reduction of adipose lipolysis. *Biochemical and biophysical research communications*. 2008;377(3):987-91.
42. Liu C, Wu J, Zhu J, Kuei C, Yu J, Shelton J, et al. Lactate inhibits lipolysis in fat cells through activation of an orphan G-protein-coupled receptor, GPR81. *The Journal of biological chemistry*. 2009;284(5):2811-22.
43. Taggart AK, Kero J, Gan X, Cai TQ, Cheng K, Ippolito M, et al. (D)-beta-Hydroxybutyrate inhibits adipocyte lipolysis via the nicotinic acid receptor PUMA-G. *The Journal of biological chemistry*. 2005;280(29):26649-52.
44. Zandi-Nejad K, Takakura A, Jurewicz M, Chandraker AK, Offermanns S, Mount D, et al. The role of HCA2 (GPR109A) in regulating macrophage function. *FASEB journal : official publication of the Federation of American Societies for Experimental Biology*. 2013;27(11):4366-74.

45. Soga T, Kamohara M, Takasaki J, Matsumoto S, Saito T, Ohishi T, et al. Molecular identification of nicotinic acid receptor. *Biochemical and biophysical research communications*. 2003;303(1):364-9.
46. Wise A, Foord SM, Fraser NJ, Barnes AA, Elshourbagy N, Eilert M, et al. Molecular identification of high and low affinity receptors for nicotinic acid. *The Journal of biological chemistry*. 2003;278(11):9869-74.
47. Nilsson NE, Kotarsky K, Owman C, Olde B. Identification of a free fatty acid receptor, FFA2R, expressed on leukocytes and activated by short-chain fatty acids. *Biochemical and biophysical research communications*. 2003;303(4):1047-52.
48. Senga T, Iwamoto S, Yoshida T, Yokota T, Adachi K, Azuma E, et al. LSSIG is a novel murine leukocyte-specific GPCR that is induced by the activation of STAT3. *Blood*. 2003;101(3):1185-7.
49. Sina C, Gavrilova O, Forster M, Till A, Derer S, Hildebrand F, et al. G protein-coupled receptor 43 is essential for neutrophil recruitment during intestinal inflammation. *Journal of immunology (Baltimore, Md : 1950)*. 2009;183(11):7514-22.
50. Gotoh C, Hong YH, Iga T, Hishikawa D, Suzuki Y, Song SH, et al. The regulation of adipogenesis through GPR120. *Biochemical and biophysical research communications*. 2007;354(2):591-7.
51. Miyauchi S, Hirasawa A, Iga T, Liu N, Itsubo C, Sadakane K, et al. Distribution and regulation of protein expression of the free fatty acid receptor GPR120. *Naunyn-Schmiedeberg's archives of pharmacology*. 2009;379(4):427-34.
52. Som P, Atkins HL, Bandyopadhyay D, Fowler JS, MacGregor RR, Matsui K, et al. A fluorinated glucose analog, 2-fluoro-2-deoxy-D-glucose (F-18): nontoxic tracer for rapid tumor detection. *Journal of nuclear medicine : official publication, Society of Nuclear Medicine*. 1980;21(7):670-5.
53. Koppenol WH, Bounds PL, Dang CV. Otto Warburg's contributions to current concepts of cancer metabolism. *Nature reviews Cancer*. 2011;11(5):325-37.
54. WEINHOUSE S, WARBURG O, BURK D, SCHADE AL. On Respiratory Impairment in Cancer Cells. *Science (New York, NY)*. 1956;124(3215):267-72.
55. Warburg O. On the Origin of Cancer Cells. *Science (New York, NY)*. 1956;123(3191):309-14.
56. Cavalli LR, Varella-Garcia M, Liang BC. Diminished tumorigenic phenotype after depletion of mitochondrial DNA. *Cell growth & differentiation : the molecular biology journal of the American Association for Cancer Research*. 1997;8(11):1189-98.
57. Morais R, Zinkewich-Peotti K, Parent M, Wang H, Babai F, Zollinger M. Tumor-forming ability in athymic nude mice of human cell lines devoid of mitochondrial DNA. *Cancer research*. 1994;54(14):3889-96.
58. Tan AS, Baty JW, Dong LF, Bezawork-Geleta A, Endaya B, Goodwin J, et al. Mitochondrial genome acquisition restores respiratory function and tumorigenic



potential of cancer cells without mitochondrial DNA. *Cell metabolism*. 2015;21(1):81-94.

59. Brand K, Leibold W, Lupp A, Schoerner C, Schulz A. Metabolic alterations associated with proliferation of mitogen-activated lymphocytes and of lymphoblastoid cell lines: evaluation of glucose and glutamine metabolism. *Immunobiology*. 1986;173(1):23-34.

60. Shim H, Chun YS, Lewis BC, Dang CV. A unique glucose-dependent apoptotic pathway induced by c-Myc. *Proceedings of the National Academy of Sciences of the United States of America*. 1998;95(4):1511-6.

61. Fantin VR, St-Pierre J, Leder P. Attenuation of LDH-A expression uncovers a link between glycolysis, mitochondrial physiology, and tumor maintenance. *Cancer cell*. 2006;9(6):425-34.

62. Altenberg B, Greulich KO. Genes of glycolysis are ubiquitously overexpressed in 24 cancer classes. *Genomics*. 2004;84(6):1014-20.

63. Walenta S, Mueller-Klieser WF. Lactate: mirror and motor of tumor malignancy. *Seminars in radiation oncology*. 2004;14(3):267-74.

64. Walenta S, Wetterling M, Lehrke M, Schwickert G, Sundfor K, Rofstad EK, et al. High lactate levels predict likelihood of metastases, tumor recurrence, and restricted patient survival in human cervical cancers. *Cancer research*. 2000;60(4):916-21.

65. Ziebart T, Walenta S, Kunkel M, Reichert TE, Wagner W, Mueller-Klieser W. Metabolic and proteomic differentials in head and neck squamous cell carcinomas and normal gingival tissue. *Journal of cancer research and clinical oncology*. 2011;137(2):193-9.

66. Singer K, Gottfried E, Kreutz M, Mackensen A. Suppression of T-cell responses by tumor metabolites. *Cancer immunology, immunotherapy : CII*. 2011;60(3):425-31.

67. Gottfried E, Kunz-Schughart LA, Ebner S, Mueller-Klieser W, Hoves S, Andreesen R, et al. Tumor-derived lactic acid modulates dendritic cell activation and antigen expression. *Blood*. 2006;107(5):2013-21.

68. Fischer K, Hoffmann P, Voelkl S, Meidenbauer N, Ammer J, Edinger M, et al. Inhibitory effect of tumor cell-derived lactic acid on human T cells. *Blood*. 2007;109(9):3812-9.

69. Dietl K, Renner K, Dettmer K, Timischl B, Eberhart K, Dorn C, et al. Lactic acid and acidification inhibit TNF secretion and glycolysis of human monocytes. *Journal of immunology (Baltimore, Md : 1950)*. 2010;184(3):1200-9.

70. Brown TP, Ganapathy V. Lactate/GPR81 signaling and proton motive force in cancer: Role in angiogenesis, immune escape, nutrition, and Warburg phenomenon. *Pharmacology & therapeutics*. 2019:107451.

71. Michalek RD, Gerriets VA, Jacobs SR, Macintyre AN, MacIver NJ, Mason EF, et al. Cutting edge: distinct glycolytic and lipid oxidative metabolic programs

are essential for effector and regulatory CD4+ T cell subsets. *Journal of immunology* (Baltimore, Md : 1950). 2011;186(6):3299-303.

72. Goetze K, Walenta S, Ksiazkiewicz M, Kunz-Schughart LA, Mueller-Klieser W. Lactate enhances motility of tumor cells and inhibits monocyte migration and cytokine release. *International journal of oncology*. 2011;39(2):453-63.

73. Baumann F, Leukel P, Doerfelt A, Beier CP, Dettmer K, Oefner PJ, et al. Lactate promotes glioma migration by TGF-beta2-dependent regulation of matrix metalloproteinase-2. *Neuro-oncology*. 2009;11(4):368-80.

74. Beckert S, Farrahi F, Aslam RS, Scheuenstuhl H, Konigsrainer A, Hussain MZ, et al. Lactate stimulates endothelial cell migration. *Wound repair and regeneration : official publication of the Wound Healing Society [and] the European Tissue Repair Society*. 2006;14(3):321-4.

75. Stern R. Hyaluronidases in cancer biology. *Seminars in cancer biology*. 2008;18(4):275-80.

76. Engelstoft MS, Park WM, Sakata I, Kristensen LV, Husted AS, Osborne-Lawrence S, et al. Seven transmembrane G protein-coupled receptor repertoire of gastric ghrelin cells. *Molecular metabolism*. 2013;2(4):376-92.

77. Lauritzen KH, Morland C, Puchades M, Holm-Hansen S, Hagelin EM, Lauritzen F, et al. Lactate receptor sites link neurotransmission, neurovascular coupling, and brain energy metabolism. *Cerebral cortex* (New York, NY : 1991). 2014;24(10):2784-95.

78. Ge H, Weizmann J, Reagan JD, Gupte J, Baribault H, Gyuris T, et al. Elucidation of signaling and functional activities of an orphan GPCR, GPR81. *Journal of lipid research*. 2008;49(4):797-803.

79. Kuei C, Yu J, Zhu J, Wu J, Zhang L, Shih A, et al. Study of GPR81, the lactate receptor, from distant species identifies residues and motifs critical for GPR81 functions. *Molecular pharmacology*. 2011;80(5):848-58.

80. Medes G, Thomas A, Weinhouse S. Metabolism of neoplastic tissue. IV. A study of lipid synthesis in neoplastic tissue slices in vitro. *Cancer research*. 1953;13(1):27-9.

81. Ookhtens M, Kannan R, Lyon I, Baker N. Liver and adipose tissue contributions to newly formed fatty acids in an ascites tumor. *The American journal of physiology*. 1984;247(1 Pt 2):R146-53.

82. Rohrig F, Schulze A. The multifaceted roles of fatty acid synthesis in cancer. *Nature reviews Cancer*. 2016;16(11):732-49.

83. Menendez JA, Lupu R. Fatty acid synthase and the lipogenic phenotype in cancer pathogenesis. *Nature reviews Cancer*. 2007;7(10):763-77.

84. Cai Y, Crowther J, Pastor T, Abbasi Asbagh L, Baietti MF, De Troyer M, et al. Loss of Chromosome 8p Governs Tumor Progression and Drug Response by Altering Lipid Metabolism. *Cancer cell*. 2016;29(5):751-66.

85. Amemiya-Kudo M, Shimano H, Hasty AH, Yahagi N, Yoshikawa T, Matsuzaka T, et al. Transcriptional activities of nuclear SREBP-1a, -1c, and -2 to different target promoters of lipogenic and cholesterologenic genes. *Journal of lipid research*. 2002;43(8):1220-35.
86. Shimano H, Yahagi N, Amemiya-Kudo M, Hasty AH, Osuga J, Tamura Y, et al. Sterol regulatory element-binding protein-1 as a key transcription factor for nutritional induction of lipogenic enzyme genes. *The Journal of biological chemistry*. 1999;274(50):35832-9.
87. Duvel K, Yecies JL, Menon S, Raman P, Lipovsky AI, Souza AL, et al. Activation of a metabolic gene regulatory network downstream of mTOR complex 1. *Molecular cell*. 2010;39(2):171-83.
88. Porstmann T, Santos CR, Griffiths B, Cully M, Wu M, Leever S, et al. SREBP activity is regulated by mTORC1 and contributes to Akt-dependent cell growth. *Cell metabolism*. 2008;8(3):224-36.
89. Carroll PA, Diolaiti D, McFerrin L, Gu H, Djukovic D, Du J, et al. Deregulated Myc requires MondoA/Mlx for metabolic reprogramming and tumorigenesis. *Cancer cell*. 2015;27(2):271-85.
90. Kuhajda FP, Jenner K, Wood FD, Hennigar RA, Jacobs LB, Dick JD, et al. Fatty acid synthesis: a potential selective target for antineoplastic therapy. *Proceedings of the National Academy of Sciences of the United States of America*. 1994;91(14):6379-83.
91. Argiles JM, Busquets S, Stemmler B, Lopez-Soriano FJ. Cancer cachexia: understanding the molecular basis. *Nature reviews Cancer*. 2014;14(11):754-62.
92. Pyne NJ, Pyne S. Sphingosine 1-phosphate and cancer. *Nature reviews Cancer*. 2010;10(7):489-503.
93. Park JB, Lee CS, Jang JH, Ghim J, Kim YJ, You S, et al. Phospholipase signalling networks in cancer. *Nature reviews Cancer*. 2012;12(11):782-92.
94. Griner EM, Kazanietz MG. Protein kinase C and other diacylglycerol effectors in cancer. *Nature reviews Cancer*. 2007;7(4):281-94.
95. Vanhaesebroeck B, Stephens L, Hawkins P. PI3K signalling: the path to discovery and understanding. *Nature reviews Molecular cell biology*. 2012;13(3):195-203.
96. De Craene B, Berx G. Regulatory networks defining EMT during cancer initiation and progression. *Nature reviews Cancer*. 2013;13(2):97-110.
97. Vo BT, Morton D, Jr., Komaragiri S, Millena AC, Leath C, Khan SA. TGF-beta effects on prostate cancer cell migration and invasion are mediated by PGE2 through activation of PI3K/AKT/mTOR pathway. *Endocrinology*. 2013;154(5):1768-79.
98. Folkman J. Role of angiogenesis in tumor growth and metastasis. *Seminars in oncology*. 2002;29(6 Suppl 16):15-8.



99. Kazlauskas A. Lysophosphatidic acid contributes to angiogenic homeostasis. *Experimental cell research*. 2015;333(2):166-70.
100. Mendelson K, Evans T, Hla T. Sphingosine 1-phosphate signalling. *Development (Cambridge, England)*. 2014;141(1):5-9.
101. Luan B, Yoon YS, Le Lay J, Kaestner KH, Hedrick S, Montminy M. CREB pathway links PGE2 signaling with macrophage polarization. *Proceedings of the National Academy of Sciences of the United States of America*. 2015;112(51):15642-7.
102. Kalinski P. Regulation of immune responses by prostaglandin E2. *Journal of immunology (Baltimore, Md : 1950)*. 2012;188(1):21-8.
103. Wang R, Green DR. Metabolic checkpoints in activated T cells. *Nature immunology*. 2012;13(10):907-15.
104. Suematsu N, Isohashi F. Molecular cloning and functional expression of human cytosolic acetyl-CoA hydrolase. *Acta biochimica Polonica*. 2006;53(3):553-61.
105. Louis P, Hold GL, Flint HJ. The gut microbiota, bacterial metabolites and colorectal cancer. *Nature reviews Microbiology*. 2014;12(10):661-72.
106. Cummings JH, Pomare EW, Branch WJ, Naylor CP, Macfarlane GT. Short chain fatty acids in human large intestine, portal, hepatic and venous blood. *Gut*. 1987;28(10):1221-7.
107. Donohoe DR, Garge N, Zhang X, Sun W, O'Connell TM, Bunker MK, et al. The microbiome and butyrate regulate energy metabolism and autophagy in the mammalian colon. *Cell metabolism*. 2011;13(5):517-26.
108. Bloemen JG, Venema K, van de Poll MC, Olde Damink SW, Buurman WA, Dejong CH. Short chain fatty acids exchange across the gut and liver in humans measured at surgery. *Clinical nutrition (Edinburgh, Scotland)*. 2009;28(6):657-61.
109. Schug ZT, Peck B, Jones DT, Zhang Q, Grosskurth S, Alam IS, et al. Acetyl-CoA synthetase 2 promotes acetate utilization and maintains cancer cell growth under metabolic stress. *Cancer cell*. 2015;27(1):57-71.
110. Comerford SA, Huang Z, Du X, Wang Y, Cai L, Witkiewicz AK, et al. Acetate dependence of tumors. *Cell*. 2014;159(7):1591-602.
111. Kamphorst JJ, Chung MK, Fan J, Rabinowitz JD. Quantitative analysis of acetyl-CoA production in hypoxic cancer cells reveals substantial contribution from acetate. *Cancer & metabolism*. 2014;2:23.
112. Hatanaka H, Tsukui M, Takada S, Kurashina K, Choi YL, Soda M, et al. Identification of transforming activity of free fatty acid receptor 2 by retroviral expression screening. *Cancer science*. 2010;101(1):54-9.
113. Tang Y, Chen Y, Jiang H, Robbins GT, Nie D. G-protein-coupled receptor for short-chain fatty acids suppresses colon cancer. *International journal of cancer*. 2011;128(4):847-56.

114. Pan P, Oshima K, Huang YW, Agle KA, Drobyski WR, Chen X, et al. Loss of FFAR2 promotes colon cancer by epigenetic dysregulation of inflammation suppressors. *International journal of cancer*. 2018;143(4):886-96.
115. Chamberland JP, Moon HS. Down-regulation of malignant potential by alpha linolenic acid in human and mouse colon cancer cells. *Familial cancer*. 2015;14(1):25-30.
116. Vara-Messler M, Pasqualini ME, Comba A, Silva R, Buccellati C, Trenti A, et al. Increased dietary levels of alpha-linoleic acid inhibit mammary tumor growth and metastasis. *European journal of nutrition*. 2017;56(2):509-19.
117. Roy S, Rawat AK, Sammi SR, Devi U, Singh M, Gautam S, et al. Alpha-linolenic acid stabilizes HIF-1 alpha and downregulates FASN to promote mitochondrial apoptosis for mammary gland chemoprevention. *Oncotarget*. 2017;8(41):70049-71.
118. Kellar A, Egan C, Morris D. Preclinical Murine Models for Lung Cancer: Clinical Trial Applications. *BioMed research international*. 2015;2015:621324.
119. Fidler IJ. Selection of successive tumour lines for metastasis. *Nature: New biology*. 1973;242(118):148-9.
120. Ohno J, Horio Y, Sekido Y, Hasegawa Y, Takahashi M, Nishizawa J, et al. Telomerase activation and p53 mutations in urethane-induced A/J mouse lung tumor development. *Carcinogenesis*. 2001;22(5):751-6.
121. Parang B, Barrett CW, Williams CS. AOM/DSS Model of Colitis-Associated Cancer. *Methods in molecular biology (Clifton, NJ)*. 2016;1422:297-307.
122. Kersten K, de Visser KE, van Miltenburg MH, Jonkers J. Genetically engineered mouse models in oncology research and cancer medicine. *EMBO molecular medicine*. 2017;9(2):137-53.
123. Fantozzi A, Christofori G. Mouse models of breast cancer metastasis. *Breast cancer research : BCR*. 2006;8(4):212.
124. Bertram JS, Janik P. Establishment of a cloned line of Lewis Lung Carcinoma cells adapted to cell culture. *Cancer letters*. 1980;11(1):63-73.
125. Lechner MG, Karimi SS, Barry-Holson K, Angell TE, Murphy KA, Church CH, et al. Immunogenicity of murine solid tumor models as a defining feature of in vivo behavior and response to immunotherapy. *Journal of immunotherapy (Hagerstown, Md : 1997)*. 2013;36(9):477-89.
126. Janker F, Weder W, Jang JH, Jungraithmayr W. Preclinical, non-genetic models of lung adenocarcinoma: a comparative survey. *Oncotarget*. 2018;9(55):30527-38.
127. Sohn OS, Fiala ES, Requeijo SP, Weisburger JH, Gonzalez FJ. Differential effects of CYP2E1 status on the metabolic activation of the colon carcinogens azoxymethane and methylazoxymethanol. *Cancer research*. 2001;61(23):8435-40.

128. Okayasu I, Hatakeyama S, Yamada M, Ohkusa T, Inagaki Y, Nakaya R. A novel method in the induction of reliable experimental acute and chronic ulcerative colitis in mice. *Gastroenterology*. 1990;98(3):694-702.
129. De Robertis M, Massi E, Poeta ML, Carotti S, Morini S, Cecchetelli L, et al. The AOM/DSS murine model for the study of colon carcinogenesis: From pathways to diagnosis and therapy studies. *Journal of carcinogenesis*. 2011;10:9.
130. Uronis JM, Muhlbauer M, Herfarth HH, Rubinas TC, Jones GS, Jobin C. Modulation of the intestinal microbiota alters colitis-associated colorectal cancer susceptibility. *PloS one*. 2009;4(6):e6026.
131. Tanaka T, Kohno H, Suzuki R, Yamada Y, Sugie S, Mori H. A novel inflammation-related mouse colon carcinogenesis model induced by azoxymethane and dextran sodium sulfate. *Cancer science*. 2003;94(11):965-73.
132. Matkowskyj KA, Marrero JA, Carroll RE, Danilkovich AV, Green RM, Benya RV. Azoxymethane-induced fulminant hepatic failure in C57BL/6J mice: characterization of a new animal model. *The American journal of physiology*. 1999;277(2):G455-62.
133. Pan Q, Lou X, Zhang J, Zhu Y, Li F, Shan Q, et al. Genomic variants in mouse model induced by azoxymethane and dextran sodium sulfate improperly mimic human colorectal cancer. *Scientific reports*. 2017;7(1):25.
134. Greten FR, Eckmann L, Greten TF, Park JM, Li ZW, Egan LJ, et al. IKKbeta links inflammation and tumorigenesis in a mouse model of colitis-associated cancer. *Cell*. 2004;118(3):285-96.
135. Srivatsa S, Paul MC, Cardone C, Holcman M, Amberg N, Pathria P, et al. EGFR in Tumor-Associated Myeloid Cells Promotes Development of Colorectal Cancer in Mice and Associates With Outcomes of Patients. *Gastroenterology*. 2017;153(1):178-90.e10.
136. Wilson JE, Petrucelli AS, Chen L, Koblansky AA, Truax AD, Oyama Y, et al. Inflammasome-independent role of AIM2 in suppressing colon tumorigenesis via DNA-PK and Akt. *Nature medicine*. 2015;21(8):906-13.
137. Guy CT, Cardiff RD, Muller WJ. Induction of mammary tumors by expression of polyomavirus middle T oncogene: a transgenic mouse model for metastatic disease. *Molecular and cellular biology*. 1992;12(3):954-61.
138. Fluck MM, Schaffhausen BS. Lessons in signaling and tumorigenesis from polyomavirus middle T antigen. *Microbiology and molecular biology reviews* : MMBR. 2009;73(3):542-63, Table of Contents.
139. Ellies LG. PyV-mT-induced parotid gland hyperplasia as detected by altered lectin reactivity is not modulated by inducible nitric oxide deficiency. *Archives of oral biology*. 2003;48(6):415-22.
140. Lin EY, Jones JG, Li P, Zhu L, Whitney KD, Muller WJ, et al. Progression to malignancy in the polyoma middle T oncoprotein mouse breast cancer model

provides a reliable model for human diseases. *The American journal of pathology*. 2003;163(5):2113-26.

141. Maglione JE, Moghanaki D, Young LJ, Manner CK, Ellies LG, Joseph SO, et al. Transgenic Polyoma middle-T mice model premalignant mammary disease. *Cancer research*. 2001;61(22):8298-305.

142. Ishay-Ronen D, Diepenbruck M, Kalathur RKR, Sugiyama N, Tiede S, Ivanek R, et al. Gain Fat-Lose Metastasis: Converting Invasive Breast Cancer Cells into Adipocytes Inhibits Cancer Metastasis. *Cancer cell*. 2019;35(1):17-32.e6.

143. Curtis M, Kenny HA, Ashcroft B, Mukherjee A, Johnson A, Zhang Y, et al. Fibroblasts Mobilize Tumor Cell Glycogen to Promote Proliferation and Metastasis. *Cell metabolism*. 2019;29(1):141-55.e9.

144. Duivenvoorden HM, Spurling A, O'Toole SA, Parker BS. Discriminating the earliest stages of mammary carcinoma using myoepithelial and proliferative markers. *PloS one*. 2018;13(7):e0201370.

145. Fischer KR, Durrans A, Lee S, Sheng J, Li F, Wong ST, et al. Epithelial-to-mesenchymal transition is not required for lung metastasis but contributes to chemoresistance. *Nature*. 2015;527(7579):472-6.

146. Gomez-Cuadrado L, Tracey N, Ma R, Qian B, Brunton VG. Mouse models of metastasis: progress and prospects. *Disease models & mechanisms*. 2017;10(9):1061-74.

147. Roswall P, Bocci M, Bartoschek M, Li H, Kristiansen G, Jansson S, et al. Microenvironmental control of breast cancer subtype elicited through paracrine platelet-derived growth factor-CC signaling. *Nature medicine*. 2018;24(4):463-73.

148. Trikha P, Sharma N, Pena C, Reyes A, Pecot T, Khurshid S, et al. E2f3 in tumor macrophages promotes lung metastasis. *Oncogene*. 2016;35(28):3636-46.

149. Coffelt SB, Kersten K, Doornebal CW, Weiden J, Vrijland K, Hau CS, et al. IL-17-producing gammadelta T cells and neutrophils conspire to promote breast cancer metastasis. *Nature*. 2015;522(7556):345-8.

150. Doornebal CW, Klarenbeek S, Braumuller TM, Klijn CN, Ciampricotti M, Hau CS, et al. A preclinical mouse model of invasive lobular breast cancer metastasis. *Cancer research*. 2013;73(1):353-63.

151. Hanson J, Gille A, Zwykiel S, Lukasova M, Clausen BE, Ahmed K, et al. Nicotinic acid- and monomethyl fumarate-induced flushing involves GPR109A expressed by keratinocytes and COX-2-dependent prostanoid formation in mice. *The Journal of clinical investigation*. 2010;120(8):2910-9.

152. Clausen BE, Burkhardt C, Reith W, Renkawitz R, Forster I. Conditional gene targeting in macrophages and granulocytes using LysMcre mice. *Transgenic research*. 1999;8(4):265-77.

153. Eguchi J, Wang X, Yu S, Kershaw EE, Chiu PC, Dushay J, et al. Transcriptional control of adipose lipid handling by IRF4. *Cell metabolism*. 2011;13(3):249-59.

154. Madison BB, Dunbar L, Qiao XT, Braunstein K, Braunstein E, Gumucio DL. Cis elements of the villin gene control expression in restricted domains of the vertical (crypt) and horizontal (duodenum, cecum) axes of the intestine. *The Journal of biological chemistry*. 2002;277(36):33275-83.
155. Duda DG, Duyverman AM, Kohno M, Snuderl M, Steller EJ, Fukumura D, et al. Malignant cells facilitate lung metastasis by bringing their own soil. *Proceedings of the National Academy of Sciences of the United States of America*. 2010;107(50):21677-82.
156. Schumacher D, Strilic B, Sivaraj KK, Wettschureck N, Offermanns S. Platelet-derived nucleotides promote tumor-cell transendothelial migration and metastasis via P2Y2 receptor. *Cancer cell*. 2013;24(1):130-7.
157. Singh N, Gurav A, Sivaprakasam S, Brady E, Padia R, Shi H, et al. Activation of Gpr109a, receptor for niacin and the commensal metabolite butyrate, suppresses colonic inflammation and carcinogenesis. *Immunity*. 2014;40(1):128-39.
158. Staubert C, Broom OJ, Nordstrom A. Hydroxycarboxylic acid receptors are essential for breast cancer cells to control their lipid/fatty acid metabolism. *Oncotarget*. 2015;6(23):19706-20.
159. Lee YJ, Shin KJ, Park SA, Park KS, Park S, Heo K, et al. G-protein-coupled receptor 81 promotes a malignant phenotype in breast cancer through angiogenic factor secretion. *Oncotarget*. 2016;7(43):70898-911.
160. Shi Y, Lai X, Ye L, Chen K, Cao Z, Gong W, et al. Activated niacin receptor HCA2 inhibits chemoattractant-mediated macrophage migration via Gbetagamma/PKC/ERK1/2 pathway and heterologous receptor desensitization. *Scientific reports*. 2017;7:42279.
161. Colegio OR, Chu NQ, Szabo AL, Chu T, Rhebergen AM, Jairam V, et al. Functional polarization of tumour-associated macrophages by tumour-derived lactic acid. *Nature*. 2014;513(7519):559-63.
162. Errea A, Cayet D, Marchetti P, Tang C, Kluza J, Offermanns S, et al. Lactate Inhibits the Pro-Inflammatory Response and Metabolic Reprogramming in Murine Macrophages in a GPR81-Independent Manner. *PloS one*. 2016;11(11):e0163694.
163. Feng J, Yang H, Zhang Y, Wei H, Zhu Z, Zhu B, et al. Tumor cell-derived lactate induces TAZ-dependent upregulation of PD-L1 through GPR81 in human lung cancer cells. *Oncogene*. 2017;36(42):5829-39.
164. Benyo Z, Gille A, Kero J, Csiky M, Suchankova MC, Nusing RM, et al. GPR109A (PUMA-G/HM74A) mediates nicotinic acid-induced flushing. *The Journal of clinical investigation*. 2005;115(12):3634-40.
165. Elangovan S, Pathania R, Ramachandran S, Ananth S, Padia RN, Lan L, et al. The niacin/butyrate receptor GPR109A suppresses mammary tumorigenesis by inhibiting cell survival. *Cancer research*. 2014;74(4):1166-78.



166. Muller WJ, Sinn E, Pattengale PK, Wallace R, Leder P. Single-step induction of mammary adenocarcinoma in transgenic mice bearing the activated c-neu oncogene. *Cell*. 1988;54(1):105-15.
167. Leystra AA, Clapper ML. Gut Microbiota Influences Experimental Outcomes in Mouse Models of Colorectal Cancer. *Genes*. 2019;10(11).
168. Wu Q, Wang H, Zhao X, Shi Y, Jin M, Wan B, et al. Identification of G-protein-coupled receptor 120 as a tumor-promoting receptor that induces angiogenesis and migration in human colorectal carcinoma. *Oncogene*. 2013;32(49):5541-50.
169. Senatorov IS, Moniri NH. The role of free-fatty acid receptor-4 (FFA4) in human cancers and cancer cell lines. *Biochemical pharmacology*. 2018;150:170-80.
170. Sivaprakasam S, Gurav A, Paschall AV, Coe GL, Chaudhary K, Cai Y, et al. An essential role of Ffar2 (Gpr43) in dietary fibre-mediated promotion of healthy composition of gut microbiota and suppression of intestinal carcinogenesis. *Oncogenesis*. 2016;5(6):e238.
171. Maslowski KM, Vieira AT, Ng A, Kranich J, Sierro F, Yu D, et al. Regulation of inflammatory responses by gut microbiota and chemoattractant receptor GPR43. *Nature*. 2009;461(7268):1282-6.
172. Smith PM, Howitt MR, Panikov N, Michaud M, Gallini CA, Bohlooly YM, et al. The microbial metabolites, short-chain fatty acids, regulate colonic Treg cell homeostasis. *Science (New York, NY)*. 2013;341(6145):569-73.
173. Kim MH, Kang SG, Park JH, Yanagisawa M, Kim CH. Short-chain fatty acids activate GPR41 and GPR43 on intestinal epithelial cells to promote inflammatory responses in mice. *Gastroenterology*. 2013;145(2):396-406.e1-10.
174. Kim M, Friesen L, Park J, Kim HM, Kim CH. Microbial metabolites, short-chain fatty acids, restrain tissue bacterial load, chronic inflammation, and associated cancer in the colon of mice. *European journal of immunology*. 2018;48(7):1235-47.
175. Thirunavukkarasan M, Wang C, Rao A, Hind T, Teo YR, Siddiquee AA, et al. Short-chain fatty acid receptors inhibit invasive phenotypes in breast cancer cells. *PloS one*. 2017;12(10):e0186334.
176. Nakajima A, Nakatani A, Hasegawa S, Irie J, Ozawa K, Tsujimoto G, et al. The short chain fatty acid receptor GPR43 regulates inflammatory signals in adipose tissue M2-type macrophages. *PloS one*. 2017;12(7):e0179696.
177. Yang L, Zhang Y. Tumor-associated macrophages: from basic research to clinical application. *Journal of hematology & oncology*. 2017;10(1):58.
178. Vanden Berghe T, Linkermann A, Jouan-Lanhouet S, Walczak H, Vandenabeele P. Regulated necrosis: the expanding network of non-apoptotic cell death pathways. *Nature reviews Molecular cell biology*. 2014;15(2):135-47.
179. Wyckoff J, Wang W, Lin EY, Wang Y, Pixley F, Stanley ER, et al. A paracrine loop between tumor cells and macrophages is required for tumor cell migration in mammary tumors. *Cancer research*. 2004;64(19):7022-9.

- 
180. Menard S, Fortis S, Castiglioni F, Agresti R, Balsari A. HER2 as a prognostic factor in breast cancer. *Oncology*. 2001;61 Suppl 2:67-72.
181. DeNardo DG, Barreto JB, Andreu P, Vasquez L, Tawfik D, Kolhatkar N, et al. CD4(+) T cells regulate pulmonary metastasis of mammary carcinomas by enhancing protumor properties of macrophages. *Cancer cell*. 2009;16(2):91-102.
182. Linde N, Casanova-Acebes M, Sosa MS, Mortha A, Rahman A, Farias E, et al. Macrophages orchestrate breast cancer early dissemination and metastasis. *Nature Communications*. 2018;9(1):21.
183. Yang L, Joseph S, Sun T, Hoffmann J, Thevissen S, Offermanns S, et al. TAK1 regulates endothelial cell necroptosis and tumor metastasis. *Cell death and differentiation*. 2019;26(10):1987-97.

## SUMMARY

Metabolites such as lactate and free fatty acids (FFAs) abundantly occur in high concentrations in tumor and stromal cells of solid malignancies. Their known functions comprise the allocation of nutrients and intermediates for the generation of cell components, the evasion of immune destruction, the induction of vessel formation and the stimulation of cell migration in order to promote tumor growth, progression and metastasis. However, the role of metabolites as signaling molecules and the downstream mechanisms of metabolite receptor mediated signaling in tumor and stromal cells is poorly understood. Our study confirms the expression of Hydroxycarboxylic acid receptor 1 (HCA1) in solid human breast tumors and the expression of Free fatty acid receptor 4 (FFA4) in solid human colorectal tumors. In addition, the expression of HCA1 in human breast cancer cell lines as well as the expression of FFA4 in human colorectal cancer cell lines was proved. Moreover, our research reveals the expression HCA2, FFA2 and FFA4 in tumor associated macrophages (TAMs).

To test whether the loss of any of the metabolite receptors affects tumor growth and progression we utilized a syngeneic Lewis lung cancer (LLC1) tumor model, an azoxymethane (AOM) – dextran sulfate (DSS) colorectal cancer model and a Mouse mammary tumor virus Polyoma Virus middle T antigen (MMTV-PyMT) breast cancer model. The loss of HCA2 did not lead to a changed outcome compared to wild type littermates in any of the models. Likewise, the deletion of FFA4 had no influence on the LLC1 model and, surprisingly, tumor number and area in the AOM-DSS model also remained unaltered. The impact of HCA1 deficiency was investigated utilizing the MMTV-PyMT model and revealed a moderately improved tumor growth. The absence of FFA2 did not affect tumor growth in the LLC1 model but led to an increased number of colorectal tumors in the AOM-DSS model while the tumor area remained unchanged. The most compelling results were obtained upon the deletion of FFA2 in the MMTV-PyMT model. Here, we demonstrate that the loss of FFA2 significantly reduces tumor latency and also significantly improves tumor growth. Nevertheless, the formation of metastases in the LLC1 model and the MMTV-PyMT model did not show any changes upon the loss of any of the metabolite receptors.

Together, our results describe a tumor-protective effect of FFA2 with an unclear impact on metastatic processes. Considerations about putative mechanisms of short chain fatty acid (SCFA) mediated FFA2 signaling suggest potential targets for pharmacological interventions to treat mammary tumors.



## **ZUSAMMENFASSUNG**

Die Behandlung von Krebserkrankungen steht vor zahlreichen Herausforderungen, die ihren Ursprung in den Eigenheiten der Erkrankungen haben. Diese Eigenschaften wurden im Jahr 2000 als die „Hallmarks of Cancer“ zusammengefasst und beinhalten Unabhängigkeit von externen Wachstumsfaktoren, Intensivität gegenüber wachstumshemmenden Faktoren, Umgehen des programmierten Zelltods in Form von Apoptose, unbegrenztes Replikationspotential, kontinuierliche Neubildung von Blutgefäßen und die Fähigkeit, in Gewebe einzudringen und Metastasen zu bilden. Diese Eigenschaften wurden erweitert um den Widerstand gegen Angriffe aus dem Immunsystem und um die Reprogrammierung des Zellstoffwechsels. Tumorzellen sind seit langem dafür bekannt, dass sie hohe Konzentrationen von Stoffwechselprodukten, sogenannter Metaboliten, enthalten können. Diese Metaboliten beinhalten zum Beispiel Laktat und freie Fettsäuren (FFAs). Bisherige Forschungsergebnisse zeigen, dass die Metaboliten wichtige Funktionen zur Förderung des Tumorwachstums, der Entwicklung und bei der Entstehung von Metastasen erfüllen. Unter anderem stellen sie Energielieferanten und Zwischenprodukte für die Bildung von Zellbestandteilen dar. Sie können die Hauptakteure der Immunantwort hemmen und die Bildung neuer Blutgefäße sowie die Zellmigration fördern. Die Funktionen der Metaboliten als Signalmoleküle und als Liganden für ihre jeweiligen Rezeptoren sowie auch die nachgelagerten Signalkaskaden sind kaum untersucht. In ihrer Funktion als Liganden können die Metaboliten G-Protein-gekoppelte Rezeptoren (GPCRs) aktivieren. Diese Arbeit betrachtet insbesondere zwei Gruppen von GPCRs, die im Metabolismus von entscheidender Bedeutung sind: Hydroxycarboxylsäurerezeptoren (HCARs) und Rezeptoren für freie Fettsäuren (FFARs). Nachfolgend werden sie als metabolische Rezeptoren bezeichnet. Unter den HCARs wird Hydroxycarboxylsäurerezeptor 1 (HCA1) durch Laktat aktiviert, während HCA2 durch Ketonkörper wie 3-Hydroxybutyrat (3-HB) aktiviert wird. In der Gruppe der FFARs findet die Aktivierung von Fettsäurerezeptor 2 (FFA2) durch kurzkettige Fettsäuren (SCFAs) wie Acetat, Butyrat und Propionat statt. Unterdessen wird FFA4 von langkettigen Fettsäuren (LCFAs) aktiviert. Die Allgegenwärtigkeit von GPCRs prädestiniert sie als Interventionspunkte der pharmakologischen Therapie. Zellen mit Expression metabolischer Rezeptoren sind nicht ausschließlich in den physiologischen Stoffwechsel involviert. Diese Zellen können auch in Tumoren auftreten. Das Stroma von Tumoren setzt sich nicht einzig aus Tumorzellen, sondern zu einem erheblichen Teil auch aus anderen Zelltypen wie Leukozyten, Fibroblasten (CAFs), Perizyten, Endothelzellen, Epithelzellen und Adipozyten zusammen. Vorliegende Daten beschreiben das Vorkommen von HCA1, HCA2, FFA2 und teilweise auch FFA4 auf Adipozyten sowie das Vorkommen von HCA2, FFA2 und FFA4 auf verschiedenen Leukozyten.

Die vorliegende Arbeit verfolgt die Hypothese, dass die autokrine oder parakrine Aktivierung metabolischer Rezeptoren durch die entsprechenden Metaboliten zu einer Modulation des Wachstums und der Entwicklung von Tumoren beitragen können. Unser Ziel war es die Expression der metabolischen Rezeptoren in Tumor- und Tumorstromazellen zu analysieren und zu überprüfen, ob der Verlust eines der Rezeptoren Wachstum, Entwicklung und Metastasierung beeinflussen kann. Da die Verwendung von konditionalen Knockouttieren dabei helfen kann, die Funktion der Rezeptoren sowie ihre nachgeordneten Signalwege in Tumor- und Tumorstromazellen aufzuklären, war die Generierung von Mäusen mit konditionalem Knockout von *Ffar4* ein weiteres Ziel dieser Arbeit.

In einer RT-qPCR-Analyse der cDNA von 425 humanen Tumoren stellten wir eine erhöhte Expression von HCA1 in Brusttumorproben sowie eine erhöhte Expression von FFA4 in Kolonkarzinomproben fest. Weitere metabolische Rezeptoren waren entweder nicht oder nur schwach in den Tumorproben exprimiert. Um erhaltenen Daten zu bestätigen, analysierten wir die Expression von HCA1 in humanen Brustkrebszelllinien und die Expression von FFA4 in humanen Kolonkarzinomzelllinien. Eine HCA1 Expression, die in etwa der in dem Tumorproben entsprach, wurde festgestellt. Die Kolonkarzinomzelllinien exprimierten FFA4; jedoch in geringerem Maß als die Tumorproben.

In Vorversuchen identifizierten wir LLC1 Zellen als die beste Zelllinie zur Durchführung eines syngenen Tumorversuchs. Die entstehenden LLC1-Tumoren zeigten im Vergleich zu anderen Tumorzelllinien das ausgeprägteste Tumorstroma und die meisten Immunzellen, die gleichzeitig metabolische Rezeptoren exprimierten. In allen Tumormodellen führten wir Immunfluoreszenzfärbungen in den Tumoren von HCA1<sup>mRFP</sup>-, HCA2<sup>mRFP</sup>-, FFA2<sup>mRFP</sup>- oder FFA4<sup>lacZ</sup>-Reporter-mäusen durch, um die Stromazellen mit Expression metabolischer Rezeptoren näher zu identifizieren. Färbungen mit den Fibroblastenmarkern PDGFR $\alpha$  und  $\alpha$ -SMA zeigten keine CAFs, die gleichzeitig einen der metabolischen Rezeptoren exprimierten. Bei Färbungen mit dem Panleukozytenmarker CD45 identifizierten wir in jedem der Modelle Fraktionen von Stromazellen, die sowohl HCA2<sup>mRFP</sup>-, FFA2<sup>mRFP</sup>- oder FFA4<sup>lacZ</sup> als auch CD45 exprimierten. Danach setzten wir die Makrophagenmarker F4/80 und CD68 ein. In allen Modellen stellten Makrophagen die größte Population der Immunzellen dar, die metabolische Rezeptoren exprimierten. Der Immunzellgehalt der Tumore unterschied sich merklich und lag bei maximal 20% in MMTV-PyMT-Brusttumoren bei FFA2<sup>mRFP</sup>-positiven Tieren. Die Populationen von tumorassoziierten Makrophagen (TAMs) waren jeweils kleiner.

Um zu testen, welchen Einfluss der Verlust von HCA2, FFA2 oder FFA4 im syngene Tumormodell hat, injizierten wir LLC1-Tumorzellen subkutan in HCA2<sup>-/-</sup>, FFA2<sup>-/-</sup> und FFA4<sup>-/-</sup>-Tiere sowie Wildtypmäuse. In allen Versuchen wurden Wurfgeschwister der rezeptordefizienten Tiere als Kontrolltiere verwendet. Die Tiere wurden 21 Tage nach der LLC1-Injektion euthanasiert oder wenn der Tumor ein Volumen von 1,7 cm<sup>3</sup> erreichte. In keiner der Knockout-Gruppen unterschied sich das Tumorstadium signifikant von dem der Wildtypen. Auch die Tumorgöße und das Tumorgewicht am Tag des Versuchsendes zeigten keinen signifikanten Unterschied. Da das LLC1-Tumormodell auch zur Untersuchung von Lungenmetastasen verwendet wird, analysierten wir die Lungen der Versuchstiere. Wir färbten die Lungen mit dem Proliferationsmarker BrdU sowie mit Hämatoxylin und Eosin. Jedoch konnten wir in keiner der Lungen Metastasierung feststellen. Somit wiesen wir nach, dass der Verlust von HCA2, FFA2 oder FFA4 keine Auswirkungen auf die Entwicklung von LLC1-Primärtumoren hat, während die nachfolgende Metastasierung in die Lunge nicht untersucht werden konnte.

Im AOM-DSS-Kolonkarzinommodell wird die Entstehung von Tumoren chemisch induziert. Die kanzerogene Substanz AOM wird intraperitoneal injiziert und verursacht Basenaustausch in der DNA und somit Mutationen. Zusätzlich erhielten die Tiere 1,8% DSS in ihrem Trinkwasser in drei Zyklen zu je fünf Tagen. DSS verursacht eine schwere Kolitis und durch die zusätzliche Gabe von AOM wird die Entstehung von Kolontumoren im Versuchszeitraum von zwölf Wochen ermöglicht. Wir verglichen Gewichtsverlust, Tumoranzahl und -fläche bei HCA2-, FFA2- und FFA4-defizienten Tieren mit Wildtypkontrollen. Der Gewichtsverlust kann als Indikator für die Schwere der Kolitis und die Tumorbilastung dienen, doch wir konnten keine signifikanten Abweichungen in der Gewichtsentwicklung beobachten. Des Weiteren fanden wir keine Unterschiede in der Tumoranzahl und -fläche zwischen HCA2- und FFA4-Knockouttieren und ihren jeweiligen Wildtypkontrollen. Daher stellten wir fest, dass der Verlust von HCA2 oder FFA4 keinen Einfluss auf die Entstehung von AOM-DSS-induzierten Kolontumoren hat. Die FFA2-Knockouttiere präsentieren eine signifikant erhöhte Anzahl von Kolontumoren verglichen mit ihren Wildtyp-Wurfgeschwistern, jedoch nivellierte sich der Effekt beim Vergleich mit der Gruppe aller verwendeten Wildtypiere. Ebenso unverändert blieb die Kolonfläche, die von Tumoren besiedelt war. Daher gibt der Versuch zwar einen Hinweis auf eine tumorprotektive Wirkung von FFA2, aber weitere Untersuchungen sind unerlässlich. Hierbei sollte beachtet werden, dass Tiere aus demselben Wurf mit denselben Haltungsbedingungen verwendet werden. Diese, wie auch der genetische Hintergrund der Tiere haben immensen Einfluss auf die Zusammensetzung des Darmmikrobioms, das durch die Fermentierung langkettiger Kohlehydrate SCFAs herstellt. Da

SCFAs als Liganden für FFA2 und teilweise auch für HCA2 dienen, ist ihre Zusammensetzung und Konzentration im Kolon von entscheidender Bedeutung für den Ausgang des Versuchs.

Für die Durchführung von Versuchen mit dem MMTV-PyMT-Brusttumormodell werden Tiere, die das MMTV-PyMT-Transgen tragen mit HCA1<sup>-/-</sup>, HCA2<sup>-/-</sup> oder FFA2<sup>-/-</sup>-Tieren verpaart. MMTV-PyMT-positive Weibchen entwickeln palpierbare Tumoren spontan mit einer Latenz von etwa acht Wochen. Die Versuchsgruppen bestanden aus MMTV-PyMT<sup>+</sup>;HCA1<sup>-/-</sup>, MMTV-PyMT<sup>+</sup>;HCA2<sup>-/-</sup> und MMTV-PyMT<sup>+</sup>;FFA2<sup>-/-</sup>-Tieren und den jeweiligen MMTV-PyMT-positiven Wildtypkontrollen und wurden bis zum Erreichen des Endpunkts, einem Gesamttumorvolumen von 1,7 cm<sup>3</sup>, beobachtet. Nach aktueller Datenlage ist HCA1 nicht in Immunzellen, jedoch stark in weißen und braunen Adipozyten exprimiert. Da das Stroma von MMTV-PyMT-Brusttumoren auf Grund der Beschaffenheit des gesunden Brustgewebes stark von Adipozyten durchsetzt ist, schlossen wir Untersuchungen an HCA1-defizienten Tieren in unsere Arbeit mit ein. Die Abwesenheit von HCA1 in Immunzellen und die Expression in benachbarten Adipozyten stellten wir mittels Immunfluoreszenzfärbung fest. Der Knockout von HCA1 führte zu einer leicht verkürzten Latenz des Auftretens erster palpierbarer Tumoren gegenüber der Vergleichsgruppe. Die Wachstumsrate der Tumoren unterschied sich nicht, was dazu führte, dass der Endpunkt in der HCA1<sup>-/-</sup>-Gruppe nur geringfügig früher erreicht wurde. Verglichen mit der Gruppe aller verwendeten Wildtypiere wurde das maximale Gesamttumorvolumen in der Gruppe der HCA1-defizienten Tiere jedoch signifikant früher erreicht. Diese Daten implizieren, dass der Verlust von HCA1 das Auftreten von MMTV-PyMT-Brusttumoren bis zu einem gewissen Grad beschleunigen kann. Im Vergleich von HCA2-defizienten Tieren mit ihren Wildtypkontrollen wurde kein Unterschied in Tumoraltenz und -wachstum sowie in der Zeitspanne bis zum Erreichen des Endpunkts festgestellt. Somit konnten wir keinerlei Auswirkungen eines Knockouts von HCA2 in MMTV-PyMT-Brusttumormodell nachweisen. Die eindrucklichsten Ergebnisse wurden durch den Knockout von FFA2 in MMTV-PyMT-positiven Tieren erzielt. Diese Gruppe entwickelte palpierbare Tumoren signifikant schneller als ihre Wildtypkontrollen (P<0,001) und auch als die Gruppe aller verwendeten Wildtypiere (P<0,0001). Durch das Fehlen von Veränderungen in den Wachstumskurven der Tumoren wurde auch der Endpunkt signifikant früher erreicht (P<0,001). Der Verlust von FFA2 führt demnach nachweislich zu einer verkürzten Latenz bis zum Auftreten von Primärtumoren im MMTV-PyMT-Brusttumormodell. Da sich das Modell gut zur Untersuchung der Metastasierung in die Lunge eignet, analysierten wir die Lungen der Versuchstiere dahingehend. Immunhistochemische Färbungen mit dem Proliferationsmarker BrdU sowie mit Hämatoxylin und Eosin zeigten Herde proliferierender Zellen in fast allen untersuchten Lungen. Jedoch konnten wir keine Unterschiede in Metastasenanzahl und -fläche zwischen den rezeptordefizienten Tieren und

den Kontrolltieren ermitteln. Die aus diesem Versuchsaufbau gewonnenen Daten können keinen Einfluss des Verlustes metabolischer Rezeptoren auf die Metastasierung im MMTV-PyMT-Brusttumormodell nachweisen.

Da der Fokus unserer Arbeit auf der Untersuchung der Entwicklung von Primärtumoren lag, waren Betrachtungen zur Metastasierung von untergeordnetem Interesse. Nachträglich muss festgestellt werden, dass die Versuchsanordnung im LLC1-Modell und im MMTV-PyMT-Modell nicht dazu geeignet waren, valide Aussagen über Auswirkungen des Verlusts von metabolischen Rezeptoren auf Metastasierungsprozesse zu treffen. Im LLC1-Modell war der Versuchszeitraum zu kurz, um eine ausreichende Metastasierung in die Lunge zu ermöglichen, beziehungsweise die durch den Primärtumor verursachte Morbidität ließ einen ausreichend langen Versuchszeitraum nicht zu. Im MMTV-PyMT-Modell wäre ein festgesetzter Zeitpunkt zur Beendigung des Versuchs nötig, um den Effekt einer kürzeren Tumorlatenz auf die Metastasierung widerzuspiegeln. Ein solcher Effekt in Form von gesteigerter Metastasenanzahl und -fläche wäre bei der Analyse der Lungen von MMTV-PyMT<sup>+</sup>;FFA2<sup>-/-</sup>-Tieren gegenüber der Kontrolle zu erwarten. Diese Untersuchungen sind ein zentraler Bestandteil weiterer Forschung mit dem Ziel, die Funktion von FFA2 in Brusttumoren aufzuklären. Die Vermeidung von Metastasen ist ein entscheidender Prognosefaktor für das Überleben von Patienten und stellt daher einen interessanten Ansatzpunkt für eine pharmakologische Intervention dar.

Die Rolle der einzelnen metabolischen Rezeptoren in verschiedenen Tumorarten wurde bisher in unterschiedlichem Maß und mit wechselnden Ergebnissen untersucht. In zahlreichen Studien wurden Tumorzelllinien verwendet, um Auswirkungen eines Rezeptorknockdowns oder einer Überexpression zu studieren. Da in diesen Modellen der Einfluss des Tumorstromas vollkommen außer Acht gelassen wird, sind sie nur bedingt aussagekräftig. Gleiches gilt für den Einsatz von Xenograftmodellen. Die Transplantation von humanen Tumorzelllinien in zwangsläufig immundefiziente Mäuse lässt zwar Rekrutierung von CAFs sowie Gefäßneubildung zu, jedoch darf auf Grund der Abwesenheit von Immunzellen eine Abbildung physiologischer Prozesse in Frage gestellt werden.

Bisher publizierte Studien am Mausmodell untersuchen vorwiegend die Rolle von HCA2 und FFA2 in der Entstehung von Kolontumoren. Eine umfassende Studie zeigt eine deutlich höhere Tumورlast in HCA2-defizienten Tieren und bietet Erklärungen für einen potentiellen Mechanismus an. Die Resultate weichen deutlich von unseren Ergebnissen ab. Hierbei können Unterschiede im genetischen Hintergrund, den Haltungsbedingungen und daraus folgend im Darmmikrobiom eine Erklärung für die Abweichungen sein. Mögliche Auswirkungen haben wir vorangehend

beschrieben. Über die Funktion von FFA2 bei der Entstehung oder Vermeidung von entzündungsbedingten Kolontumoren gibt es ebenso widersprüchliche Auffassungen. Generell lässt sich allerdings feststellen, dass die Mehrzahl der Studien zu ähnlichen Ergebnissen wie unsere Untersuchungen kommt. Als mögliche Mechanismen für vermehrte Tumorentwicklung in FFA2-defizienten Tieren werden verminderte Autophagie durch einen Wegfall der Stimulation von FFA2 in neutrophilen Granulozyten durch Acetat sowie die Hemmung antiinflammatorischer Signale durch fehlende FFA2-Aktivierung in regulatorischen T-Zellen genannt. Die Rolle von FFA2 in Brusttumoren ist bislang unbekannt. Jedoch zeigt eine Studie, dass Überexpression von FFA2 in Adipozyten zu einer vermehrten Ausschüttung von Tumornekrosefaktor  $\alpha$  (TNF- $\alpha$ ) aus Makrophagen des antiinflammatorischen M2-Typs im Fettgewebe führt. Da das Tumorstroma von MMTV-PyMT-Brusttumoren Adipozyten enthält und hauptsächlich von Makrophagen des M2-Typs durchsetzt ist, lässt sich der beschriebene Mechanismus möglicherweise auf das Modell übertragen. Die Aktivierung des Rezeptors für TNA- $\alpha$  stimuliert durch das Wirken von Caspase-8 den programmierten Zelltod in Form von Apoptose oder Nekroptose. Demnach könnte der Verlust von FFA2 zu verringerter TNF- $\alpha$  Ausschüttung und somit zur Vermeidung von Apoptose oder Nekroptose der Tumorzellen führen. Zusammenfassend kann festgestellt werden, dass weitere Forschungsarbeit erforderlich ist, um die Funktion von FFA2 im Brusttumorstroma sowie die nachfolgenden Signalwege aufzuklären. Unsere Ergebnisse lassen vermuten, dass die Antagonisierung von FFA2 die Entstehung von entarteten Zellen und die daraus folgende Entwicklung von Brusttumoren im MMTV-PyMT-Modell hemmen kann. Als GPCR ist FFA2 ein attraktives Ziel für pharmakologische Interventionen und könnte neue Möglichkeiten zur Behandlung von Brusttumoren eröffnen.

### ACKNOWLEDGEMENTS

First, I would like to thank Prof. Dr. Stefan Offermanns for giving me the opportunity to carry out my research at the Max-Planck-Institute for Heart and Lung Research. Without his continuous scientific and methodical support, it would not have been possible to conduct this research. I sincerely appreciate his invaluable guidance.

I wish to show my gratitude to Prof. Dr. Nina Wettschureck for providing her advice and support and to Dr. Boris Strilic for his practical help and for introducing me to substantial research methods.

Moreover, I would like to thank my lab mate and friend Dr. Sarah Tonack for supporting me with her great scientific knowledge and for always encouraging me.

I thank my friends and research colleagues, Dr. Sorin Tunaru, Xinyi Chen, Dr. Rémy Bonnavion, Dr. András Iring, Dr. Shun Lu, Dagmar Magalei, Kathrin Heil, Daniel Heil, Martina Finkbeiner, Sabrina Kurz, Alan LeMercier, Kenneth Roquid, Adriana Vucetic, Dr. Sayali Joseph, Dr. Julián Albarrán, Dr. Denise Tischner, Dr. Carola Meyer and Dr. Lida Yang, for their amazing support. It was a special experience sharing the laboratory with you for the past years.

I take the opportunity to thank all the people in the institute who have supported me to complete the research directly or indirectly.

Additionally, I would like to extend my gratitude to Svea Hümmer for secretarial assistance and for consistent caring.

Last but not least, a special thanks to my husband Fabian, my parents and my sister for their love, advice and encouragement throughout this experience.

## CURRICULUM VITAE

### Isabell Brandenburger

#### Pharmacist

Barbarastraße 2, 61231 Bad Nauheim

Tel.: 0049151-44339285

E-Mail: isabell.brandenburger@yahoo.de

Born: 15. November 1988 in Bad Belzig

#### Practical Experiences

---

- |                 |   |
|-----------------|---|
| 02/2015-01/2020 | <b>Max-Planck-Institute for Heart and Lung Research,<br/>Department of Pharmacology, Bad Nauheim</b><br>PhD project supervised by Prof. Dr. Stefan Offermanns |
| 10/2014-01/2015 | <b>Pfalz-Apotheke, Ingelheim</b><br>Pharmacist  |
| 11/2013-04/2014 | <b>Schwanen Apotheke, Mainz</b><br>Internship for students of pharmacy  |
| 05/2013-10/2013 | <b>Bundesinstitut für Arzneimittel und Medizinprodukte</b><br>Internship for students of pharmacy at the department of clinical trials                        |
| 11/2012-04/2013 | <b>Novartis Pharma GmbH Nürnberg</b><br>Internship for students of pharmacy at the department of quality assurance  |

#### Education

---

- |                 |   |
|-----------------|---|
| 06/2014         | <b>License to practice as a pharmacist</b>  |
| 10/2012-09/2013 | <b>Pharmacy (Diploma degree program)</b><br>Novartis Pharma GmbH Nürnberg and Friedrich-Schiller-University Jena, supervision by Prof. Dr. Dagmar Fischer |
| 10/2008-10/2012 | <b>Pharmacy (state examination)</b><br>Friedrich-Schiller-University Jena   |
| 06/2008         | University-entrance diploma acquired at Fläming-Gymnasium in Belzig   |



---

## LEBENS LAUF

### Isabell Brandenburger

#### Apothekerin

Barbarastraße 2, 61231 Bad Nauheim

Tel.: 0049151-44339285

E-Mail: isabell.brandenburger@yahoo.de

geboren 15. November 1988 in Belzig

#### Berufliche Erfahrungen

---

02/2015- 01/2020	<b>Max-Planck-Institut für Herz- und Lungenforschung, Abteilung Pharmakologie, Bad Nauheim</b> Promotion betreut von Prof. Dr. Stefan Offermanns
10/2014-01/2015	<b>Pfalz-Apotheke, Ingelheim</b> Apothekerin
11/2013-04/2014	<b>Schwanen Apotheke, Mainz</b> Pharmaziepraktikum
05/2013-10/2013	<b>Bundesinstitut für Arzneimittel und Medizinprodukte</b> Pharmaziepraktikum im Fachgebiet Klinische Prüfung
11/2012-04/2013	<b>Novartis Pharma GmbH Nürnberg</b> Pharmaziepraktikum in der Abteilung Qualitätssicherung

#### Bildung

---

06/2014	<b>Approbation</b>
10/2012-09/2013	<b>Pharmazie (Diplom)</b> Novartis Pharma GmbH Nürnberg und Friedrich-Schiller-Universität Jena, Betreuung durch Prof. Dr. Dagmar Fischer
10/2008-10/2012	<b>Pharmazie (Staatsexamen)</b> Friedrich-Schiller-Universität Jena
06/2008	Abitur am Fläming-Gymnasium in Belzig

## Schriftliche Erklärung

### Erklärung

Ich erkläre hiermit, dass ich mich bisher keiner Doktorprüfung im Mathematisch-Naturwissenschaftlichen Bereich unterzogen habe.

---

Ort, Datum

---

Unterschrift

### Versicherung

Ich erkläre ehrenwörtlich, dass ich die dem Fachbereich Biochemie, Chemie und Pharmazie der Johann Wolfgang Goethe-Universität Frankfurt am Main zur Promotionsprüfung vorgelegte Dissertation mit dem Titel

#### **The role of metabolite receptors in tumor progression**

am Max-Planck-Institut für Herz- und Lungenforschung unter Betreuung und Anleitung von Prof. Dr. Stefan Offermanns selbständig angefertigt und mich anderer Hilfsmittel als der in ihr angegebenen nicht bedient habe, insbesondere, dass alle Entlehnungen aus anderen Schriften mit Angabe der betreffenden Schrift gekennzeichnet sind. Ich versichere, die Grundsätze der guten wissenschaftlichen Praxis beachtet, und nicht die Hilfe einer kommerziellen Promotionsvermittlung in Anspruch genommen zu haben.

---

Ort, Datum

---

Unterschrift